# Maneuver Prediction for Motion Cueing

MSc. Thesis

J. M. Eppink

Delft University of Technology

TU Delft

# Maneuver Prediction for Motion Cueing

## MSc. Thesis

by

J.M. Eppink

to obtain the degree of Master of Science
at the Faculty of Aerospace Engineering,
Department of Control & Simulation,
Delft University of Technology

Student number: 4290429
Date: October 29, 2020
Supervisors: Prof. Dr. Ir. M. Mulder, TU Delft
Dr. Ir. D. M. Pool, TU Delft
Dr. Ir. J. Venrooij, BMW Group
Ir. M. J. C. Kolff, BMW Group

An electronic version of this thesis is available at http://repository.tudelft.nl/.

TU Delft BMW GROUP

# List of Tables

# List of Figures

# List of Symbols

## Greek symbols

| | |
|---|---|
| $\alpha$ | two-thirds law fitting parameter |
| $\Gamma$ | lateral acceleration |
| $\Gamma_{max}$ | maximum lateral acceleration |
| $\Delta C_{max}$ | maximum curvature deviation |
| $\delta$ | driver control input position |
| $\dot{\delta}$ | driver control input velocity |
| $\delta_{s_{required}}$ | required steering wheel angle |
| $\delta_{s_{error}}$ | steering wheel error |
| $\theta$ | pitch |
| $\kappa$ | curvature |
| $\boldsymbol{\rho_i}$ | length of actuator $i$ |
| $\rho_{min}$ | minimum actuator length |
| $\rho_{min}$ | maximum actuator length |
| $\tau_v$ | time delay of the human's error response |
| $\phi$ | roll |
| $\psi$ | yaw |
| $\omega$ | angular velocity |
| $\omega_{split_x}$ | cut-off frequency used to split longitudinal vehicle acceleration into translational and tilt movement of the platform |

## Latin symbols

| | |
|---|---|
| $A$ | adjustment acceleration |
| $A_i$ | lower hinge point of actuator $i$ |
| $a$ | acceleration |
| $a_0$ | initial acceleration of the vehicle |
| $a_{acc,max}$ | maximum possible acceleration |
| $a_{brake,max}$ | maximum possible deceleration |
| $a_{lim}$ | acceleration limit |
| $\boldsymbol{a_i}$ | distance between the lower hinge point and the center of the inertial reference frame of actuator $i$ |
| $\bar{a}$ | mean of the vehicle's maximum possible acceleration and deceleration |
| $B$ | big acceleration |
| $B_{r,i}$ | upper hinge points |
| $\boldsymbol{b_{r,i}}$ | distance between the upper hinge point of actuator $i$ and the center of the platform, in the body reference frame |
| $C$ | body reference frame |
| $D_{PD}$ | $D$-value of the $PD$-controller of the acceleration- and jerk limiter |
| $\boldsymbol{d_s}$ | platform positions |
| $\boldsymbol{d_{s,max}}$ | maximum platform positions |
| $dT_a$ | TETP rate of change threshold |

| | |
|---|---|
| $E$ | emergency acceleration |
| $f_{s_{max}}$ | maximum specific force throughout the excursion |
| $H_c$ | control horizon |
| $H_{o_e}$ | linear portion of the human error response |
| $H_p$ | prediction horizon |
| $H_u$ | control horizon |
| $j$ | jerk |
| $j_{lim}$ | jerk limit |
| $K$ | inner loop gain of the acceleration- and jerk limiter |
| $K_e$ | gain of the human error response |
| $K_x$ | gain on the translational $x$-acceleration |
| $k$ | time step |
| $L_i$ | linear actuator i |
| $M$ | medium acceleration |
| $N$ | negative acceleration |
| $O$ | inertial reference frame |
| $P$ | position |
| $P_{PD}$ | $P$-value of the $PD$-controller of the acceleration- and jerk limiter |
| $P_{sim}$ | position of the platform's center |
| $\boldsymbol{R}$ | rotation (matrix) |
| $\boldsymbol{r}$ | position of the platform center in the inertial reference frame |
| $s$ | track distance |
| $T_b$ | braking threshold |
| $T_d$ | deceleration threshold |
| $^T$ | matrix transpose |
| $T_{L,e}$ | lead time constant of the human error response |
| $T_{l,e}$ | lag time constant of the human error response |
| $\boldsymbol{u}_s$ | angular rates and translational accelerations provided to the platform |
| $\boldsymbol{u}_{s,max}$ | maximum angular rates and translational accelerations provided to the platform |
| $V$ | velocity of the vehicle |
| $V_{sim}$ | velocity of the platform's center |
| $v_0$ | initial velocity of the vehicle |
| $v_d$ | prediction of the desired velocity when neglecting road curvature |
| $v_1$ | prediction of the velocity used to anticipate curve 1 |
| $v_2$ | prediction of the velocity used to anticipate curve 2 |
| $P_{x_{PP,min}}$ | minimum prepositioning position |
| $P_{x_{PP,max}}$ | maximum prepositioning position |
| $S$ | small acceleration |
| $t$ | time |
| $\bar{u}_f$ | future acceleration averaged over a time interval |
| $\bar{u}_h$ | historic acceleration averaged over a time interval |

## Other symbols

| | |
|---|---|
| ⊗ | universal joint |
| ∅ | sliding joint |
| ⊙ | ball joint |

# List of Abbreviations

| | |
|---|---|
| AD | absolute difference |
| ADAS | advanced driver assistance systems |
| CHMM | coupled hidden Markov models |
| COW | constant orientation workspace |
| DID | driver intention detection |
| DOF | degree of freedom |
| ETP | extended tangent point |
| FPR | false positive rate |
| HMM | hidden Markov model |
| LSTM | long short-term memory |
| MCA | motion cueing algorithm |
| MPC | model predictive control |
| MW | maximal workspace |
| NN | neural network |
| OW | orientation workspace |
| DTW | dynamic time warping |
| PMI | perceived motion incongruence |
| PP | prepositioning |
| PR | post-hoc rating |
| RNN | recurrent neural network |
| SPR | section-wise post-hoc rating |
| TETP | time to extended tangent point |
| TLC | time to line crossing |
| TOW | total orientation workspace |
| TP | tangent point |
| TPR | true positive rate |
| ROC | receiver operating characteristic |
| RMS | root mean square |
| VAF | variance accounted for |
| WS | workspace |

# Contents

# Introduction

## Background

Driving simulators are used as tools in research since the early 1960s, as means to obtain insights in interactions between the driver and his/her environment. Various reasons make it beneficial or necessary to conduct experiments in a simulated environment opposed to on the real road. Driving simulators offer a controlled environment, assuring safety and reproducibility. Moreover, simulator studies are generally less expensive when compared to studies with real vehicles. Lastly, a lack of readiness of a concept of which one wants to investigate the interactions with a human driver can make studies with a real vehicle impossible. Currently, simulator experiments in the field of driving with higher levels of automation are becoming increasingly popular, introducing new use cases. Examples of novel experiments on user behavior are system acceptance [1], takeover behavior [2] and cooperative strategies [3]. The growing number of use cases, combined with the increasing levels of realism that can be reached due to technological advances in the last decades, makes driving simulation a topic which is researched extensively. [4]

A driving simulator is a device set up to provide a combination of stimuli to the driver, known as cues. Important cues are visuals, sound and force feedback of the steering wheel. Many driving simulators include a platform that provides motion cues, which can yield an increase in the behavioral validity of a simulator experiment as a means to substitute a real driving experiment [5, 6]. Moreover, motion cues can decrease simulator sickness, which is a common cause for the drop-out of participants in simulator experiments [7]. Due to the limits on the acceleration, velocity and deflection of the actuators of motion platforms, a one-to-one reproduction of the dynamics of a simulated vehicle is seldom possible. The calculation of realizable platform motions is performed by a motion cueing algorithm (MCA). Many types of MCAs exist, ranging from simple filter-based approaches to advanced optimization-based solvers. Providing motion cueing is not trivial and often results in missing cues, cues where no stimulus is demanded (false cues), phase errors and scaling errors. [8]

A distinction can be made between passive driving experiments, where a participant is driven around, and active driving experiments, where the participant controls the virtual vehicle. In the latter case, motion cueing is complicated by the lack of knowledge on the oncoming sequence of maneuvers, while having to provide cues in real-time. This lack of knowledge mostly applies to longitudinal behavior, which is highly influenced by the participant's driving style, compared to lateral dynamics, which is mostly influenced by the roughly predefined trajectory [9].

Conventionally, only the outputs from the model of the simulated vehicle are used as inputs for MCAs. This leaves potentially useful information from the driver inputs and the road environment unused. The aim of this research is to increase the understanding of the predictive value of this information and its potential to improve online motion cueing. This project is done in cooperation with the BMW Group, which operates a number of motion-based driving simulators and is continually seeking to improve their motion cueing. Recorded data logs of 37 drives from a previously performed experiment in a static simulator at the BMW Group [10] will be analyzed in a search for ways to predict braking and acceleration in a simulated environment and a method to exploit knowledge of future maneuvers in active driving experiments.

## Research scope, objective and questions

The effectiveness of predictions in motion cueing will not only depend on the accuracy of the predictions, but also on the MCA to which the predictive feature are added and on the method used to incorporate predictions in simulator movement. The classical washout filter MCA is a well-known MCA capable of providing motion cueing in active driving tasks. BMW has an in-house developed version available, which will be adapted for this study. Considering the conversion of predictions to simulator movement, the focus will be on simulator prepositioning, an established predictive feature in motion cueing with classical washout filter MCAs [9, 11**?** , 12]. Lastly, the scope is defined by the set of recorded simulator drives made available by BMW, which contains rural road with curves, hilltops, changing legal speed limits and a passage through a village. Based on the previously described problem and resources, the following research objective is stated:

> *The objective of this research is to assess the suitability of driver inputs and information from the simulation environment as triggers for prepositioning of a dynamic driving simulator, by means of establishing a prediction model from driving data and evaluating prepositioning rules as extension to a classical washout filter MCA for a small hexapod motion platform.*

In order to achieve this research objective, various sub-objectives are defined:

- *SO1:* Review the state-of-the-art of longitudinal prepositioning in motion cueing for driving simulation.
- *SO2:* Review the state-of-the-art of longitudinal driver modeling and maneuver prediction.
- *SO3:* Propose and evaluate prediction models to predict longitudinal maneuvering.
- *SO4:* Design prepositioning based on these prediction models.
- *SO5:* Perform a human-in-the-loop experiment to evaluate the proposed prepositioning.

These sub-objectives define the work packages for this project, of which a graphical overview including interactions is provided in Figure 1.

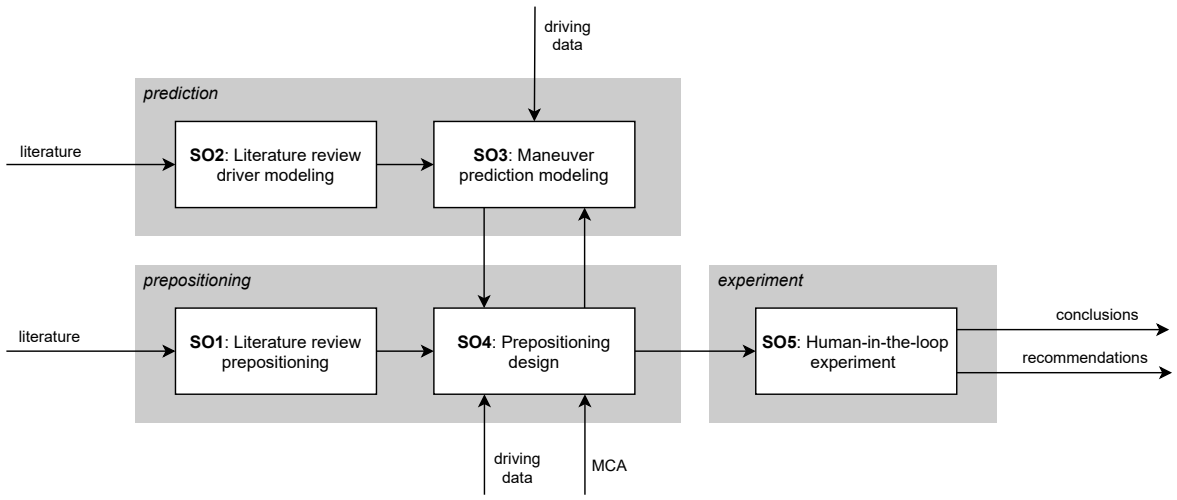


Figure 1: Schematic overview of the project.

In line with the stated objectives, the following research questions are defined:

- *RQ1:* To what extent can longitudinal maneuvers be predicted in a driving simulation environment?
  - *a)* What information can be used to predict longitudinal driving maneuvers?
  - *b)* Under what conditions can longitudinal driving maneuvers be predicted accurately?
- *RQ2:* To what extent can motion cueing quality of a classical washout filter MCA be improved using prepositioning based on predictions of longitudinal maneuvers?
  - *a)* How should predictions be converted to prepositioning that can be incorporated in a classical washout filter MCA?
  - *b)* What is the effect of prepositioning based on predictions of longitudinal maneuvering on the workspace usage of a hexapod-based driving simulator?
  - *c)* What is the effect of prepositioning based on predictions of longitudinal maneuvering on motion cueing quality as perceived by driving simulation participants?

# Report Outline

Part I: **Scientific paper**
In the scientific paper, the knowledge from the literature reviews and preliminary analysis as presented in the Preliminary thesis, was used to create a prediction model and prepositioning algorithm. Moreover, the results of the human-in-the-loop experiment performed to test the algorithm are discussed. From these results, conclusions are drawn and recommendations for future research were presented.

Part II: **Preliminary thesis**
The preliminary thesis consists of a literature reviews on i) the state-of-the-art of prepositioning in driving simulation and ii) driver modeling, both with a focus on longitudinal dynamics. Moreover, a preliminary analysis was done wherein the preliminary set of driving data was analyzed. Lastly, an experiment design was drafted, to evaluate the final PP design.

Part III: **Appendices**
Eight appendices are attached to this thesis. In the first appendix, the effect of the workspace limiting on motion cueing quality is described. Appendix B provides results of the post-hoc questionnaire, which were omitted in the scientific paper. The subsequent appendices describe the briefing, post-hoc motion cueing questionnaire and Latin square design used in the human-in-the-loop experiment. A potential effect of the drive number on the subjective ratings is discussed in Appendix F. The effect of the thresholds on the prediction scores is shown in Appendix G. Lastly, Appendix H provides a comparison between the prepositioning algorithm proposed in this thesis and a prepositioning algorithm available in literature.

# I

# Scientific paper

# Probabilistic Maneuver Prediction for Motion Cueing in Driving Simulation

J. M. Eppink
Control & Simulation, Faculty of Aerospace Engineering
Delft University of Technology
email: jesseeppink@gmail.com

***Abstract*—Potential usage of the workspace of driving simulators is restricted by a lack of knowledge on oncoming maneuvers, due to the unpredictable nature of human drivers. This research aims to explore the possibility of using information from driver inputs, dynamic vehicle states, and features of the road environment to improve motion cueing through simulator prepositioning. Probabilistic models were established to predict longitudinal maneuvering for a short scenario consisting of a drive on a two-lane road through a rural area. By combining the accelerator deflection, the vehicle's velocity and the future speed limit in a logistic regression model, the area under the receiver operating characteristic curve was 0.84 for acceleration prediction and 0.77 for deceleration prediction, using a look-ahead time of 5 seconds. In order to use these predictions for motion cueing, the prediction model was extended to a prepositioning module. The proposed design was tested in combination with a classical washout algorithm on a small hexapod-based driving simulator in a human-in-the-loop experiment. No distinguishable results were obtained in objective and subjective evaluation of the motion cueing quality, as possibilities to improve motion cueing were limited with the experimental setup used. Nevertheless, the workspace usage was improved significantly. The average distance that could be maintained from the edge of the simulator's workspace, could be increased from 0.025 meter to 0.084 meter, for equivalent motion cueing.**

***Index Terms*—motion cueing, driving simulation, prepositioning, maneuver detection**

## I. Introduction

Driving simulators are used since the early 1960s as cost-efficient means to obtain insights in interactions between drivers, the car automation and the road environment [1]. They offer a controlled environment, assure safety and improve reproducibility. Currently, many simulator experiments in the field of driving with higher levels of automation are becoming cunducted, introducing new use cases. Examples of novel experiments on user behavior focus on system acceptance [2], takeover behavior [3] and cooperative strategies [4].

Various cues (i.e., stimuli) can be provided to the driver in a simulator. Many driving simulators contain a motion system, as motion cueing can yield an increase in the behavioral validity of a simulator experiment [5], [6]. Moreover, motion cueing can reduce the risk of simulator sickness, a common cause of drop-out of participants [7].

Due to the limits on the acceleration, velocity and deflection of the actuators of motion simulation systems, a one-to-one reproduction of the dynamics of a real vehicle is seldom possible. Translation of vehicle motion into simulator displacements within the limited workspace of a motion system is performed by a motion cueing algorithm (MCA) [8]. Various types of MCAs exist, ranging from simple filter-based approaches to advanced optimization-based solvers [9].

Providing motion cueing can be complicated and often results in missing cues, false cues (i.e., cues where no stimuli are demanded), phase errors, and scaling errors [9]. In simulator experiments where participants actively control the virtual vehicle, motion cueing is often tuned conservatively, to account for the lack of knowledge on oncoming maneuvers. This lack of knowledge especially applies to longitudinal maneuvering, as differences in driving styles result in a high inter-driver variability of longitudinal acceleration when compared to lateral acceleration [10].

Some driving maneuvers cause motion renderings that are almost unidirectional. In this case, a simulator generally moves in this direction during a maneuver and returns to the neutral position when the maneuver ends. If it is possible to predict future motion renderings, the simulator's neutral position can be offset with a displacement opposing the direction of the predicted motion. This displacement is referred to as prepositioning (PP) [11]. As successful PP makes more workspace available in the direction of the expected maneuver, one can intensify cueing. This is not without risk, however, as movements in unanticipated directions can bring the simulator closer to the edge of its workspace [11].

Hansson & Stenbeck [12] assumed it impossible to predict whether acceleration or deceleration will occur, due to the non-deterministic human nature. In their PP implementation for a curvy race track, the possibilities of braking and accelerating were taken into account at all times. The mean of the range of possible vehicle accelerations was then calculated from the maximum possible acceleration and deceleration, depending on the vehicle's velocity. From this mean, a reference PP offset was calculated.

Pitz et al. [13] used legal speed limit signs, road crossings, pedestrian crossings, and traffic lights as potential triggers for PP. Without reporting on the exact PP implementation, they reported no significant differences in objective and subjective motion cueing quality when comparing an MCA with longitudinal PP to another MCA without longitudinal PP. It is reasoned that this was a consequence of longitudinal driving behavior being dominated by individual driving style rather

than road layout.

Being merely a tool to improve workspace usage, not motion cueing quality, PP ideally happens imperceptibly. Consequently, it is usual to limit a reference PP signal on an acceleration- and jerk level [12], [13], as both were found to have an effect on how motion is perceived [14]. A control scheme with saturation limits, a PD-controller and a feedforward loop from Fischer [15] can be used for this purpose [12].

Next to motion cueing implementations in which PP is calculated explicitly, a class of MCAs exist in which PP can result from optimization. In these MCAs, which are based on model predictive control (MPC), an optimal sequence of dynamic simulator states is calculated for a limited time horizon by means of minimizing a cost function, while explicitly taking into account workspace constraints [16]. Grottoli et al. [17] showed that in the hypothetical case of having perfect predictions of future vehicle dynamics, the performance of MPC-based cueing improves. As in reality, these are unknown, constant dynamics were conventionally assumed [16]. Recently, efforts have been made to obtain better predictions in the real-time simulation environment. Mohammadi et al. [18] used an artificial neural network to predict future accelerations out of historic accelerations to objectively improve motion cueing of an MPC-based MCA.

Generally, only current dynamic vehicle states are used as inputs for MCAs. This leaves potentially useful information from the driver inputs and the road environment unused. Efforts have been put into predictions of future vehicle movement to improve MCAs [8], [12], [18]–[21], but none combined driver inputs, dynamic vehicle states and features of the road environment. The current research aims to assess the suitability of these sources of information as triggers for PP of a dynamic driving simulator, by means of i) establishing prediction models for longitudinal maneuvering from driving data, and ii) evaluating PP logic based on those predictions. The effect of this PP design on workspace usage and motion cueing quality are evaluated in a human-in-the-loop experiment using a classical washout MCA and a small hexapod-based driving simulator.

This paper is structured as follows: First, Section II describes how recorded data logs were analyzed to create an acceleration prediction model for a simulated environment. Hereafter, the prediction model was extended to a PP algorithm, which is described in Section III. The human-in-the-loop experiment done to evaluate the PP algorithm is described in Section IV. Results are provided in Section V, followed by a discussion in Section VI and conclusions in Section VII.

## II. Prediction

### A. Scenario

The scenario investigated in this paper involves driving along a two-lane road through a rural area, containing multiple speed limit signs, a small village, various curves (maximum curvature: 0.029 $m^{-1}$) and a number of hills (maximum slope: 14%). An overview of the scenario is provided in Figure 1. The scenario is driven in both directions, southward and northward.

The preliminary data set used to fit and evaluate the prediction models is taken from a previously performed simulator experiment [22]. It contains 21 southward drives and 16 northward drives. The sections in which longitudinal maneuvering takes place are denoted S1 to S4 and N1 to N4. An overview of the characteristics of these sections is provided in Table I. Starting and stopping maneuvers were excluded, as these are considered exceptions to normal continuous driving behavior and would therefore need a separate approach. Traffic was only present on the opposite lane. The vehicle model constitutes a 2018 BMW 530i with a 4 cylinder 2.0 L engine and automatic transmission.

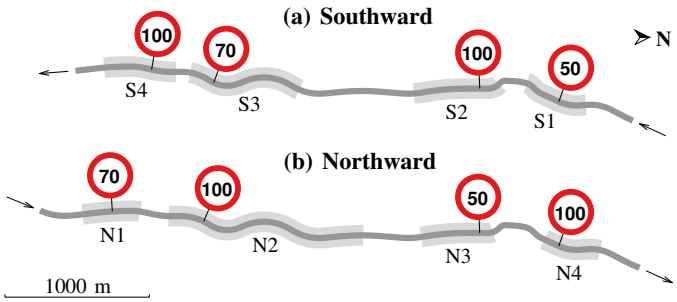


Fig. 1. Scenarios used to fit and evaluate the prediction models.

Table I
Sections with sustained acceleration/deceleration

| | Description | Speed limits (km/h) |
|---|---|---|
| S1 | Entering village | 100 → 50 |
| S2 | Leaving village | 50 → 100 |
| S3 | Sharp turn, reduced speed limit | 100 → 70 |
| S4 | Sharp hilltop, increased speed limit | 70 → 100 |
| N1 | Sharp hilltop, reduced speed limit | 100 → 70 |
| N2 | Sharp turn, increased speed limit | 70 → 100 |
| N3 | Entering village | 100 → 50 |
| N4 | Leaving village | 50 → 100 |

### B. Model output

As the output of the designed prediction model will be used as input for a PP module, it could have been opted to predict the future platform excursion that is to be anticipated. However, this would have made the prediction algorithm restricted to the MCA and dependent on its tuning parameter set. The vehicle's surge acceleration, $a_x$, is the input for the MCA's surge channel and will be used as model output instead. It is found that an imperceptible PP excursion of 0.30 m (i.e., covering most of the workspace of the small hexapod-based simulator used in this paper) can take up to 4.1 seconds [23]. In order to be able to apply PP before a maneuver commences, it is desired to predict oncoming accelerations with a larger look-ahead time. For this purpose, the peak acceleration between

the current time and 5 seconds ahead, $a_{x,peak}[t \cdots t+5]$ as in (1) was predicted. More specifically, the probability that this peak acceleration is larger than 0.5 m/s$^2$ or smaller than -0.5 m/s$^2$ was estimated. Instances where this holds, were labeled *acceleration* and *deceleration*, respectively. A histogram of $a_{x,peak}[t \cdots t+5]$ for the recorded drives is shown in Fig. 2. The classes *acceleration* and *deceleration* both make up 33% of the data points, whereas in 34% of the data points no maneuver is about to occur.

$$a_{x,peak}[t] = \begin{cases} \max(a_x[t]) & \max(a_x[t]) \geq |\min(a_x[t])| \\ \min(a_x[t]) & \max(a_x[t]) < |\min(a_x[t])| \end{cases} \quad (1)$$

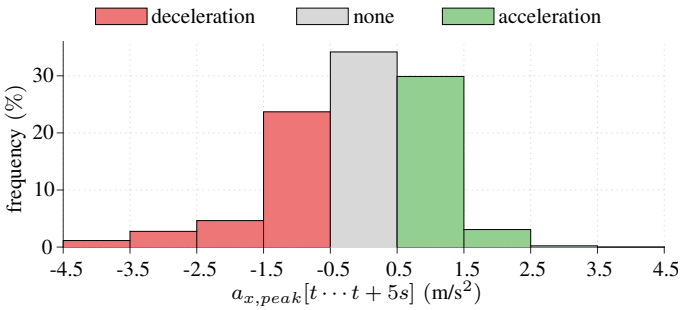


Fig. 2. Distribution of $a_{x,peak}[t \cdots t+5s]$ for all drives combined.

### C. Model type

MCAs are generally re-tuned for each scenario and motion platform [24]. It was therefore desired to create a prediction model of which the decisions are easy to understand, as this simplifies adaptation and potential troubleshooting. Conditional probability tables (CPTs) and a logistic regression model were evaluated as means to achieve this goal.

*1) CPTs:* Possible values for model inputs were subdivided into segments. The probability that a maneuver occurs in the near future, $p$, was calculated for all combinations of model input segments and assumed valid for the center of these segments. The resulting CPTs were linearly interpolated/extrapolated to calculate $p$ for any exact set of model inputs. Each CPT contained $\prod_{i=1}^{n} m_i$ parameters, where $n$ is the number of predictor variables and $m_i$ is the number of segments of variable $i$. For simplicity, equally sized segments spanning the complete range of sample data were used. The amount of segments was a trade-off between resolution (i.e., more segments) and accuracy (i.e., more data per segment). Empirically, an $m_i$ of 8 was chosen when one predictor variable was used. When using two predictor variables, a lower $m_i$ of 5 was chosen, to compensate for the further segmentation of the data. CPTs were used to compare predictor variables, as they were straight-forward to use. A drawback of the CPTs was the large amount of parameters.

*2) Logistic regression:* The best predictor variables found using the CPTs were used to train a logistic regression model. In logistic regression, a linear relationship as in (2) is assumed between the predictor variables, $x$, and the log-odds of the probability that a maneuver occurs in the near future, $\ell$ [25]. Each model contained only $n+1$ parameters. Matlab's `mnrfit` function was used to fit the model's parameters, $\beta$.

$$\ell = \log \frac{p}{1-p} = \beta_0 + \sum_{i=1}^{n} \beta_i x_i \quad (2)$$

### D. Model inputs

The vehicle's velocity, legal speed limits and driver control inputs were considered as potential predictor variables (i.e., model inputs). Earlier analysis showed that other road environment attributes, such as road curvature, slope and road width, are less relevant for velocity control in the current scenario [23].

*1) Vehicle velocity and legal speed limits:* As Hansson & Stenbeck's PP algorithm [12] uses the vehicle's velocity as the only input, predicting acceleration behavior from solely velocity was also tried in the current analysis. It could be expected that the vehicle's velocity in itself is not very informative, as acceleration can occur at high velocities and likewise, deceleration can occur at low velocities.

Another predictor is obtained by subtracting the legal speed limit, $V_r$, from the vehicle's velocity, $V_{veh}$. Drivers anticipate to upcoming road signs well before reaching them. To account for this, another predictor was created using the speed limit further down the road instead of the speed limit at the vehicle's position. For this purpose, the speed limit that applies $dt$ seconds in advance, $\hat{V}_{r,t+dt}$, is calculated, assuming the vehicle velocity to remain constant.

*2) Control inputs:* Next to information from the road environment and the vehicle's velocity, control inputs were used to predict future maneuvering. As the model aims to predict longitudinal maneuvering, the accelerator- and brake pedals (denoted $\delta_a$ and $\delta_b$, respectively) were considered. The relative pedal deflections in a $[0, 1]$ range, and the time derivative of the relative accelerator deflection (denoted $\dot{\delta}_a$) were tested as potential predictor variables.

### E. Model selection

To prevent overfitting of the model on the training data, the southward drives were used for model creation and northward drives were used for model evaluation. The outputs of CPTs and logistical regression models are the probabilities that acceleration and deceleration is about to occur, i.e., $p\left(a_{x,peak}[t \cdots t+5s] > 0.5\right)$ and $p\left(a_{x,peak}[t \cdots t+5s] < -0.5\right)$. Generally, a classification threshold is selected to determine above which $p$-value a maneuver is predicted. Receiver operator characteristic (ROC) curves [26] were created to be able to see how the true positive rate (TPR) and false positive rate (FPR) change for various threshold values. The area under the curve (AUC) was used as a performance metric independent of the selected threshold. Moreover, $F_1$-scores [27] were calculated for each threshold, so as to find the optimal classification thresholds and their

Table II
AUCs AND OPTIMAL F-SCORES FOR ACCELERATION- AND DECELERATION CPTs MADE USING VARIOUS PREDICTORS

| | Acceleration | | Deceleration | |
|---|---|---|---|---|
| **Predictor variable(s)** | **AUC** | **$F_1$** | **AUC** | **$F_1$** |
| $V_{veh}$ | 0.54 | 0.46 | 0.50 | 0.39 |
| $V_{veh} - V_r$ | 0.66 | 0.47 | 0.53 | 0.38 |
| $V_{veh} - \hat{V}_{r,t+4s}$ | 0.73 | 0.51 | 0.65 | 0.42 |
| $V_{veh} - \hat{V}_{r,t+8s}$ | 0.74 | 0.54 | 0.75 | 0.55 |
| $\delta_a$ | 0.81 | 0.60 | 0.71 | 0.53 |
| $\delta_b$ | 0.54 | 0.45 | 0.64 | 0.43 |
| $\delta_a$, $\delta_b$ | 0.81 | 0.60 | 0.73 | 0.51 |
| $\delta_a$, $\dot{\delta_a}$ | 0.81 | 0.60 | 0.70 | 0.53 |
| $V_{veh} - \hat{V}_{r,t+8s}$, $\delta_a$ | <u>0.84</u> | <u>0.64</u> | <u>0.77</u> | 0.53 |
| $V_{veh} - \hat{V}_{r,t+8s}$, $\delta_b$ | 0.74 | 0.54 | 0.76 | <u>0.57</u> |

corresponding scores. Both scores are in a $[0, 1]$ range, where 1 indicates perfect predictions.

The AUCs and optimal $F_1$-scores for the models of various (combinations of) predictor variables are provided in Table II, where the best scores are underlined. It can be seen that subtracting the legal speed limit from the vehicle velocity yielded improved predictions. Even better results were obtained when a look-ahead time of 8 seconds was used for speed limits. When looking at the control inputs, it was found that the accelerator pedal deflection predicts both acceleration and deceleration better than the brake pedal deflection. Adding the time derivative of the accelerator deflection did not improve predictions and even yielded a reduced AUC for deceleration prediction. Generally, the best prediction scores were obtained using the vehicle's velocity w.r.t. the legal speed limit 8 seconds ahead combined with the accelerator pedal deflection ($V_{veh} - \hat{V}_{r,t+8s}$, $\delta_a$).

A graphical representation of the CPTs based on $V_{veh} - \hat{V}_{r,t+8s}$ and $\delta_a$ is given in Fig. 3. These probabilities were interpolated to obtain finer predictions. In the top right corner, probabilities are unknown, as this represents a considerable accelerator deflection while the vehicle's velocity is much higher than the legal speed limit, which does not occur in the training data. Model outputs in this region are obtained through linear extrapolation. It can clearly be seen that generally, a higher $V_{veh} - \hat{V}_{r,t+8}$ decreases the chance of acceleration and increases the chance of deceleration, whereas a higher $\delta_a$ increases the chance of acceleration and decreases the chance of deceleration.

Using the optimal predictors from the CPT-based models for logistic regression, the models displayed in Figure 4 were obtained. One can see that they roughly show the same behavior as the CPT-based models, but now no interpolation/extrapolation is required. The ROC curves of both model architectures are shown in Fig. 5. Points with optimal $F_1$-scores are denoted +. No large differences are found between

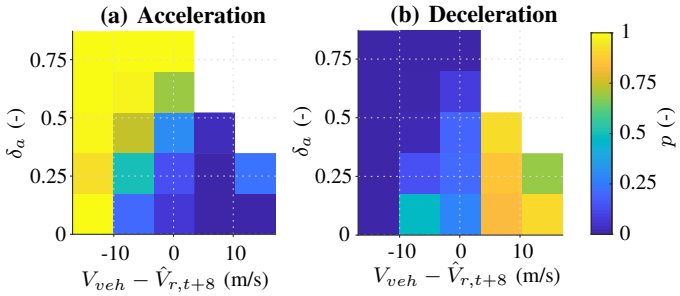


Fig. 3. CPTs for acceleration/deceleration prediction with predictor variables $V_{veh} - \hat{V}_{r,t+8s}$ and $\delta_a$.

the two model types. Table III presents the AUC and optimal $F_1$-scores for both model architectures. For acceleration prediction, the AUC and $F_1$-score are slightly better for the CPT. For deceleration prediction, the optimal $F_1$-score is slightly better for the logistic regression model. As the logistic regression model consists of only 3 parameters per maneuver, compared to the 25 parameters of the CPT, it is used throughout the remainder of this paper. The exact relationships between the predictor variables and the predicted probabilities of acceleration, deceleration and no maneuver ($\hat{p}_{acc}$, $\hat{p}_{dec}$ and $\hat{p}_{none}$, respectively) are provided in Eq. (3).

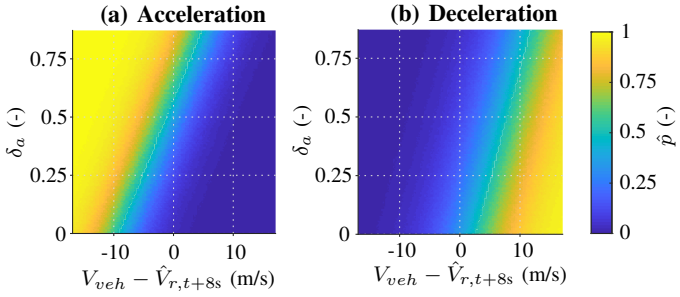


Fig. 4. Logistic regression models for acceleration/deceleration prediction with predictor variables $V_{veh} - \hat{V}_{r,t+8s}$ and $\delta_a$.

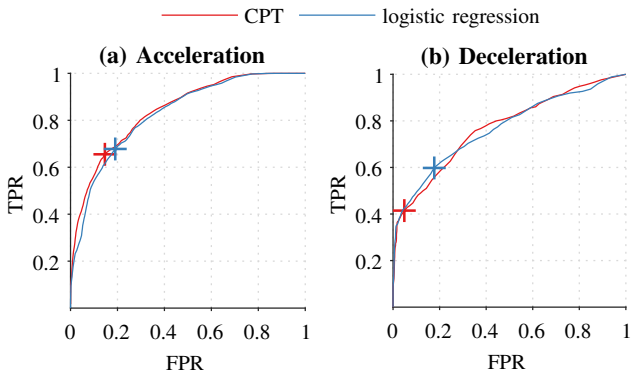


Fig. 5. ROC curves for acceleration/deceleration prediction models with predictor variables $V_{veh} - \hat{V}_{r,t+8}$ and $\delta_a$. Points with optimal $F_1$-scores are denoted +.

Table III
AUCs AND OPTIMAL F-SCORES FOR ACCELERATION- AND DECELERATION USING CPTs AND LOGISTIC REGRESSION WITH PREDICTOR VARIABLES $V_{veh} - \hat{V}_{r,t+8}$ AND $\delta_a$

| | **Acceleration** | | **Deceleration** | |
|---|---|---|---|---|
| **Model architecture** | **AUC** | **$F_1$** | **AUC** | **$F_1$** |
| CPT | 0.84 | 0.64 | 0.77 | 0.53 |
| Logistic regression | 0.83 | 0.62 | 0.77 | 0.55 |

$$\hat{p}_{acc}(t) = \left(1 + e^{3.3+0.35(V_{veh}-\hat{V}_{r,t+8})-5.6\delta_a}\right)^{-1} \quad (3a)$$

$$\hat{p}_{dec}(t) = 1 - \left(1 + e^{-0.62+0.25(V_{veh}-\hat{V}_{r,t+8})-2.6\delta_a}\right)^{-1} \quad (3b)$$

$$\hat{p}_{none}(t) = 1 - \hat{p}_{acc}(t) - \hat{p}_{dec}(t) \quad (3c)$$

## III. PREPOSITIONING

### A. Design

The suitability of the newly designed prediction model for PP was tested in combination with the classical washout MCA implementation from Ellensohn [10], which was chosen for its simplicity and widespread use. A schematic representation is given in Fig. 6. In this MCA, linear high-pass filters (HPFs) and low-pass filters (LPFs) are used to present high frequency vehicle accelerations in the translational channel and provide low frequency vehicle accelerations in the tilt coordination channel, respectively. Translational accelerations are transformed from body reference frame $B$ to inertial reference frame $I$ using the simulator's orientation ($\phi_{sim}$, $\theta_{sim}$, $\psi_{sim}$). More HPFs are present in the translation and rotation channels to facilitate washout in the inertial frame. Linear scaling and cut-off frequencies are set independently per degree-of-freedom.

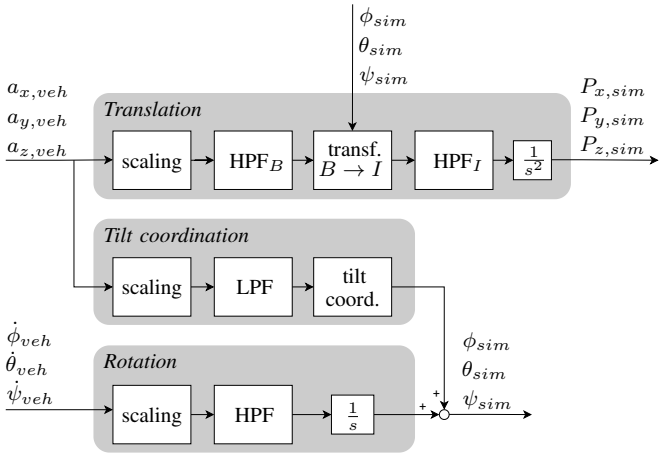


Fig. 6. Classical washout MCA used in this paper.

In the current section, a PP logic is designed that calculates a reference PP signal from the acceleration and deceleration probabilities calculated using the proposed prediction model. The acceleration and jerk of this reference signal will be limited by a controller proposed by Fischer [15], as shown in Fig. 7. Thresholds for acceleration and jerk will be set to 0.05 m/s$^2$ and 0.1 m/s$^3$, respectively, as these values have empirically been found acceptable for PP [12]. The final PP output is added to the MCA's output before being sent through the workspace limiting block, which ensures smooth behavior in case one of the simulator's actuators exceeds 95% of the maximum deflection potential. The remaining 5% of the deflection potential was empirically found sufficient to smoothly stop the simulator. An overview of the proposed architecture is given in Figure 8.

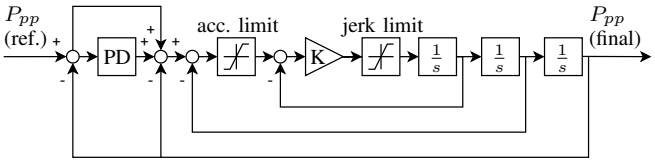


Fig. 7. PP controller with acceleration and jerk limiting. Adapted from [12]

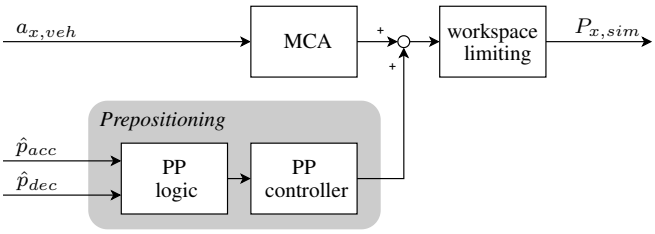


Fig. 8. Merging of prediction-based PP with the MCA's surge output.

Two types of logic were used to calculate a reference PP signal from the acceleration/deceleration probabilities. In both types, the longitudinal simulator position shifts to anticipate acceleration and deceleration ($P_{pp,acc}$ and $P_{pp,dec}$, respectively), are calculated separately at every sampling instance. In both PP algorithms, these two PP results are summed before being forwarded to the PP controller.

*1) Threshold-based PP logic:* If the probability of acceleration/deceleration exceeds a threshold, the platform is commanded to its maximum PP offset, denoted $P_{pp,min}$ and $P_{pp,max}$ for the maximum rear and front positions, respectively. The thresholds for acceleration and deceleration were set 0.51 and 0.30, respectively, as with these thresholds optimal $F_1$ scores were obtained in Section II-E. Note that the corresponding points on the ROC curves are shown in Fig. 5. The resulting logic is shown in (4).

$$P_{pp,acc}(t) = \begin{cases} 0 & \hat{p}_{acc}(t) < 0.51 \\ P_{pp,min} & \hat{p}_{acc}(t) \geq 0.51 \end{cases} \quad (4a)$$

$$P_{pp,dec}(t) = \begin{cases} 0 & \hat{p}_{dec}(t) < 0.30 \\ P_{pp,max} & \hat{p}_{dec}(t) \geq 0.30 \end{cases} \quad (4b)$$

*2) Linear PP logic:* In this second PP logic, the platform is prepositioned based on a linear scaling with the acceleration/deceleration probabilities, as in (5).

$$P_{pp,acc}(t) = \hat{p}_{acc}(t) \cdot P_{pp,min} \tag{5a}$$

$$P_{pp,dec}(t) = \hat{p}_{dec}(t) \cdot P_{pp,max} \tag{5b}$$

Fig. 9 shows the PP reference signal resulting from both types of PP logic and the limited signal resulting from the PP controller, for a part of one drive including section N3. It can be seen that the PP controller yields a smooth output for both approaches, which is slightly delayed w.r.t. the reference signal. When using the threshold-based logic, a short excitation of the reference position yields almost no response in the final PP signal.

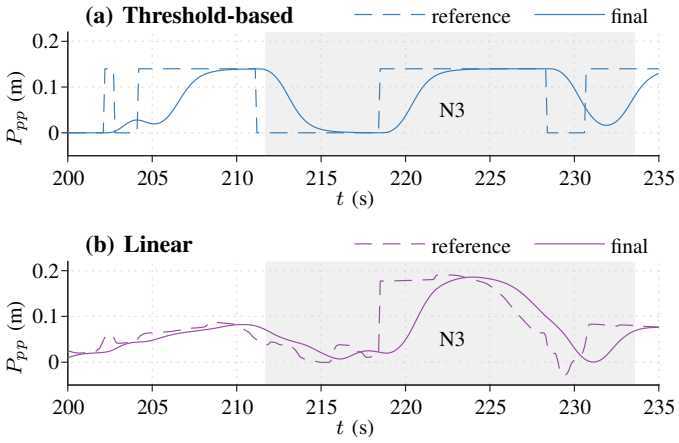


Fig. 9. Threshold-based and linear PP for a drive including section N3.

## B. Evaluation

The described types of PP logic were evaluated using computer simulations (i.e., without the actual driving simulator). For both types, the potential increase of surge motion cueing intensity that could be provided without exceeding the workspace limits of BMW's Portable Motion Simulator (PMS) in any of the 16 recorded northward drives was calculated. The PMS is a small hexapod-based motion system with 400 mm stroke actuators. Further details on the simulator are given in Section IV-D. The tuning set shown in Table IV was used as a starting point. It was previously created for the same simulator and scenario [22].

Intensifying surge motion cueing could be either done by decreasing the cutoff frequency of the high-pass filter for translational surge acceleration ($\omega_{HPF,x}$), or by increasing the translational surge gain, $K_x$. The latter method was chosen for its straightforwardness, as a multiplication of the gain yields an equal multiplication of the magnitude of the simulator's response. The maximum $K_x$ that could be set without activating the workspace limiting in any of the 16 drives, $K_{x,max}$, was calculated for both types of PP logic. A grid search was performed to find the optimal combination of $P_{pp,min}$ and $P_{pp,max}$ for each type of PP logic. The final results are presented in Table V.

Table IV
MCA TUNING PARAMETERS FROM A FORMER EXPERIMENT [22]

| | $x$ | $y$ | $z$ | $\phi$ | $\theta$ | $\psi$ |
|---|---|---|---|---|---|---|
| $K$ | 0.13 | 0.10 | 0.13 | 4.30 | 4.00 | 2.00 |
| $\omega_{HPF}$ (rad/s) | 4.30 | 4.00 | 2.00 | - | - | 0.80 |
| $K_{tilt}$ | 0.13 | 0.10 | - | - | - | - |
| $\omega_{LPF,tilt}$ (rad/s) | 0.35 | 1.50 | - | - | - | - |
| $\omega_{HPF,washout}$ (rad/s) | 0.15 | 0.20 | 1.00 | 0.80 | 1.20 | 0.50 |
| $\zeta_{HPF,washout}$ | 1.50 | 1.50 | 1.00 | - | - | - |

Table V
MAXIMUM SURGE GAIN AND CORRESPONDING $P_{pp,min}$ AND $P_{pp,max}$

| **PP logic** | $K_{x,max}$ | $P_{pp,min}$ | $P_{pp,max}$ |
|---|---|---|---|
| None | 0.24 | - | - |
| Threshold-based | 0.34 | -0.10 m | 0.14 m |
| Linear | 0.33 | -0.14 m | 0.20 m |

$K_{x,max}$ was found to be 0.34 and 0.33 for the threshold-based and linear PP logic, respectively. As these values are equivalent, more performance criteria were used to choose between these PP logic types. These extra criteria were the amount of movement induced by PP (i.e., false cues) and the minimum margin kept from the edge of the simulator's workspace (i.e., the available workspace to improve motion cueing) per drive. In order to allow for a fair comparison, $K_x$ was set to 0.33 for both types of PP logic in this analysis.

The root mean square of the acceleration induced by PP, $a_{pp,rms}$, was calculated per drive to compare the amount of false cues due to PP activity. The minimum margin from the workspace edge in surge direction, $d_{ws,x,min}$, was calculated discretely using the constant orientation workspace (COW) as in Kurutas [28]. Due to coupling between the degrees-of-freedom of a hexapod system, the workspace differs per platform orientation. This is accounted for by recalculating the workspace using the orientation at each time step.

An example of the COW of the current simulator in its neutral position is given in Fig. 10(a). Only 95% of the maximum actuator deflection was accounted for, as hereafter workspace limiting overrides the MCA. In the 2D cross-section at the simulator's heave position shown in Fig. 10(b), the front and rear distances between the platform's centroid and the workspace edge, $d_{ws,front}$ and $d_{ws,x,rear}$ are indicated. The minimum of $d_{ws,front}$ and $d_{ws,x,rear}$ over each drive was taken as $d_{ws,x,min}$.

Box plots of the two additional PP performance metrics for the 16 northward drives are shown in Figure 11. For equivalent motion cueing, the linear PP logic maintained a larger margin from the workspace edge, with lower PP accelerations. For

this reason, the linear PP logic is considered more effective than the threshold-based approach and is used throughout the remainder of this paper.

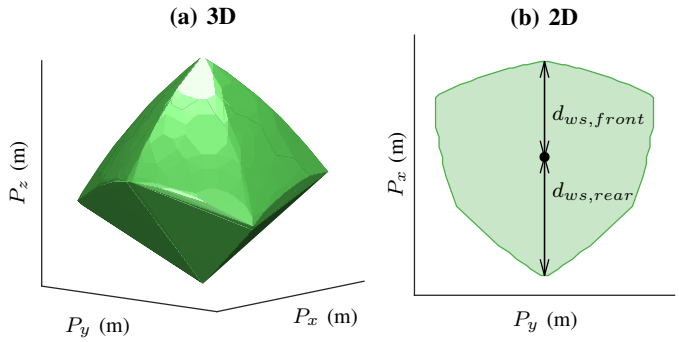


Fig. 10. COW of the Portable Motion Simulator, where • indicates the platform's centroid.

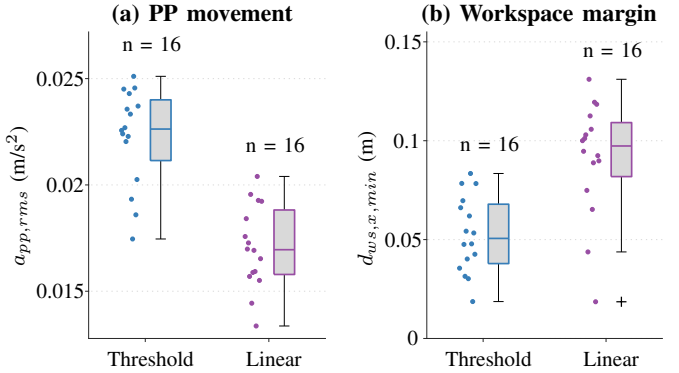


Fig. 11. PP movement and workspace margin for the threshold-based and linear PP logic.

## IV. Experiment

The effectiveness of the proposed PP design was investigated with a within-subjects experiment, where participants drove the northward scenario shown in Fig. 1(b) with various motion conditions. The goal of the experiment was to investigate the effect of the proposed PP on workspace usage and the possibility to noticeably improve motion cueing quality.

### A. Experimental conditions

The tested experimental conditions are shown in Table VI. Condition C1 served as baseline, against which the effects of adding PP and increasing the translational surge gain ($K_x$) were tested. All other MCA tuning parameters are as shown in Table IV. In condition C2, PP was active, but $K_x$ was kept as in condition C1. This condition is added to test the hypotheses that adding PP improves the workspace management and that adding PP does not have an effect on the motion cueing quality, which is made based on the limiting of the jerk and the acceleration with the PP controller. In condition C3, $K_x$ was increased to 0.33, so as to completely use the workspace that was expected to be made available by PP. It was hypothesized that the combined effect of adding PP and intensifying surge motion results in an increase in motion cueing quality, as PP was assumed to happen imperceptibly and intensifying surge motion would reduce the error between the specific forces in the simulated vehicle and the platform. The difference between the motion cueing between the three conditions for an acceleration maneuver is demonstrated in Fig. 12, where $f_{s,x}$ denotes the forward specific force.

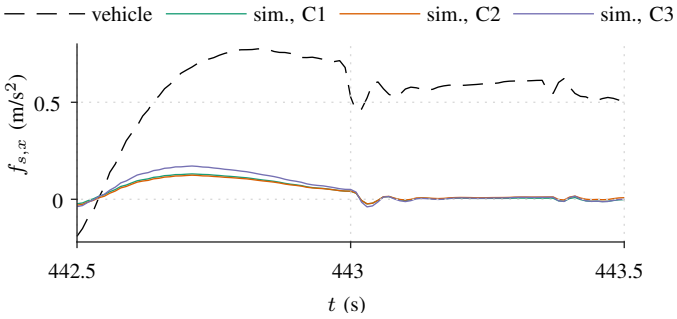


Fig. 12. Response to an acceleration maneuver per experimental condition.

Table VI
Experimental conditions

| Condition | PP | $K_x$ |
|---|---|---|
| C1 | off | 0.24 |
| C2 | on | 0.24 |
| C3 | on | 0.33 |

### B. Dependent measures

*1) Workspace management:* Evaluation of the workspace management was done by comparing the minimum margin from the workspace edge in surge direction, $d_{ws,x,min}$, which was calculated post-hoc from recorded time traces of the summed MCA and PP outputs as explained in Section III-B. The starting and stopping procedures were not included in this analysis, as the MCA and the PP module were not tuned for those. To allow for a fair comparison, the effect of the workspace limiting block (see Fig. 8) was omitted in this analysis. A larger margin indicates that there is more workspace available to potentially intensify cueing or anticipate unexpected maneuvering, without activating workspace limiting.

*2) Motion cueing quality:* Evaluation of the motion cueing quality was done both objectively and subjectively. The absolute difference (AD) as introduced by Grottoli et al. [17] was used as an objective measure. It represents the normalized error between the specific forces in the vehicle and the simulator. The AD was calculated post-hoc from the recorded time traces of the vehicle and simulator dynamics using (6). Only the specific force in surge direction was considered, as for all other degrees-of-freedom, the motion

condition was equivalent for all conditions. Again, starting and stopping maneuvers were excluded from the analysis.

$$\text{AD} = \frac{\int |f_{s,veh} - f_{s,sim}| dt}{\int |f_{s,veh}| dt} \tag{6}$$

As a subjective measure, the perceived motion incongruence (PMI) was orally rated by the participants. The PMI is defined as the deviation between the expected vehicle motion and the perceived simulator motion [29]. An 11-point scale from 0-10 was used, where 0 indicates perfect motion and 10 indicates that the motion is highly unrealistic. Participants were asked to only rate the longitudinal motion, as this was the only degree-of-freedom that was varied throughout the experiment. The PMI data were collected by means of post-hoc ratings (PR) and section-wise post-hoc ratings (SPR). In PR, participants rated the PMI of an entire drive after it has ended. SPR is a novel measurement method, in which the PMI is orally rated at the end of each section of interest as announced by the experiment leader [10]. For this purpose, sections N1 to N4 as described in Table I were used.

Moreover, the statements shown in Table VII were queried in a post-hoc motion cueing evaluation questionnaire after each drive, to obtain insights into possible causes of differences in PMI ratings. All statements were evaluated using 5-point Likert scales [30]. For statements Q1 to Q4, the agreement was asked (strongly disagree, disagree, undecided, agree, strongly agree). For statements Q5 and Q6, the occurence was asked (never, rarely, sometimes, often, always).

Table VII
MOTION CUEING QUESTIONNAIRE

| | **Statement** | **Scale** |
|---|---|---|
| Q1 | Acceleration felt realistic | agreement |
| Q2 | Braking felt realistic | agreement |
| Q3 | Motion was too weak | agreement |
| Q4 | Motion was too strong | agreement |
| Q5 | No motion was provided when motion was expected | occurence |
| Q6 | Motion was provided when no motion was expected | occurence |

### C. Participants

Due to participant recruitment limitations imposed by the COVID-19 pandemic, the participant group consisted of 34 employees of the BMW Group (32 males, 2 females). They were aged between 18 and 63 years ($\mu = 37.7$ years, $\sigma = 13.4$ years). All were in possession of a driver license. The yearly mileage was on average 18,161 km ($\sigma = 9,585$ km). Participation was on a voluntary basis and informed consent was provided before an experiment commenced. The study was approved by the BMW Group and TU Delft's Human Research Ethics Committee.

### D. Apparatus

The simulator used for the experiment was BMW's Portable Motion Simulator, as shown in Fig. 13. The simulator has an open cabin and is based on the Cruden 406 hexapod, with 400 mm stroke actuators. High-frequency vibrations from the road surface and engine were provided using a separate vibration system. Visuals were shown on three 42" screens. The steering wheel provided haptic feedback. Sounds from the engine, other vehicle's and wind were provided. BMW's SPIDER simulation environment [31] was used to control the distributed real-time simulation. The vehicle model is the same as in the preliminary data (i.e., a 2018 BMW 530i with a 4 cylinder 2.0 L engine and automatic transmission).

Fig. 13. Portable Motion Simulator at the BMW Group.

### E. Procedure

Preceding the measurement phase, several training sessions with all motion conditions were performed, to get participants used to the simulator and the rating method. Thereafter, each participant drove each condition twice, resulting in a total of six measurement drives per participant. A 5-minute break was held after the third measurement drive. Randomized Latin square matrices were used to balance out order effects in condition testing. Participants were asked to drive a predefined trajectory on a rural two-lane road as they would do during everyday driving, without time pressure and while respecting road regulations. Simulated traffic was only present in the opposite lane.

## V. RESULTS

The results are subdivided into two parts. Section V-A discusses the accuracy of the prediction model throughout the experiment. Section V-B presents the effects of adding PP based on this prediction model on motion cueing.

### A. Prediction

The AUC of the maneuver prediction model across all experimental drives was 0.80 for acceleration and 0.73 for deceleration. Both scores were lower than those calculated using the preliminary data set and presented in Table III. When averaging over all drives, the RMS of the longitudinal vehicle

acceleration found for the experimental data ($\mu = 0.77$ m/s$^2$) was 34% higher than that of the preliminary data ($\mu = 0.54$ m/s$^2$). This indicates that participants drove more aggressively in the current experiment when compared to [22].

As a means to analyze the prediction performance over distance, the acceleration and deceleration prediction errors ($\epsilon_{\hat{p}_{acc}}$ and $\epsilon_{\hat{p}_{dec}}$, respectively) are calculated using (7a-b). In these equations, $y_{acc}$ and $y_{dec}$ denote binary variables indicating whether $a_{x,peak}[t \cdots t+5\text{s}]$ exceeded the acceleration/deceleration threshold, as in (7c-d).

Fig. 14 shows the median and IQR of the prediction errors against the track distance. A positive prediction error indicates an overestimation of the probability that maneuvering will occur (i.e., false positives), and likewise, a negative prediction error indicates an underestimation (i.e., false negatives). An $\epsilon_{\hat{p}}$ of zero indicates correct predictions. This was approximately true for a major part of the track distance. Identified causes of poor predictions are anticipation to slope, speeding and anticipation to road curvature. Examples of these phenomena are denoted by ①, ② and ③ in Fig.14, respectively, and will be discussed in more detail.

$$\epsilon_{\hat{p}_{acc}}(t) = \hat{p}_{acc}(t) - y_{acc}(t) \tag{7a}$$

$$\epsilon_{\hat{p}_{dec}}(t) = \hat{p}_{dec}(t) - y_{dec}(t) \tag{7b}$$

$$y_{acc}(t) = \begin{cases} 1 & a_{x,peak}[t \cdots t+5\text{s}] \geq 0.5 \\ 0 & a_{x,peak}[t \cdots t+5\text{s}] < 0.5 \end{cases} \tag{7c}$$

$$y_{dec}(t) = \begin{cases} 1 & a_{x,peak}[t \cdots t+5\text{s}] \leq -0.5 \\ 0 & a_{x,peak}[t \cdots t+5\text{s}] > -0.5 \end{cases} \tag{7d}$$

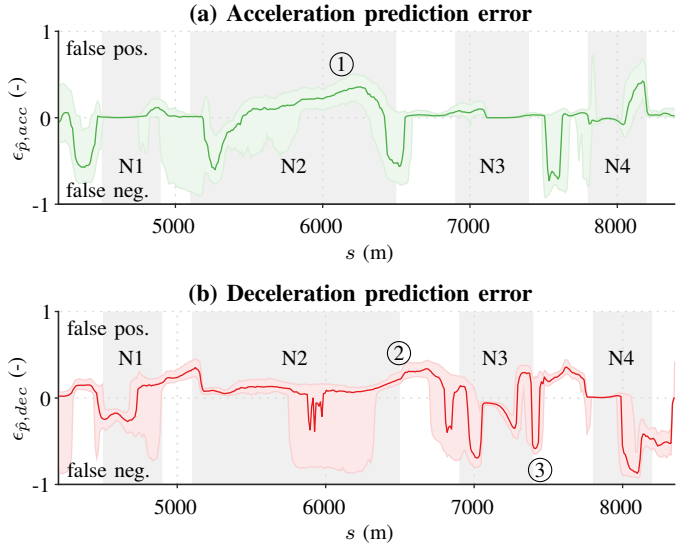


Fig. 14. Medians and IQRs of the acceleration and deceleration prediction errors of all experimental drives against track distance.

*1) Slope:* A preliminary analysis showed that the slope of the road did not play a major role in the velocity choice in the current scenario [23]. However, Fig. 15 shows that in example ① , the accelerator deflection is increased so as to maintain a desired velocity while driving a road with a varying slope, $\alpha$. As the accelerator deflection was increased merely to maintain speed, and thus not to accelerate, $\hat{p}_{acc}$ was overestimated.

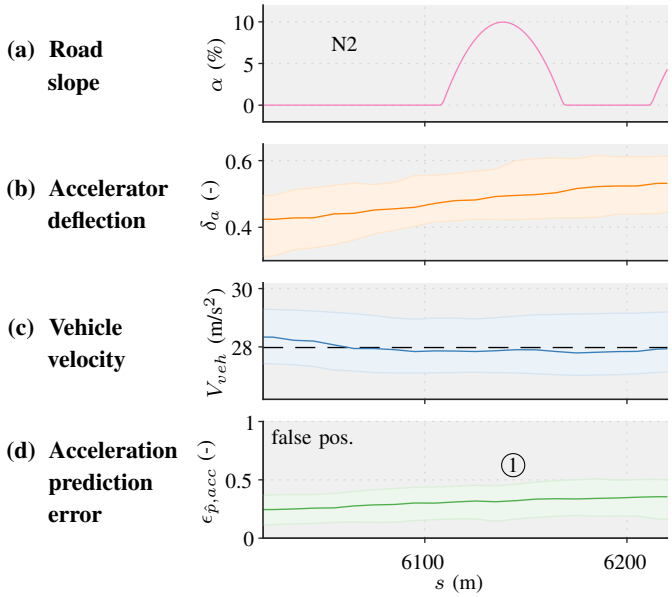


Fig. 15. Medians and IQRs of the road's slope, accelerator pedal deflection, vehicle's velocity (the legal speed limit is denoted by - - -) and acceleration prediction error while driving uphill.

*2) Speeding:* At ②, many participants drove faster than the legal speed limit, which is clearly visible in Fig. 16(a). When the velocity is higher than the legal speed limit, a deceleration maneuver is expected. However, since drivers maintained their velocity (or even increased it, as speeding was apparently intended) $\hat{p}_{dec}$ was overestimated.

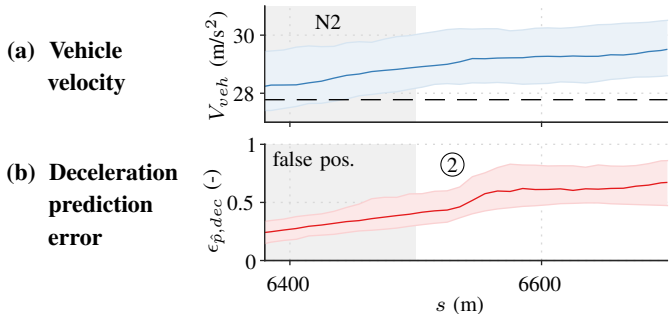


Fig. 16. Medians and IQRs of the vehicle's velocity (the legal speed limit is denoted by - - -) and deceleration prediction error while speeding.

*3) Curvature:* Compared to speed limits, road curvature only played a small role in velocity choice in the current scenario. An exception to this was found at ③, where drivers brake as a response to the curvature shortly after section N3. This is shown in Fig. 17, where $\kappa$ denotes curvature. As road curvature is not accounted for in the proposed prediction model, $\hat{p}_{dec}$ was underestimated.

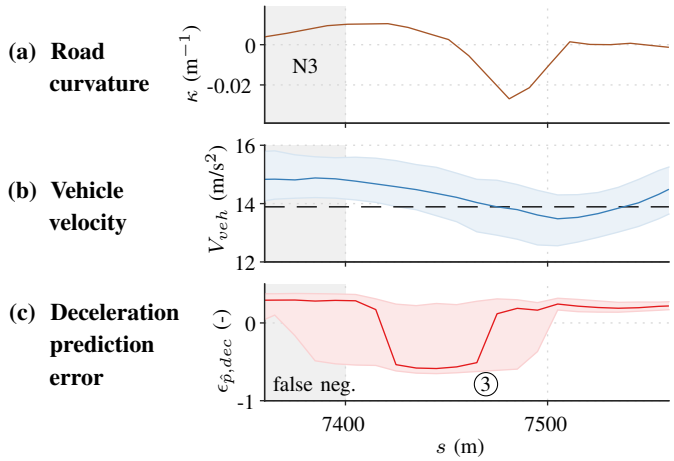


Fig. 17. Medians and IQRs of the road's curvature, vehicle's velocity (the legal speed limit is denoted by - - -) and deceleration prediction error while negotiating a curve.

## B. Prepositioning

This subsection discusses the findings on the proposed PP resulting from the human-in-the-loop experiment. An analysis of the workspace management is presented in Section V-B1. Measurements of objective and subjective motion cueing quality are presented in Sections V-B2 and V-B3, respectively. As each participant drove twice with each motion condition, averaged data points are used in these analyses.

*1) Workspace management:* The position of the simulator against the track distance for all experimental drives per experimental condition is shown in Fig. 18. Cases in which workspace limits of the simulator were reached are denoted by •. The number of involved drives, $n$, is shown per cluster. By comparing conditions C1 and C2, it can clearly be seen that adding PP centered the simulator's trajectory around the neutral point. This generally prevented reaching the workspace limits in sections N1, N3 and N4. Increasing $K_x$ in condition C3 re-introduced occurrences where workspace limits were reached in sections N1 and N3.

The measurement variable used to evaluate workspace margin (i.e., the minimum workspace margin kept per drive for each condition) is shown in Fig. 19. A significant overall effect was found using a repeated measures ANOVA, $F(2, 66) = 37.8, p < 0.05$. Post-hoc testing revealed that when comparing C1 ($\mu = 0.025$ m) to C2 ($\mu = 0.084$ m), a significant increase in workspace margin was found, $t(33) = 7.38,\ p < 0.05$. The increase in margin obtained using PP is used to intensify cueing in C3, resulting in a decreased workspace margin ($\mu = 0.020$ m). The presence of negative workspace margins

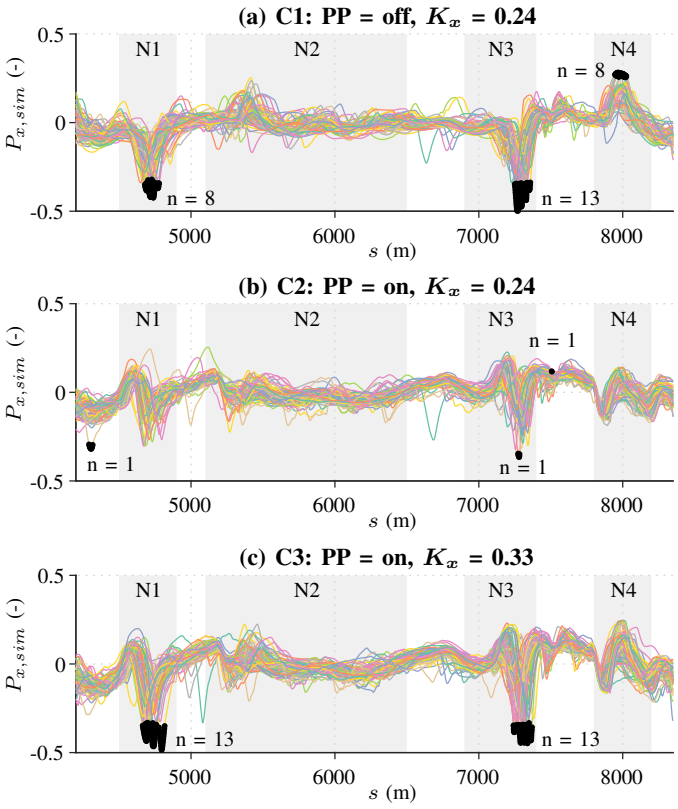


Fig. 18. Demanded simulator position against track distance for all drives, where • denotes that workspace limiting was activated.

indicates that workspace limits were reached in a considerable number of drives. This was the case for 37%, 4% and 34% of the drives under conditions C1, C2 and C3, respectively. Reaching the workspace limits could result in false cues due to braking of the simulator and missing cues due to the inability to accelerate further in the direction of the workspace edge. As further elaborated in Appendix A, this could negatively influence both the objective and subjective motion cueing quality. For this reason, drives where workspace limits were reached were omitted in the following analysis on motion cueing quality.

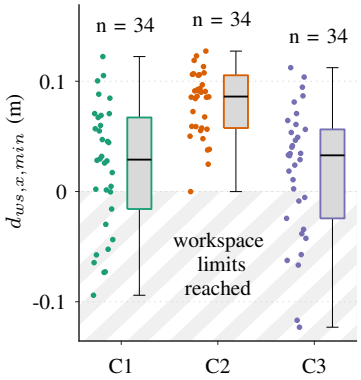


Fig. 19. Minimum workspace margin.

*2) Objective motion cueing quality:* The objective motion cueing quality per experimental condition is shown in Fig. 20. A repeated measures ANOVA was used to test statistical significance. Drivers with missing data due to reaching the workspace limits were completely excluded from this analysis. A significant main effect was found, $F(2, 44) = 10.6,\ p < 0.05$. It can be seen that the absolute difference in conditions C1 and C2 was comparable, which is in line with the hypothesis that PP itself does not have an effect on the motion cueing quality. When comparing condition C1 ($\mu = 0.934$) to C3 ($\mu = 0.927$), a paired samples t-test indicated a significant difference, $t(22) = 4.27,\ p < 0.05$. This confirms the hypothesis that simultaneously adding PP and increasing surge motion yields an improvement in motion cueing quality. Nevertheless, the small magnitude of this difference makes it questionable whether this effect is meaningful.

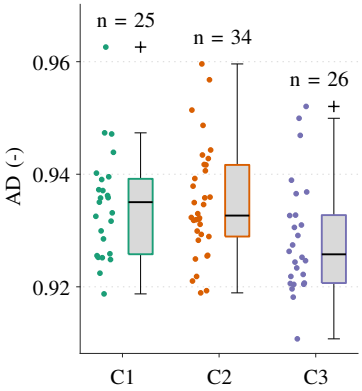


Fig. 20. Objective motion cueing quality, excluding drives in which workspace limits were reached.

*3) Subjective motion cueing quality:* The SPR results are presented in Fig. 21. No substantial differences are found between conditions in any of the sections. The post-hoc motion cueing questionnaire and the PR measurements are omitted, as they included the starting and stopping maneuver, in which workspace limits were reached in most of the drives, and it is not possible to distinguish the effect of workspace limiting and motion cueing. For completeness, those data are shown in Appendix B.

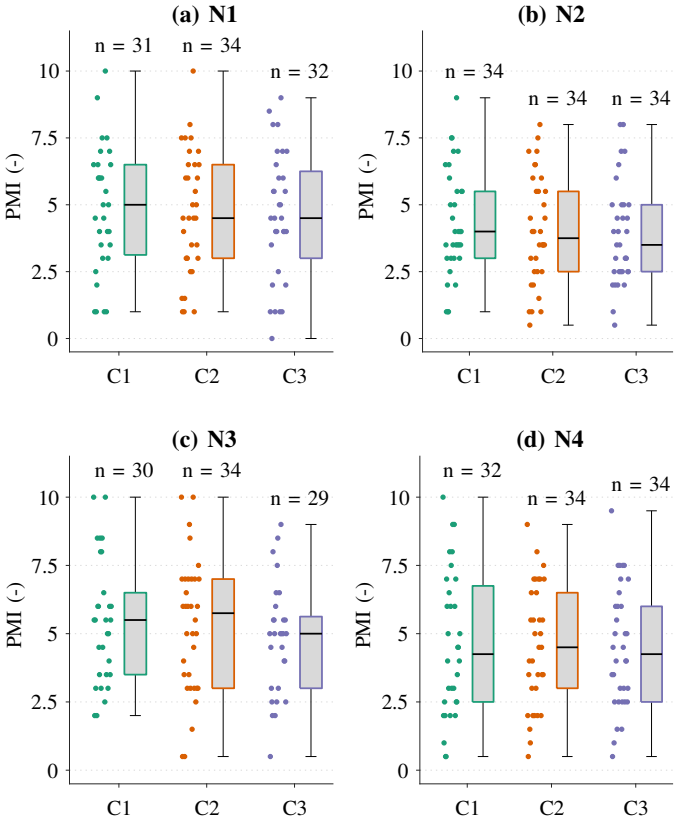


Fig. 21. Subjective ratings of the motion cueing quality per section, excluding drives in which workspace limits were reached.

## VI. Discussion

### A. Prediction

Although acceleration behavior differs per driver, it could be predicted with reasonable accuracy for the current scenario using only the accelerator, vehicle velocity and speed limits. In literature, predicting longitudinal driving behavior was considered hard or impossible, due to the non-deterministic nature of longitudinal driving behavior [12], [13]. In the current research, a stochastic approach was applied in order to account for this. AUCs of 0.80 and 0.73 were obtained for acceleration and deceleration prediction, respectively.

That the acceleration and deceleration prediction AUCs obtained using the experimental drives were respectively 8% and 5% lower than those in the drives initially used for model evaluation in Section II-E, is believed to be caused by a difference in driving style. The RMS of the longitudinal vehicle acceleration was 43% higher for the experimental drives. This could be due to the result of intrusiveness of the current subjective measurement paradigm. That is, even though participants were explicitly asked to drive as they would do in everyday driving, having to rate longitudinal motion cueing might have been an incentive to drive more aggressively.

The working principle of the current model (i.e., a high velocity w.r.t. the speed limit and a larger accelerator deflection yield a higher chance of acceleration and vice versa), is likely to be generally applicable. The risk of overfitting on the current scenario was mitigated by using only three model parameters per maneuver. Nevertheless, one should be careful when extending the findings in this research to other driving tasks and scenarios, where driving behavior might differ. Shortcomings of the prediction model as encountered in the current experiment are the inability to account for slopes and curves. Moreover, maneuvers other than continuous driving (e.g., a stopping maneuver) will be poorly predicted by the current model. As a one-size-fits-all approach is expected to complicate modeling, a more effective approach would be to use a separate prediction logic for such maneuvers.

Improvement of the prediction accuracy of the current model can likely be achieved by correcting the accelerator

pedal position for the slope of the road. If successfully implemented, accelerator deflections aimed to compensate for the slope will not yield erroneous predictions. The correction would have to be calculated using a simplified vehicle model. Moreover, road curvature could be incorporated in the model. In literature, various relationships are found between road curvature and the maximum velocity [32], [33]. It can be opted to use the maximum (future) curve-driving velocity instead of the legal speed limit at instances where it is lower than the legal speed limit.

The success of prediction-based PP in the current scenario can clearly be seen when comparing the simulator traces in Fig. 18(a-b), where it can be seen that reaching the workspace limits was generally prevented when the simulator was pre-positioned based on the proposed prediction model. Fig. 18(c) shows that in the high surge gain condition, the workspace is likely to be reached in sections N1 and N3. This can be explained by erroneous predictions. Looking at Fig. 14, it can be seen that at these locations in section N2 and N3, the probability that a deceleration is about to occur was often underestimated.

In the current paper, the AUC was used as the metric to select the optimal predictor, as it is a frequently used method to calculate test scores for classification models [34]. For the use case of PP, however, the severity of an incorrect prediction can differ per situation. A false positive acceleration prediction is for instance worse when decelerating than when driving stationary, as in the first case the MCA output and the PP yield a simulator excursion in the same direction. A model score tailored to the use-case of PP that emphasizes on critical instances could help to select a more suitable prediction model.

With more driving data, that contain a larger range of driving behavior in more diverse driving scenarios, more advanced prediction models could be trained with the aim of reaching higher prediction accuracy, which would lead to an improvement of the PP. In the field of driver intent detection, time-series techniques such as hidden Markov models [35] and long short-term memory algorithms [36] were used to predict driving behavior. Moreover, it was found that adding driver gaze can improve prediction scores [37]. It could be worthwhile to develop comparable models for the driving simulation environment, so as to obtain a higher prediction accuracy at the cost of increased model complexity.

### *B. Prepositioning*

The human-in-the-loop experiment demonstrated that PP based on the proposed prediction model was able to improve workspace usage of a classical washout MCA for the current driving scenario, as for equivalent motion cueing settings the average margin that was kept from the workspace, was increased from 0.025 m to 0.084 m. With this improved workspace usage, cueing was objectively improved slightly by increasing the surge gain. The mean AD of the condition with PP and intensified motion cueing (C3) was 0.927, whereas that of the condition without PP (C1) was 0.934. That this difference is only small when compared to ranges of AD found in previous research [17], [24] could explain the lack of distinction between the subjective ratings.

Various causes are identified for the lack of significant differences in the subjective ratings when activating PP and increasing the surge gain. First, the simulator has a small workspace due to its maximum actuator stroke of just 400 mm. To provide motion cueing with this limited workspace, low gains (0.24 and 0.33) and a high cut-off frequency (4.30 rad/s) are set for surge motion, resulting in little movement. A 38% higher $K_x$-value resulted in a stronger representation of high-frequency surge motion. However, still only little surge motion can could be represented by translational movement of the platform. In previous works where PP was tested, larger motion systems consisting of both a hexapod and a $x, y$-sled were used [12], [19]. Consequently, this is advised for future research on prepositioning in motion cueing.

Second, increasing the motion cueing gain to intensify cueing amplifies the shortcomings of the classical washout MCA. This is clearly visible in Fig. 22, which shows the forward specific force of the MCA's response to a step input. Here, ④, ⑤ and ⑥ indicate translational simulator movement at the onset, low frequency tilt coordination and the false cue after the response, respectively. Clearly, cueing at the onset at ④ resembles the vehicle's motion more closely when increasing $K_x$ from 0.24 (conditions C1 and C2) to 0.33 (condition C3). However, this comes at the cost of an increased magnitude of the false cue at ⑥. A nonlinear extension that prevents false cues as in [19] can be implemented to prevent this phenomenon in future work.

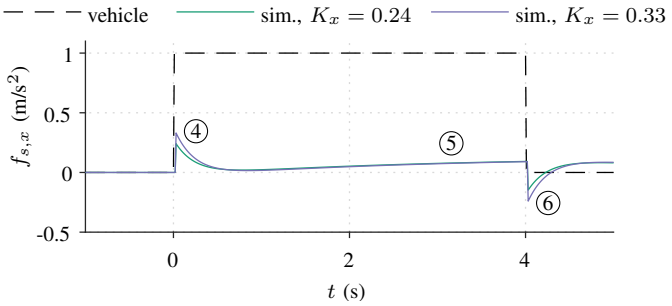


Fig. 22. Step response of the MCA for both experimental gain settings.

In previous research on predictive cueing, more sophisticated methods were applied to make use of improved workspace management due to PP. Hansson & Stenbeck [12] decreased the cut-off frequencies of the complementary HPF and LPF that split surge motion between tilt-coordination and translational movement. This was not opted for in this paper, as in the original tuning set, tilt coordination and translation filters were not complementary (i.e., mid-frequency motion was not presented by the platform). It was chosen not to re-tune tilt coordination, to make a fair comparison possible. In the work of Pitz [19], the classical washout MCA was replaced by an MCA based on non-linear scaling, to optimally utilize the asymmetrical workspace obtained by PP. Testing the PP approach presented in this paper with more sophisticated

MCAs is an essential next step. Ultimately, it is advised to integrate probabilistic prediction models in MPC-based MCAs, so as to improve the state-of-the-art of motion cueing.

Another undesired effect of increasing $K_x$ in the setup used in the experiment is the amplification of vehicle model imperfections. For example, it is known that the vehicle model used throughout this experiment contains gear switches which are found to be obtrusive, considering that it should model automatic transmission of a modern luxury car (i.e., a 2018 BMW 530i). An example of this phenomenon is shown in Fig. 23. The upper plot shows an increasing accelerator input in a section of one of the experimental drives. The lower plot shows the resulting surge acceleration, $a_x$, where the effect of two gear switches are marked ⑦. As these contain high-frequency motion, a higher $K_x$-value will increase the cueing intensity of this undesired motion more than that of desired low frequency accelerations. In conclusion, obtaining an improved vehicle model is essential, before the gain on high-frequency motion cueing can be further increased.

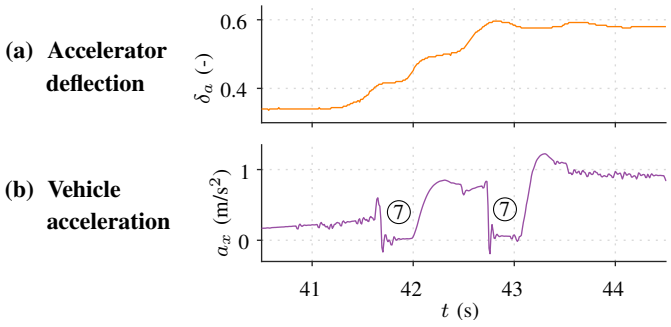


Fig. 23. Accelerator deflection and the resulting longitudinal acceleration, including automatic gear switches.

Moreover, it is advised to test interaction effects with lateral PP, of which various implementations can be found in literature [11], [12], [19], [38]. In case of using a hexapod-based motion system, interaction effects can occur, as the degrees-of-freedom are coupled. In the driving scenario used in this paper, the route was predefined. Work of Ellensohn [10] showed that for predefined routes, the variability of lateral accelerations and yaw rates between drivers is relatively low. Consequently, a deterministic approach can be suitable here. In case drivers are allowed to navigate freely, a probabilistic approach as presented in this paper can be applied.

The section-wise post-hoc measurement method has been shown particularly useful, as the post-hoc measurements were obscured, due to reaching the workspace limits in the start-up and stopping procedures. Nevertheless, it remains questionable whether this method is suitable to identify small differences in motion cueing. It is therefore advised to first examine the results in AD, before designing the experiment. In case of small differences, a continuous rating (CR) technique could be used, as it can yield insights into the motion incongruence during driving simulation with a higher spatial resolution [39]. CR can, however, not be used in active driving tasks, as the measurement method would be intrusive.

## VII. Conclusions

Driver inputs, dynamic vehicle states, and features of the road environment that are available in a real-time driving simulation can be effectively combined to predict probabilities of longitudinal driving maneuvers. The area under the receiver operator characteristic curve was 0.84 for acceleration prediction and 0.77 for deceleration prediction, using a model based on the accelerator pedal position, the vehicle's velocity, and the future speed limit. In a human-in-the-loop experiment with a short scenario of a two-lane road through a rural area, the prediction scores were slightly lower (i.e., 0.80 and 0.73), but still accurate enough to improve the workspace management of a classical washout algorithm for a small hexapod-based simulator.

As a result, the average distance that was kept from the workspace edge was increased from 0.025 m to 0.084 m, while providing equivalent motion cueing. Increasing the surge gain of the motion cueing algorithm to utilize the improved workspace management, yielded a small decrease in the normalized absolute error between the specific force of the vehicle and platform, from 0.934 to 0.927. Subjective ratings did not provide evidence for improved nor deteriorated motion cueing quality using the current setup. Nevertheless, the observed improvement in workspace management demonstrated the potential of combining information from dynamic vehicle states, driver inputs and the road environment within the real-time simulation environment.

## References


[1] P. Hock, J. Kraus, F. Babel, M. Walch, E. Rukzio, and M. Baumann, "How to design valid simulator studies for investigating user experience in automated driving - Review and hands-on considerations," *Proceedings - 10th International ACM Conference on Automotive User Interfaces and Interactive Vehicular Applications, AutomotiveUI 2018*, no. September, pp. 105–117, 2018.

[2] C. J. Van Driel, M. Hoedemaeker, and B. van Arem, "Impacts of a Congestion Assistant on driving behaviour and acceptance using a driving simulator," *Transportation Research Part F: Traffic Psychology and Behaviour*, vol. 10, no. 2, pp. 139–152, 2007.

[3] S. Brandenburg and E. M. Skottke, "Switching from manual to automated driving and reverse: Are drivers behaving more risky after highly automated driving?" *2014 17th IEEE International Conference on Intelligent Transportation Systems, ITSC 2014*, pp. 2978–2983, 2014.

[4] F. Seeliger, G. Weidl, D. Petrich, F. Naujoks, G. Breuel, A. Neukum, and K. Dietmayer, "Advisory warnings based on cooperative perception," *IEEE Intelligent Vehicles Symposium, Proceedings*, no. Iv, pp. 246–252, 2014.

[5] I. Siegler, G. Reymond, A. Kemeny, and A. Berthoz, "Sensorimotor integration in a driving simulator: contributions of motion cueing in elementary driving tasks," *Proceedings of the Driving Simulation Conference*, no. September, pp. 21–32, 2001. [Online]. Available: http://experts.renault.com/dsc2001/sensorimotor-integration.pdf

[6] B. J. Correia Grácio, *The effects of specific force on self-motion perception in a simulation environment*, 2013.

[7] B. Aykent, F. Merienne, C. Guillet, D. Paillot, and A. Kemeny, "Motion sickness evaluation and comparison for a static driving simulator and a dynamic driving simulator," *Proceedings of the Institution of Mechanical Engineers, Part D: Journal of Automobile Engineering*, vol. 228, no. 7, pp. 818–829, 2014.

[8] B. Augusto and R. Loureiro, "Motion cueing in the Chalmers driving simulator: A model predictive control approach," Ph.D. dissertation, Chalmers University of Technology, 2009. [Online]. Available: http://publications.lib.chalmers.se/records/fulltext/98871.pdf

[9] N. J. I. Garrett and M. C. Best, "Driving simulator motion cueing algorithms–a survey of the state of the art," *Proceedings of the 10th International Symposium on Advanced Vehicle Control (AVEC)*, pp. 183–188, 2010.

[10] F. Ellensohn, "Urban Motion Cueing Algorithms – Trajectory Optimization for Driving Simulators," Ph.D. dissertation, TU München, 2019.

[11] C. Weiß, "Control of a Dynamic Driving Simulator : Time-Variant Motion Cueing Algorithms and Prepositioning," Ph.D. dissertation, Deutsches Zentrum für Luft- und Raumfahrt, 2006.

[12] P. Hansson and A. Stenbeck, "Prepositioning of driving simulator motion systems," MSc. dissertation, Chalmers University of Technology, 2014.

[13] J. Pitz, T. Rothermel, M. Kehrer, and H. Reuss, "Predictive motion cueing algorithm for development of interactive assistance systems," in *Internationales Stuttgarter Symposium*, 2016, pp. 213–226.

[14] P. R. Grant and B. Haycock, "Effect of jerk and acceleration on the perception of motion strength," *Journal of Aircraft*, vol. 45, no. 4, pp. 1190–1197, 2008.

[15] M. Fischer, "Motion-Cueing-Algorithmen für eine realitätsnahe Bewegungssimulation (Dissertation)," *Berichte aus dem DLR-Institut für Verkehrssystemtechnik*, 2009.

[16] M. Dagdelen, G. Reymond, A. Kemeny, M. Bordier, and N. Maïzi, "Model-based predictive motion cueing strategy for vehicle driving simulators," *Control Engineering Practice*, vol. 17, no. 9, pp. 995–1003, 2009.

[17] M. Grottoli, D. Cleij, P. Pretto, Y. Lemmens, R. Happee, and H. H. Bülthoff, "Objective evaluation of prediction strategies for optimization-based motion cueing," *Simulation*, vol. 95, no. 8, pp. 707–724, 2018.

[18] A. Mohammadi, H. Asadi, S. Mohamed, K. Nelson, and S. Nahavandi, "Future reference prediction in model predictive control based driving simulators," *Australasian Conference on Robotics and Automation, ACRA*, vol. 2016-Decem, no. March 2017, pp. 177–184, 2016.

[19] J.-O. Pitz, *Vorausschauender Motion-Cueing-Algorithmus für den Stuttgarter Fahrsimulator*. Springer Vieweg, 2017.

[20] M. Bruschetta, C. Cenedese, A. Beghi, and F. Maran, "A motion cueing algorithm with look-Ahead and driver characterization: Application to vertical car dynamics," *IEEE Transactions on Human-Machine Systems*, vol. 48, no. 1, pp. 6–16, 2018.

[21] F. Ellensohn, M. Spannagl, S. Agabekov, J. Venrooij, M. Schwienbacher, and D. Rixen, "A hybrid motion cueing algorithm," *Control Engineering Practice*, vol. 97, no. January, p. 104342, 2020. [Online]. Available: https://doi.org/10.1016/j.conengprac.2020.104342

[22] A. Parduzi, J. Venrooij, and S. Marker, "The Effect of Head-Mounted Displays on the Behavioural Validity of Driving Simulators," in *DSC 2020 Europe*, Antibes, 2020, pp. 125–132.

[23] J. Eppink, "Maneuver Prediction for Motion Cueing," Unpublished, Preliminary MSc. dissertation, Delft University of Technology, 2020.

[24] M. Kolff, J. Venrooij, D. M. Pool, and M. Mulder, "Comparison of Quality Metrics between Motion Cueing Algorithms in a Virtual Test Environment," pp. 9–11, 2020.

[25] A. Dobson and A. Barnett, *An Introduction to Generalized Linear Models*, third edit ed. Chapman & Hall/CRC, 2008.

[26] C. Metz, "Basic Principles of ROC Analysis," *Seminars in Nuclear Medicine*, vol. VIII, no. 4, pp. 283–298, 1978.

[27] N. Chinchor, "MUC-4 Evaluation Metrics," in *Proceedings of the Fourth Message Understanding Conference*, 1992, pp. 22–29.

[28] S. Kurutas, "Modellierung der Dynamik eines Hexapods," Ph.D. dissertation, Universität Duisburg-Essen, 2006.

[29] Advisory Group for Aerospace Research and Development, "Fidelity of simulation for pilot training," 1980.

[30] R. Likert, "A technique for the measurement of attitudes," *Archives of Psychology*, vol. 22 140, no. 55, 1932.

[31] M. Strobl, "SPIDER - Das innovative Software-Framework der BMW Fahrsimulation," *VDI-Berichte*, no. 1745, pp. 303–320, 2003.

[32] G. Reymond, A. Kemeny, J. Droulez, and A. Berthoz, "Role of lateral acceleration in curve driving: Driver model and experiments on a real vehicle and a driving simulator," *Human Factors*, vol. 43, no. 3, pp. 483–495, 2001.

[33] P. Bosetti, M. Da Lio, and A. Saroldi, "On Curve Negotiation: From Driver Support to Automation," *IEEE Transactions on Intelligent Transportation Systems*, vol. 16, no. 4, pp. 2082–2093, 2015.

[34] Z. Elamrani Abou Elassad, H. Mousannif, H. Al Moatassime, and A. Karkouch, "The application of machine learning techniques for driving behavior analysis: A conceptual framework and a systematic literature review," *Engineering Applications of Artificial Intelligence*, vol. 87, no. March 2019, p. 103312, 2020. [Online]. Available: https://doi.org/10.1016/j.engappai.2019.103312

[35] X. Zhao, S. Wang, J. Ma, Q. Yu, Q. Gao, and M. Yu, "Identification of driver's braking intention based on a hybrid model of GHMM and GGAP-RBFNN," *Neural Computing and Applications*, vol. 31, no. s1, pp. 161–174, 2019. [Online]. Available: https://doi.org/10.1007/s00521-018-3672-1

[36] Y. Liu, P. Zhao, D. Qin, G. Li, Z. Chen, and Y. Zhang, "Driving Intention Identification Based on Long Short-Term Memory and A Case Study in Shifting Strategy Optimization," *IEEE Access*, vol. 7, pp. 128 593–128 605, 2019.

[37] M. Wu, T. Louw, M. Lahijanian, W. Ruan, X. Huang, N. Merat, and M. Kwiatkowska, "Gaze-based Intention Anticipation over Driving Manoeuvres in Semi-Autonomous Vehicles," *IEEE International Conference on Intelligent Robots and Systems*, pp. 6210–6216, 2019.

[38] T. Chapron, J.-p. Colinot, and P. S. a. Peugeot-citroën, "The new PSA Peugeot-Citroën Advanced Driving Simulator Overall design and motion cue algorithm," *DSC 2007 North America*, 2007.

[39] D. Cleij, J. Venrooij, P. Pretto, D. M. Pool, M. Mulder, and H. H. Bülthoff, "Continuous subjective rating of perceived motion incongruence during driving simulation," *IEEE Transactions on Human-Machine Systems*, vol. 48, no. 1, pp. 17–29, 2018.

# II

# Preliminary thesis

# 1

# Prepositioning a driving simulator

Some driving maneuvers cause motion renderings which are almost unidirectional with respect to a linear degree of freedom. In this case, the simulator will leave its neutral position to move in this direction during a maneuver and return to the neutral position at the end of the maneuver. When it is possible to predict future motion renderings, it can be helpful to offset the simulator's neutral position with a displacement opposing the predicted simulator excursion. This displacement is called prepositioning (PP) [13]. As there is now more space available in the direction of the expected maneuver, one can make use of the larger motion capabilities by modifying the MCA tuning parameters. However, this is not without risk. If a less conservative MCA tuning is chosen, movements in unanticipated directions can drive the simulator into its limitations.

This chapter will start with a description of the kinematics and workspace definitions for hexapod motion systems in Section 1.1, in order to clarify its limitations. The rest of this chapter will describe motion cueing implementations. When designing a PP algorithm, one can distinguish between the logic that determines the PP reference position and the controller used to reach this desired position while preventing false cues. These are discussed in Sections 1.2 and 1.3, respectively. Section 1.4 covers model predictive control (MPC)-based MCAs, which do not explicitly include PP, but can nevertheless yield PP as result of optimization schemes based on predictions. The chapter will be concluded with a discussion of the state-of-the-art in Section 1.5.

## 1.1. Workspace of a hexapod motion platform

The hexapod motion platform is a parallel robotic manipulator first described by Gough and Whitehall [14] as a means to test tires for automobiles in 1956. Nine years later, Stewart [15] developed a comparable concept for a flight simulator motion base, which is shown in Figure 1.1. Ever since, the hexapod platform is extensively used in flight- and driving simulation. It is characterized by high force-torque capacity and high structural rigidity [16].

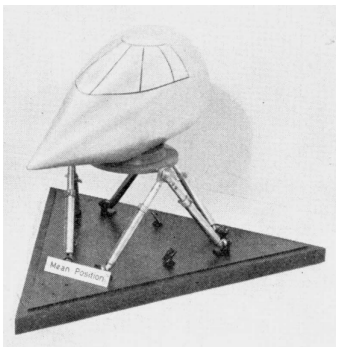


Figure 1.1: Stewart's flight simulator design. [15]

### 1.1.1. Topology

Figure 1.2 shows the topological structure of a hexapod-based simulator [17]. The system consists of a fixed basis and a moving platform, interconnected by 6 linear actuators ($L_1$-$L_6$). The position and orientation of the platform are determined by the length of the actuators, which provide a total of 6 degrees of freedom (DOF).

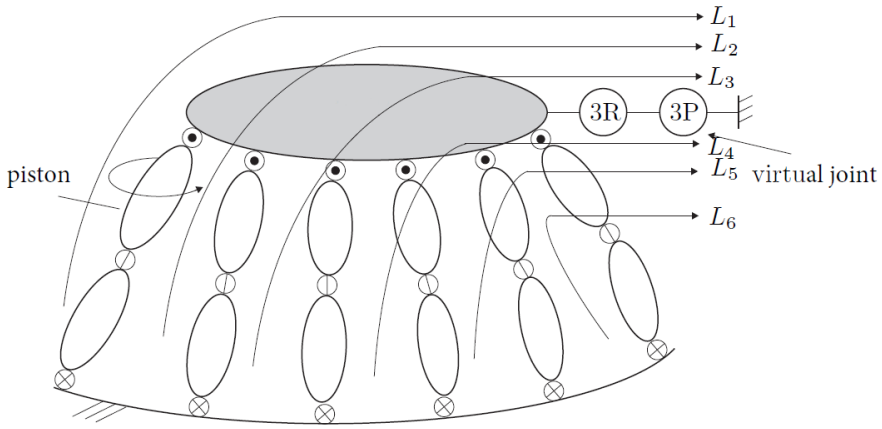


Figure 1.2: Topological structure of a hexapod motion system. The symbol ⊗ denotes a universal joint, ⊘ denotes a sliding joint and ⊙ denotes a ball joint. The virtual joint has three rotational (R) and three translational (P) degrees of freedom. [17]

### 1.1.2. Inverse kinematics

Inverse kinematics is the inference of the length of each actuator with the knowledge of the position and orientation of the platform. It can be useful to analyze a motion system's limitations. A schematical representation of a hexapod motion system is given in Figure 1.3. Two reference frames are used for calculation of inverse kinematics. The inertial reference frame, $O$, is fixed to the center of the basis. The body reference frame, $C$, is fixed to the center of the platform. Both reference systems are right-handed, as in Figure 1.4.

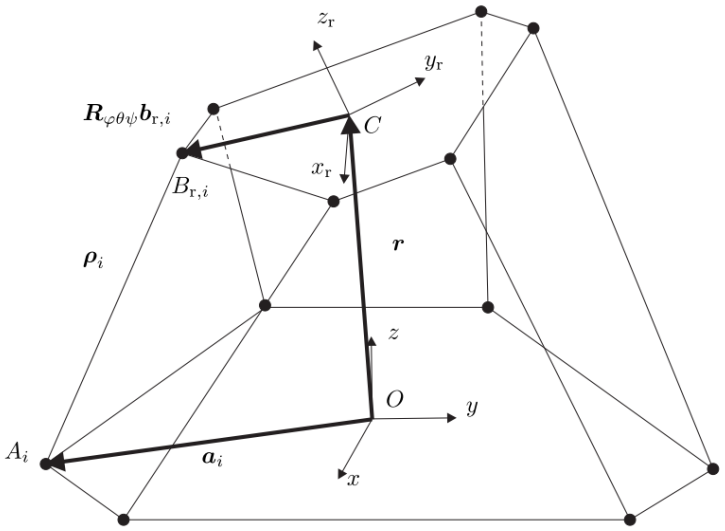


Figure 1.3: Schematical representation of a hexapod motion system. [17]

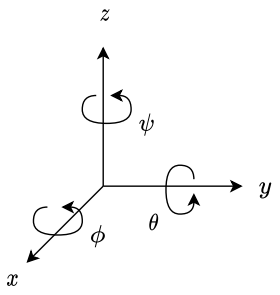


Figure 1.4: Right-handed reference system.

For each actuator $i$, the distance between the lower hinge point ($A_i$) and the center of the basis is constant and denoted by vector $\boldsymbol{a}_i$. The distance between the (rotated) upper hinge point ($B_{r,i}$) and the center of the platform is constant too and denoted $\boldsymbol{b}_{r,i}$, in the body reference frame. In order to express vector $\boldsymbol{b}_i$ in the inertial reference frame, rotation matrix $\boldsymbol{R}_{\phi\theta\psi}$ is used as given in Equations 1.1 and 1.2.

Note that the first rotation is around the z-axis (yaw), followed by the y-axis (pitch) and x-axis (roll).

$$\boldsymbol{R}_{\phi\theta\psi} = \boldsymbol{R}_{\phi}\boldsymbol{R}_{\theta}\boldsymbol{R}_{\psi} \tag{1.1}$$

$$\boldsymbol{R}_{\phi} = \begin{bmatrix} cos(\phi) & -sin(\phi) & 0 \\ sin(\phi) & cos(\phi) & 0 \\ 0 & 0 & 1 \end{bmatrix}, \boldsymbol{R}_{\theta} = \begin{bmatrix} cos(\theta) & 0 & sin(\theta) \\ 0 & 1 & 0 \\ -sin(\theta) & 0 & cos(\theta) \end{bmatrix}, \boldsymbol{R}_{\psi} = \begin{bmatrix} 1 & 0 & 0 \\ 0 & cos(\psi) & -sin(\psi) \\ 0 & sin(\psi) & cos(\psi) \end{bmatrix} \tag{1.2}$$

The length of actuator $i$, $\rho_i$, is defined by the distance between hinge points $A_i$ and $B_{r,i}$ and can be calculated using Equation 1.3, where $\boldsymbol{r}$ denotes the position of the platform's center in inertial frame $O$.

$$\boldsymbol{\rho}_i = \boldsymbol{r} - \boldsymbol{a}_i + \boldsymbol{R}_{\phi\theta\psi}\boldsymbol{b}_{r,i} \tag{1.3}$$

### 1.1.3. Workspace definitions and visualization

The workspace can be defined as the reachable set of positions and orientations by the platform's center [17]. For hexapod-based simulators, this is limited by the actuator length range $[\rho_{min}\ \rho_{max}]$. Since coupling exist between all 6 DOFs, the workspace of a hexapod simulator is 6-dimensional. A possible approach for representing the workspace of a hexapod is to fix the position/orientation in one or more dimensions [18]. The workspace can then be plotted for the remaining DOFs. When fixing all three rotational DOFs, one obtains the constant orientation workspace (COW), as shown in Figure 1.5. In case of fixing all translational DOFs, the orientation workspace (OW) is obtained, as shown in Figure 1.6. Other definitions of workspace are given in Table 1.1. [17]

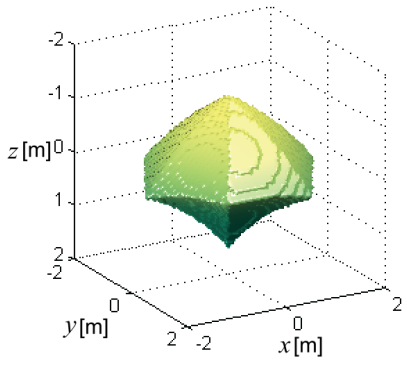


Figure 1.5: COW of DLR's SimCar driving simulator. [17]

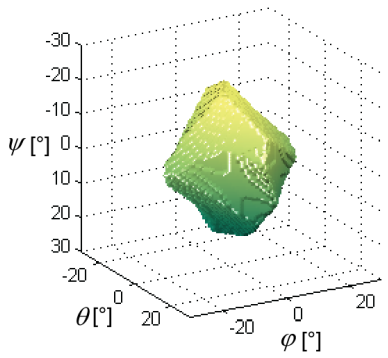


Figure 1.6: OW of DLR's SimCar driving simulator. [17]

Table 1.1: Workspace definitions. [17, 19]

| Nomenclature | Definition |
|---|---|
| Maximal workspace (MW) | All positions reachable in at least one orientation. |
| Constant orientation workspace (COW) | All positions reachable in a defined orientation. |
| Total orientation workspace (TOW) | All positions reachable for a defined range of orientations. |
| Orientation workspace (OW) | All orientations reachable at a defined position. |

## 1.2. Prepositioning logic

Various studies on motion cueing contain an implementation of longitudinal PP [9, 11–13]. One can distinguish between two types of PP logics. In the first variant, one identifies a driving situation and deduces that a certain maneuver is expected. This will be referred to as situation-based PP and is described in Section 1.2.1. The second variant uses only the vehicle's current velocity, is referred to as velocity-based PP and is discussed in Section 1.2.2. Note that PP can also be applied laterally [9, 11**?** , 12], but this is considered to be outside the scope of the current study.

### 1.2.1. Situation-based

The first documented effort on PP in driving simulation was by Weiß [13]. It is proposed to start at a PP position (i.e., at an offset from the original neutral position) when a driving situation is detected in which an approximately unidirectional linear movement is expected. At the end of the driving situation, the simulator will return to the former neutral position. The solution presented by Weiß allowed the longitudinal PP to be either off, to the front or to the rear. Weiß does not describe an implementation and evaluation of PP logic. Nevertheless, the suggestions as shown in Table 1.2 are provided. Lastly, Weiß claimed that a vast amount of information is needed in order to provide reasonable PP.

Table 1.2: Suggestions for maneuver prediction based on situations by Weiß [13].

| Maneuver | Situation |
|---|---|
| Braking | Presence of other vehicles in the vicinity<br>Transition from straight road to curve<br>Traveling at a speed near to or above the speed limit |
| Acceleration | Driving at a low speed<br>Transition from a curve to straight road |

Work by Pitz [9] on predictive cueing uses legal speed limits and presence of road crossings, pedestrian crossings and traffic lights as triggers for PP. A situational analysis functionality with a finite prediction horizon is established to process information from the environment. Road and environment attributes have a discrete form and are positioned w.r.t. the track distance variable $s$. Figure 1.7 shows some environment attributes on a road. Pitz did not elaborate on how the desired PP position was obtained from these attributes, however.

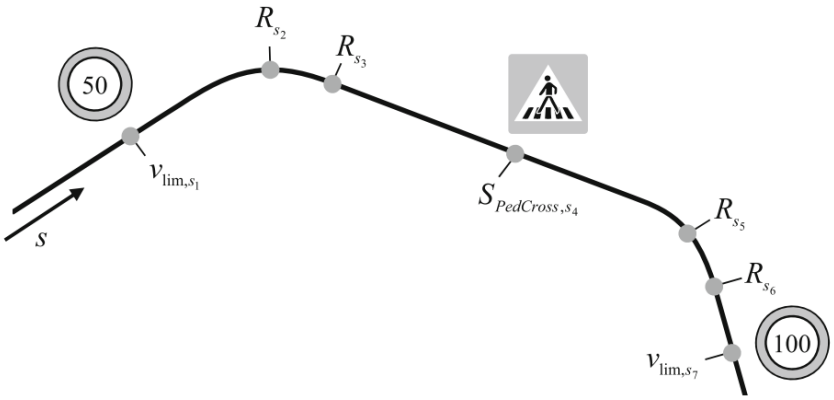


Figure 1.7: Attributes of the road and environment. [20]

Pitz noted that high-pass filters used in classical washout filter MCA's have symmetric behavior, and thus do not optimally exploit the workspace, which has become asymmetric due to PP. In order to solve this, nonlinear scaling is applied to the acceleration of the MCA. Figure 1.8 shows what scaling factor is used, depending on the simulator position and velocity, which are denoted by $P_{sim}$ and $V_{sim}$, respectively. In contrast to a classical washout filter, non-linear scaling does not return the simulator to its center position. A PD-controller is added, to provide a neutral push. When looking at the RMS values of accelerations, no significant differences were found between the Predictive MCA as proposed by Pitz and a classical washout filter MCA without PP. This is explained by longitudinal behavior being dominated by the driving style of the test person and not just the road layout [9].

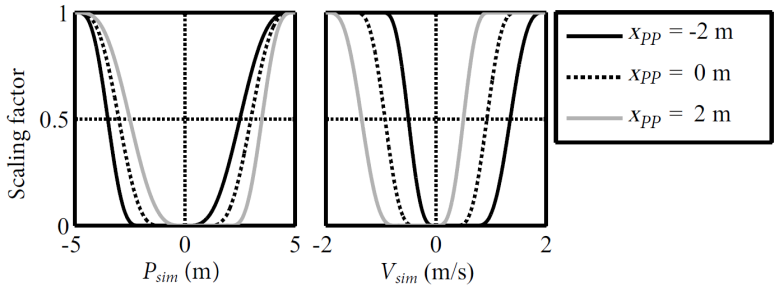


Figure 1.8: Nonlinear scaling used by Pitz [20] to obtain asymmetric workspace usage.

### 1.2.2. Velocity-based

Chapron & Colinot [11] implemented longitudinal prepositioning based on the modeled vehicle acceleration/deceleration characteristics. These are time-varying and depend on the vehicle's velocity as well as the gear ratio. Hansson & Stenbeck [12] implemented longitudinal PP using the same principle and documented the specifications of their implementation. Considering it impossible to predict when acceleration or braking was to occur due to the non-deterministic human nature, both possibilities are taken into account at any time. The mean of the range of possible vehicle accelerations, $\bar{a}$, as a function of the vehicle's velocity, $(V)$, is calculated from the maximum possible acceleration, $a_{acc,max}$, and the maximum possible deceleration, $a_{brake,max}$ as in Equation 1.4. Equation 1.5 is used to convert this value to an ideal platform neutral point. In the latter equation, $x_{PP,max}$ denotes the maximum PP position.

$$\bar{a}(V) = \frac{a_{acc,max}(V) + a_{brake,max}}{2} \tag{1.4}$$

$$x_{PP}(V) = -x_{PP,max}\frac{\bar{a}(V)}{\max\left(\bar{a}(V_{max}), |\bar{a}(V_{min})|\right)} \tag{1.5}$$

The relationship between $a_{acc,max}$ and $V$ for each gear of the Saab 93 model used by Hansson & Stenbeck is given in Figure 1.9. A piecewise function as shown in Figure 1.10 and described in Equation 1.6 was fitted. $a_{brake,max}$ is independent of the vehicle's velocity and equal to -5 m/s$^2$. Figure 1.11 shows the mean of the vehicle's maximum possible acceleration and deceleration against the vehicle's velocity.

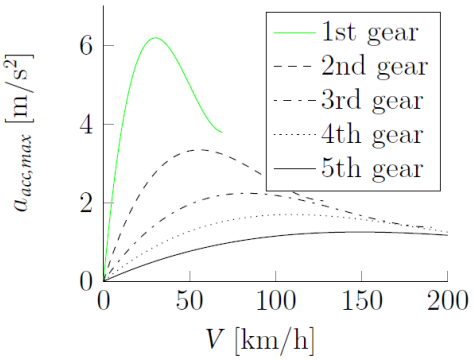


Figure 1.9: Maximum acceleration w.r.t. velocity per gear. [12]

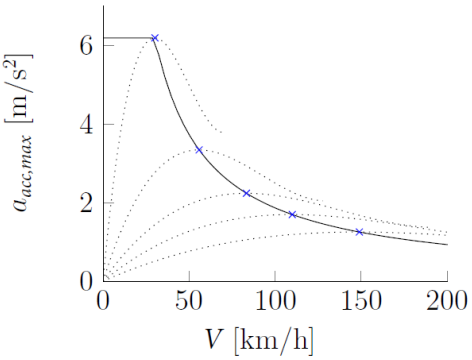


Figure 1.10: Curve fitted max. acceleration w.r.t. velocity. [12]

$$a_{acc,max} = \begin{cases} 6 & V \leq 8.64 \text{ (m/s)} \\ 51.84 \cdot V^{-1} & V > 8.64 \text{ (m/s)} \end{cases} \tag{1.6}$$

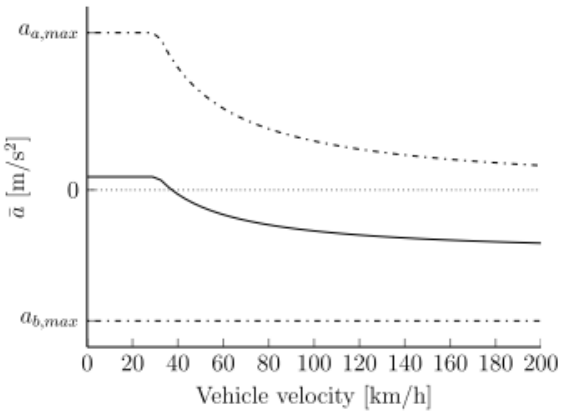


Figure 1.11: Mean of the maximum possible acceleration and deceleration against velocity velocity. [12]

Hansson & Stenbeck made use of the virtually enlarged workspace resulting from PP by decreasing $\omega_{split_x}$, the cut-off frequency used to split longitudinal vehicle acceleration into translational motion represented by a motion sled and tilt coordination of a hexapod platform. This yields the two conditions as shown in Table 1.3, which are evaluated both analytically and by means of a human-in-the-loop experiment. Computer simulations show that in Condition 2, an increase of 25% RMS translational acceleration by the motion sled was obtained, while reducing the maximum longitudinal tilt rate throughout the ride by 29.9%. The study is concluded with a subjective evaluation, where participants are asked to drive a rural road, for both motion conditions. Significant differences in favour of the PP condition were found for the questions *"Did the acceleration feel realistic?"* and *"Did the braking feel realistic?"*.

Table 1.3: Experimental conditions tested by Hansson & Stenbeck [12].

| Condition | Prepositioning | $\omega_{split_x}$ |
|---|---|---|
| 1 | off | 0.65 |
| 2 | on | 0.55 |

## 1.3. Prepositioning controllers

The goal of a PP controller is to reach a desired reference position, while minimizing perceived stimuli by the driver. Knowledge of human perception (thresholds) is thus key and will be discussed in Section 1.3.1. Hereafter, two types of controllers used in literature will be discussed in Sections 1.3.2 and 1.3.3.

### 1.3.1. Perception thresholds

Human self-motion perception is imperfect. Motion of low amplitude can in some cases not be perceived by humans. Benson et al. [21] studied perception thresholds for linear horizontal acceleration, while eliminating all auditory and visual cues. Thresholds for longitudinal acceleration were found to differ between participants. A mean threshold for longitudinal acceleration of 0.063 m/s$^2$ was found when using a cosine-shaped velocity trajectory with a duration of 3 seconds. Moreover, it was found that higher thresholds are found when the acceleration is achieved at a lower rate. It was thus concluded that the sensory system that senses linear movement is sensitive to both acceleration and jerk (i.e., the rate of change of acceleration).

In later work of Grant and Haycock [22], the paired-comparison methodology was used to compare profiles of longitudinal translation with various acceleration profiles consisting of jerk-limited acceleration square waves. A plot of the test scores for all profiles can be found in Figure 1.12, where a higher score denotes a higher relative motion strength. It was confirmed that the perceived motion strength depends on acceleration and jerk. Moreover, it was found that an increase of the duration of acceleration significantly affects the perceived motion strength. Although as of yet, no explicit thresholds are known, it can be concluded that both acceleration and jerk will thus have to be limited in order to minimize perception of PP.

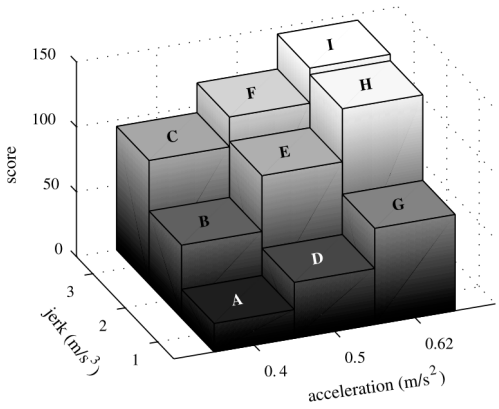


Figure 1.12: Paired-comparison scores for the perceived motion strength of jerk-limited square wave accelerations [22].

### 1.3.2. Low-pass filter

As discussed in Section 1.2.1, Weiß [13] proposed longitudinal PP that is either inactive, to one specified position in the front or to one specified position in the rear. Adding this signal to the longitudinal position resulting from the MCA would yield an undesirable uncontrolled transition. In order to prevent this, the PP position signal is low-pass filtered. Weiß noted that the most important characteristics of a PP controller are the time to reach a desired position and the shape of the step-response of the controller. The first has to comply with the look-ahead of the PP logic, while the second has to result in minimal perception by the human test participant. In order to attain smoothness, filters with a minimum order $n = 2$ were tested. Step-responses of filters ranging from $n = 2$ till $n = 5$ that reach 95% of the intended excursion within 3 seconds have been examined. Weiß recommended the second order filter, since higher order filters need more time to reach the intended position. Moreover, it was noted that when filters are tuned so that overshoot is prevented, noticeable accelerations are obtained. In order to reduce these, second order filters with a slight overshoot (damping ratio < 1) as shown in Table 1.4 are suggested. Here, $f_{s_{max}}$ denotes the maximum specific force throughout the excursion in case of a PP excursion of 0.7 m within 3 seconds. A maximum overshoot of 3% is chosen, because it is found to yield a good result with the PP excursion magnitude and workspace of the simulator used. It can be seen that a reduction of $f_{s_{max}}$ is obtained when the overshoot is increased.

Table 1.4: Prepositioning controllers proposed by Weiß [13].

| Overshoot (%) | Transfer function | $f_{s_{max}}$ |
|---|---|---|
| 1 | $\frac{1}{0.7056s^2+1.3944s+1}$ | 0.4271 |
| 3 | $\frac{1}{0.9025s^2+1.4250s+1}$ | 0.3719 |
| 5 | $\frac{1}{1.0816s^2+1.9968s+1}$ | 0.2807 |

### 1.3.3. Acceleration and jerk limiter

As opposed to the discrete PP logic proposed by Weiß, the logic implemented by Hansson & Stenbeck [12] yields a reference position that is continuous and can have any value within predefined range $[P_{x_{PP,min}}\ P_{x_{PP,max}}]$. Nevertheless, high amplitudes of acceleration and jerk have to be prevented while reaching the desired position. In order to do so, a controller from Fischer [23] is used, which can be found in Figure 1.13. Saturation blocks are used to limit acceleration and jerk to 0.05 m/s$^2$ and 0.1 m/s$^3$, respectively. The first is chosen to be below the 0.063 m/s$^2$ threshold as found by Benson et al. [21]. The latter was tuned empirically by the authors, so that no movement was noticed at the onset of the proposed PP. A PD controller is used in combination with a feedforward loop to prevent sustained oscillations.

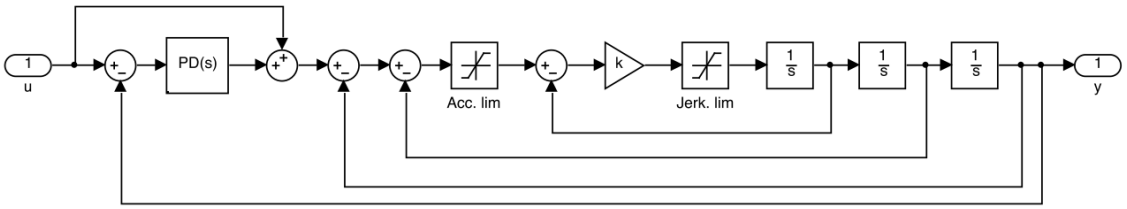


Figure 1.13: Acceleration and jerk limiter as proposed by Hansson & Stenbeck [12].

The effect of the controller on a position-level can be seen in Figure 1.14. One can note that the controller yields a delay in case of large fluctuations of the desired PP position. This delay is not necessarily a problem, since the motion is not perceivable. Chapron & Colinot [11] and Pitz [9] also report the use of nonlinear filters that limit acceleration and jerk.

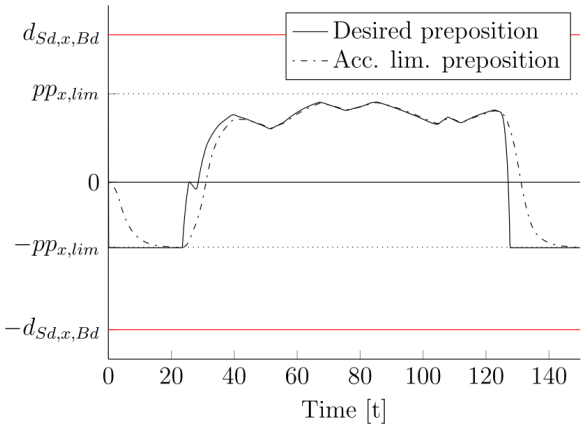


Figure 1.14: Desired and limited PP signal using the controller proposed by Hansson & Stenbeck [12].

## 1.4. Prepositioning in MPC-based MCAs

PP consisting of a PP logic and PP controller as described in Sections 1.2 and 1.3 are designed for use in combination with conventional MCAs that are based on filters. A novel MCA type first described by Dagdelen et al. [24] is based on model predictive control (MPC). A brief explanation on the working principles, advantages and disadvantages of MPC-based MCAs is given in Section 1.4.1. MPC-based MCAs optimize simulator motion using expectations of future vehicle motion, which can result in the use of PP. Sections 1.4.2 until 1.4.4 discuss efforts to describe the effectiveness of various predictors used in MPC-based MCAs.

### 1.4.1. MPC-based MCA

In MPC-based MCAs, the system behavior is predicted for a finite prediction horizon $H_p$ at each time step, $k$. An optimal sequence of control input commands (i.e., dynamic simulator states) is calculated for a limited control horizon $H_u$ by means of minimizing a cost function which penalizes e.g. the difference between vehicle and simulator motion, deviations from the neutral state and deviations between two successive inputs. Constraints such as those on the simulator workspace are taken into account explicitly for a limited constraint horizon $H_c$. The first input of the optimal control sequence is applied and hereafter the process is repeated for the next time step. An example of a scheme showing relevant signals and horizons is shown in Figure 1.15. Here, $\boldsymbol{u_s}$ and $\boldsymbol{u_{s,max}}$ denote the angular rates and translational accelerations provided to the platform, and their maxima. $\boldsymbol{d_s}$, and $\boldsymbol{d_{s,max}}$ denote the platform's positions and its maxima [25].

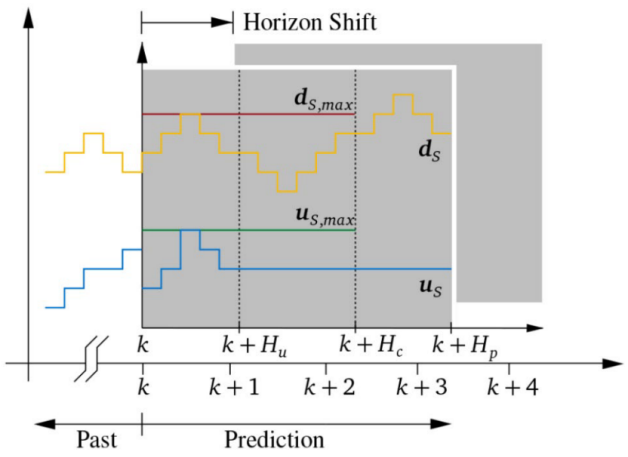


Figure 1.15: Schematic diagram of MPC horizons. [25]

Multiple studies have reported superiority of MPC-based concepts w.r.t. classical washout filter MCAs. It is found that MPC-based MCAs use a larger part of the simulator's workspace and yield a reduced difference between vehicle and simulator dynamics [24, 26]. Moreover, experiments have been performed in which MPC-based MCAs have outperformed classical washout filter MCAs using subjective ratings [24, 27]. Taking the simulator's workspace constraints into account is a clear advantage when comparing to classical washout MCAs, since it eliminates the need to tune for the worst-case scenario [8]. Moreover, it is possible to include a model of human perception in the optimization scheme of an MPC-based MCA, in order to optimally reduce sensory conflicts [24].

A major disadvantage associated with MPC is the computational expensiveness, given that an optimization problem is solved for a larger time horizon at each individual time step [26]. This is further complicated by a varying computation time per time step [28]. Another disadvantage of MPC-based MCAs is their complexity in comparison to a filter-based MCA, which complicating implementation and modification of such algorithms [8]. Lastly, a notable difficulty considering MPC is the lack of knowledge on the vehicle motion throughout the prediction horizon, as the input from the driver to the motion simulator is not known beforehand. This problem is usually worked around by assuming the future vehicle accelerations to be equal to the acceleration at the latest time step. This unrealistic assumption prevents providing optimal results [29].

### 1.4.2. Effectiveness of improved predictions

Grottoli et al. [30] noted that next to actually improving predictions, it is also of key importance to obtain an understanding of the effect of improved predictions on the motion cueing quality of MPC-based MCAs. In their study, the MCA's output is compared for two prediction strategies. The first strategy is a constant reference strategy, as conventionally used in MPC-based MCAs [29]. The second strategy uses perfect prediction (i.e., the future vehicle dynamics are known exactly) and is referred to as *oracle*. Note that the *oracle* strategy is not possible in active driving tasks, where time traces of future vehicle dynamics are never fully known. The quality of motion cueing is observed in terms of correlation, delay and absolute error. It was found that all are superior in case of perfect prediction, confirming the assumption that the cueing quality of MPCs can be improved by increasing the accuracy of predictions of future vehicle accelerations. Moreover, it was noted that PP is applied by the MCA in case of a known future maneuver. Lastly, it was found that the workspace is used more extensively in case of improved predictions. This evaluation is done by means of comparing the volumes of the convex hulls of the simulator positions and orientations throughout the experiments.

### 1.4.3. Predictions using reference drives

Bruschetta et al. [28] used a recorded reference drive to predict future vehicle accelerations, by means of aligning the current vehicle position with a position on the reference drive and extracting the future accelerations in the time domain. In case the reference provides unreliable predictions, the implemented algorithm switches to constant predictions instead. A case study is performed, considering only vertical

accelerations. It is noted that the reference-based predictions improve cueing performance when using a large enough look-ahead time. This comes at the cost of a higher computational load, which typically increases exponentially with the size of the prediction horizon [31]. It should be noted that since this case study is performed for vertical acceleration only, it does not guarantee success for the case of longitudinal acceleration, which is considered highly dependent on driving style opposed to road layout [9].

In an implementation proposed by Ellensohn et al. [32], optimized cueing is calculated offline using an optimization-based MCA and deviations between the reference drive and actual drive are accounted for online by a classical washout filter MCA. The offline cueing is aligned based on the coordinates in the virtual environment and cued together with the classical online MCA. This concept is only applied to lateral dynamics, since variations between drivers are found to be too large for longitudinal maneuvering. The optimization-based MCA which is used offline can be viewed as an MPC with a prediction horizon spanning the whole ride. The novel MCA is compared with a classical washout MCA in a human-in-the loop experiment. Here a significant decrease of perceived motion incongruence (PMI) is found, which indicates improved motion cueing.

### 1.4.4. Predictions without reference drives

Augusto & Loureiro [26] compared the performance of an MPC-based MCA for three prediction methods without any reference information on the future trajectory. The three models that are compared are i) assuming constant accelerations (conventional approach), ii) assuming constant control inputs and predicting vehicle dynamics by using a simplified vehicle model and iii) assuming constant derivatives of control inputs, again combined with a simplified vehicle model. Simplification of the vehicle model is necessary to reduce computation times. It was found that the controllers using the vehicle model did not have better results than the controller that assumed constant acceleration. Only the resulting cueing was evaluated, and thus no comparison of the accuracy of the predictions is provided.

Mohammadi et al. [29] used an artificial neural network (NN) to predict future accelerations $\bar{u}_f$ out of historic accelerations $\bar{u}_h$. A limited time history and future are divided into regions of varying intervals, as shown in Figure 1.16. Higher resolutions are taken for regions closer to the current sampling time. An implementation is made and evaluated for longitudinal motion, with a prediction horizon of 0.4 seconds. It is found that the RMS error of the specific force of the MPC-based MCA is decreased using the proposed prediction in comparison to the same MPC-based MCA that predicts constant vehicle accelerations.

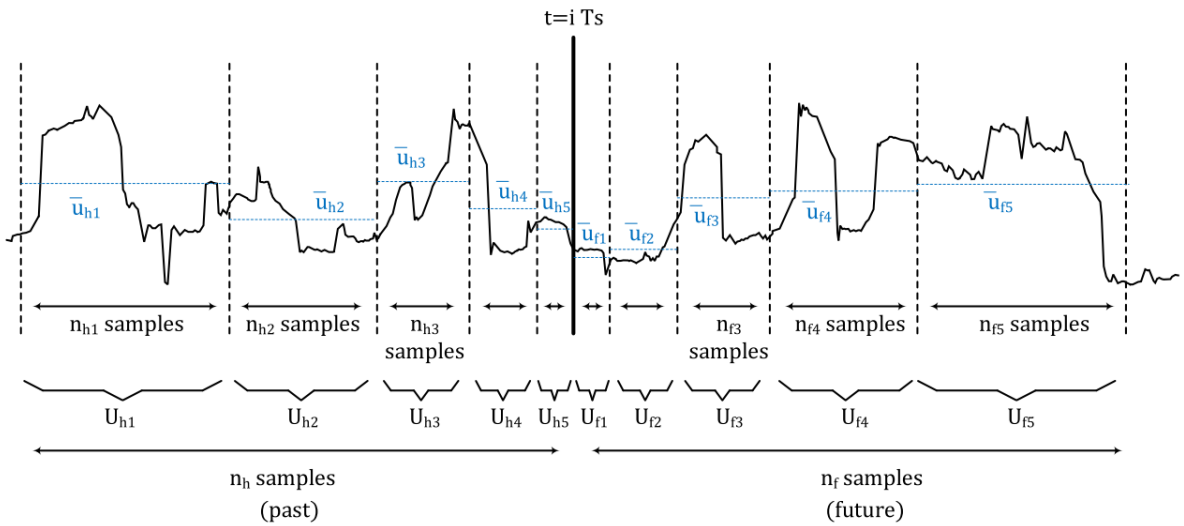


Figure 1.16: Intervals of historic and future samples as proposed by Mohammadi et al. [29].

## 1.5. Discussion

Explicit use of PP is currently limited to filter-based MCAs. Accurate logic is required, since maneuvers in unanticipated directions can yield a conflict with the simulator's workspace boundaries, which are strongly coupled for hexapod-based simulators. Considering PP logic, one can distinguish between situation-based and velocity-based PP. In situation-based PP, driving situations are identified and appropriate PP is calculated based on these situations. Although suggestions are given in literature, no implementations are described. It is assumed that a vast amount of information is needed in order to reasonably perform situation-based PP. In contrast, velocity-based PP is only based on the current velocity of the vehicle. The physical capabilities of the vehicle are considered, while not making assumptions on the likeliness of acceleration and braking maneuvers. Since detailed implementation is provided in literature, this form of PP can be used as a baseline throughout the current study. Since a PP excursion does not resemble vehicle motion, it is key to minimize the perceptiveness of it. In the majority of literature on PP, an acceleration- and jerk limiter are used, since both are known to play a role in human motion perception. Such controller will be used in the current study to calculate a PP position that can be fed to the simulator out of a desired PP position.

MPC-based MCAs, which can yield PP as output of more advanced optimization schemes, also depend on predictions of future vehicle states. Predictions based on previously recorded reference drives have been proven successful for cueing in $y$- and $z$-direction, but not for accelerations and braking, since these are considered harder to predict. Inclusion of a vehicle model does not necessarily improve predictions, since one would still need to predict future inputs to this vehicle model. The only successful approach for longitudinal prediction improvements in MPC-based MCAs is using NN. However, no details are given on the complexity of the driving task. Furthermore, the short prediction window of 0.4 s suggests that it is more a matter of improved scaling than of PP, since the latter would need more time. Lastly, it should be noted that for the described predictions in MPC-based MCA's, features such as road curvature and legal speed limits are not taken into account. It can be concluded that although the use cases for prediction in motion cueing are plentiful, little is known about the acquisition of predictions of longitudinal maneuvering in a driving simulation environment.

# 2

# Driver modeling

Understanding human driving behavior in the context of the driving scene and surrounding environment is considered of interest for multiple reasons. In the field of road design, knowledge on human driving behavior is used to strive for *design consistency*, ensuring harmonized driver behavior and thereby minimizing accidents [33]. In the field of vehicle design, the human-like models are required to increase system acceptance at higher levels of automation [34]. Although driving a car is a familiar task for many people, its stochastic nature makes modeling driver control far from straightforward [35]. Section 2.1 aims to describe characteristics of the human driver using control theory. Sections 2.2.1 and 2.2.2 describe acceleration and velocity in everyday driving. The latter contains a focus on velocity choice in curve negotiation, as for this confined task various general mechanisms have been proposed that describe how the human driver chooses longitudinal velocity in real world driving tasks. Where the aforementioned fields focus on how drivers control a vehicle, the emerging field of driver intent detection (DID), solely aims to detect driving intent in real-time using advanced data-based models. The state-of-the-art of DID will be discussed in Section 2.3. Lastly, Section 2.4 provides an overview of the driver modeling techniques discussed in this chapter, as well as a discussion of their suitability to be used for prepositioning in driving simulation.

## 2.1. Driving from a control perspective

Limited tasks, such as path-following and headway control, can be investigated from the perspective of control theory [36–38]. Here, the human driver is considered a control system: *a system consisting of subsystems and processes (or plants) assembled for the purpose of obtaining a desired output with desired performance, given a specified input* [39]. A simplified description of such system is given in Figure 2.1. The human driver can be considered an adaptive, nonlinear controller, of which the human physiology, adaptability and preview utilization are important aspects [36].

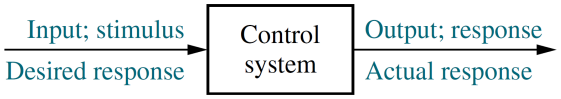


Figure 2.1: Simplified description of a control system. [39]

### 2.1.1. Physiology

Physiological limitations influence the human as a control system. Processing times and information transmission times cause delays. Information can only be sensed by a human when it exceed certain thresholds. Moreover, human cognition imposes limitations on the human control capabilities. This makes us for example unable to optimally predict ahead and estimate rate information [36]. Inputs for drivers are vision, motion, tactile and auditory inputs. Often, there is redundancy in information during driving, which can help drivers to confirm decisions more quickly or yield better estimations [36]. The visual system can extract position and velocity information separately, where the saccadic (jump-like) response of the eye is used for position determination and the smoother pursuit mode is used to track

velocity [40]. Extracting velocity from visual scenes is done using optical flow from the surrounding visual scenes [41]. When a moving visual scene is observed, a feeling of self-motion is induced. If this happens for a stationary observer, this is referred to as vection [6]. As a means of driver aid, velocity is also shown on a velocity gauge and for some vehicles numerically on a digital display. Driving simulator studies have shown that motion perceived by the vestibular system in the inner ear also plays a role when controlling a vehicle [5, 6]. Tactile forces are noticed by humans using the somatosensory system, which consists of various receptors sensitive to pressure, stretch and vibration [42]. Lastly, it is known that velocity estimations are enhanced using auditory inputs [43].

### 2.1.2. Adaptability

A key property of the human driver is its ability to adapt to the controlled vehicle dynamics as well as the operating conditions. This feature, referred to as *adaptability*, was observed by McRuer & Jex [44]: *"The human is a multimode, adaptive, learning controller capable of exhibiting an enormous variety of behavior".* For the general case of controlling a visual-only, single-axis, compensatory tracking task with (quasi-)random perturbations as illustrated in Figure 2.2, McRuer & Jex proposed the generally accepted *simplified precision model* to describe the linear portion of the human error response, $H_{o_e}$. In this model, which can be found in Equation 2.1, $\tau_v$ denotes the human's time delay, resulting from physical delays. Gain $K_e$, lead and lag time constants $T_{L,e}$ and $T_{l,e}$ are parameters that the human operator adapts in order to make open-loop system dynamics in the crossover region (i.e., the region in the frequency domain where the open-loop gain equals 1) resemble a single integrator.

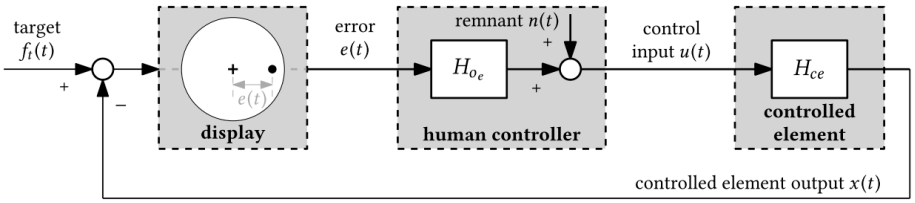


Figure 2.2: Control diagram of a human performing a compensatory target-tracking task with a (quasi-)random target signal. [45]

$$H_{o_e}(j\omega) = K_e \frac{1 + T_{L,e} j\omega}{1 + T_{l,e} j\omega} e^{-\tau_v j\omega} \tag{2.1}$$

### 2.1.3. Preview

Another key property of the human driver is the use of preview information about the trajectory that is to be followed in the future. By means of preview, upcoming maneuvers are anticipated [45]. This implies a substantial difference with compensatory tracking tasks, for which the *crossover model* was developed. Preview models proposed by Sheridan [46] that make use of preview, form the basis for many later models. The investigated task here was *forced-paced*, indicating that the human controller only manipulates lateral maneuvering. This is a simplification of real driving, where drivers also control the velocity of a vehicle (referred to by Sheridan as *self-paced*). More recent work of Van der El [45] on *forced-paced* driving showed that drivers use two distinct feedforward responses, based on a *near* and *far* viewpoint. An illustration of the driving task and control loop as used by Van der El is provided in Figure 2.3. Longitudinal maneuvering is studied and modeled less extensively than lateral maneuvering. Control traits such as delay and preview are assumed to apply to longitudinal control too [36]. However, fundamental experimental studies that address these, as done for lateral dynamics by McRuer & Jex, Sheridan and Van der El, are lacking.

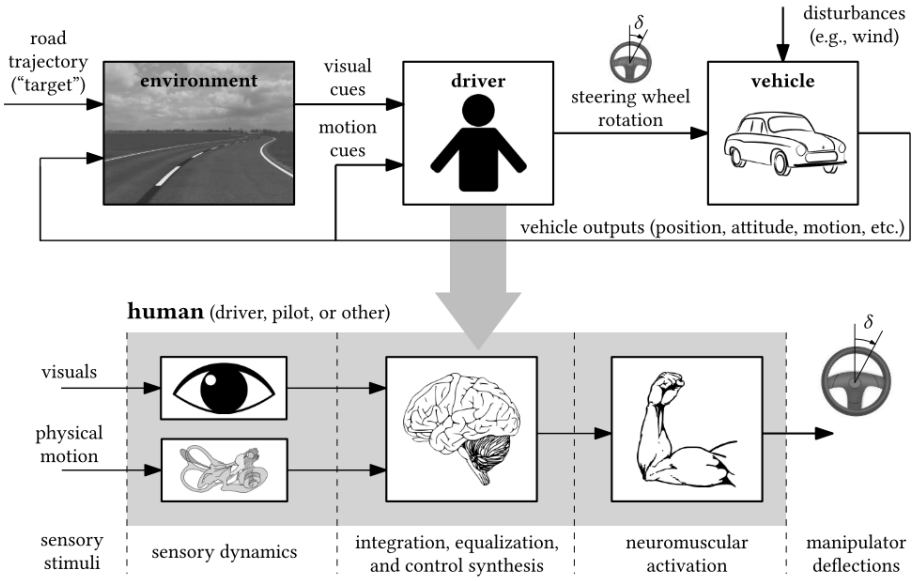


Figure 2.3: Illustration of the closed-loop task of driver steering on a winding road (top), with a detailed view of the human's stimulus-response relation (bottom). [45]

## 2.2. Naturalistic driving behavior

In contrast to the *forced-paced* studies discussed using control theory, naturalistic driving studies study everyday driving tasks, either with the use of instrumented vehicles, or with driving simulators. The focus in naturalistic driving studies is on driver behavior. This differs from control theoretic modeling (Figure 2.1), since in real driving, the desired response can have many forms. In Section 2.2.1, levels of acceleration common in naturalistic driving are discussed. Section 2.2.2 describes how drivers choose their velocity. For the confined task of curve driving, various theories that have been developed to describe how drivers choose their velocity will be discussed in detail.

### 2.2.1. Acceleration levels in naturalistic driving

Lechner and Perrin [47] studied longitudinal and lateral acceleration in everyday driving and compared the occuring accelerations to the vehicle's capabilities. The latter is often referred to as the tire *friction circle* or *friction ellipse* and describes the maximum simultaneous longitudinal and lateral acceleration that can be sustained without loss of control of the vehicle. Large differences are found between individuals when driving the same vehicle on the same road, but generally drivers operate well within the boundaries posed by the vehicle. Later work of Bielaczek [48] confirms this finding. Bielaczek distinguished between average and sportive drivers and plotted acceleration maxima as shown in Figure 2.4. It can be concluded that although tire friction constrains vehicle control, these friction constraints are not a suitable basis to model a driver during everyday driving.

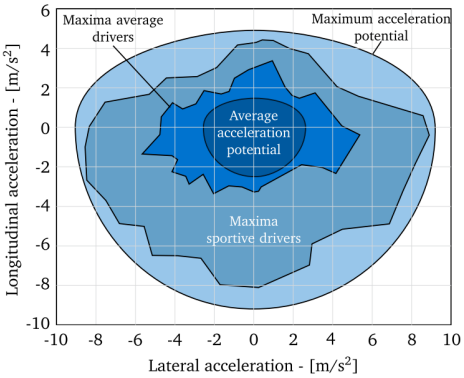


Figure 2.4: Acceleration maxima for average and sportive drivers compared to average and maximum vehicle acceleration. [48]

When a driver requires deceleration, this can be achieved either by pressing the brake pedal or by releasing the accelerator pedal to make use of engine braking, rolling resistance and aerodynamic drag. In a data set containing real driving data from urban roads, extra-urban roads and motorways with roundabouts, ramps and intersections, Bosetti et al. [49] found the imperical distribution shown in Figure 2.5. Peaks are found at 0 m/s$^2$ for stationary driving and around -0.35 m/s$^2$ for engine braking.

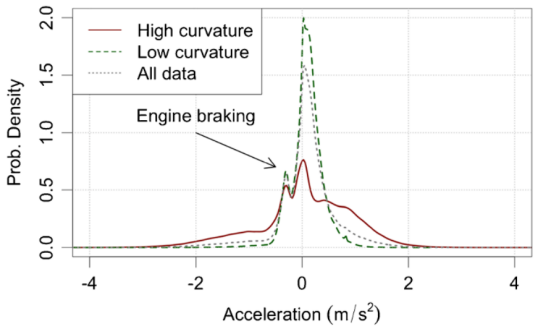


Figure 2.5: Distribution of longitudinal acceleration from Bosetti et al.'s [49] data.

Ritchie et al. [50] compared levels of acceleration for various levels of forward velocity when driving curves and found a strong inverse relationship for velocities higher than 10 m/s. Later research confirmed this finding [47–49, 51]. It is hypothesized that the observed decrement in lateral force maxima is due to a decreased sense of *safety* at higher velocities [50]. Bosetti et al. [49] have visualized this with scatter plots of lateral and longitudinal accelerations versus forward velocity as shown in Figures 2.6 and 2.7. It is found that unlike lateral acceleration, longitudinal acceleration levels seem to be relatively independent of forward velocity. Lateral acceleration is usually a consequence of curve negotiation, which will be discussed in further detail in Section 2.2.2.

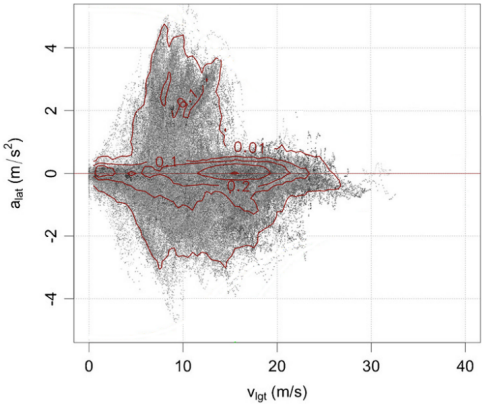


Figure 2.6: Lateral acceleration vs. forward velocity. [49]

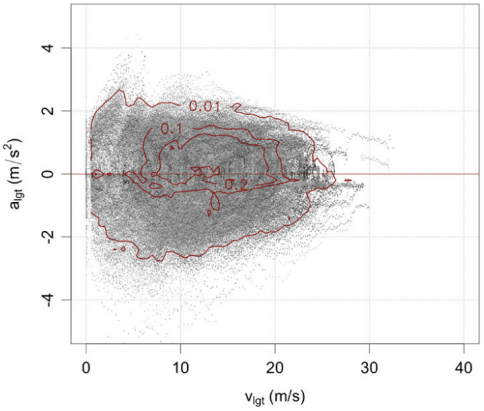


Figure 2.7: Longitudinal acceleration vs. forward velocity. [49]

## 2.2.2. Velocity choice in naturalistic driving

Next to levels of acceleration, the choice of velocity for certain driving scenarios is a characteristic that attracted attention from various researchers. Levison [52] used the term *free speed* for the driver's desired speed when there is no need to slow down or stop for an event such as a crossing or interfering traffic. The following factors are distinguished for the determination of *free speed*:

1. *Legal considerations*: maximum velocity chosen w.r.t. the speed limit, based on driving style
2. *Vehicle limitations*: maximum velocity reachable by the vehicle
3. *Comfort*: maximum velocity which is considered comfortable (e.g. accelerations, vibrations)
4. *Safety*: maximum velocity under which the driver assumes adequate control of the vehicle

The first factor, *legal considerations*, can be related to the driving environment. The second, *vehicle limitations*, is considered primarily relevant for heavy utility vehicles. Relating *comfort* and *safety* to a driving scenario is complex. However, various statistical studies have been performed that directly relate environment attributes to the velocity chosen by drivers. As an example, Cruzado & Donnel [53] investigated factors affecting driver velocity choice using a large data set containing 2,859 drivers along 20 transition zones of two-lane rural highways. Linear regression is used to estimate the reduction in velocity between high-speed and low-speed zones, which is referred to as the *velocity differential*. Higher *velocity differentials* were found for larger initial speeds, reduced road widths, an increased amount of driving lanes, presence of intersections, warning signs and the presence of curves. Real world driving scenarios generally consist of a multitude of such attributes and the chosen anticipation is known to vary considerably between drivers [32].

Of all factors that influence the velocity choice, road curvature is studied most extensively [33]. Over the course of the last decades, a vast quantity of curve velocity models have been developed in the fields of road and vehicle design. Four models with different underlying mechanisms are discussed in this section. Next to these studies, a large quantity of statistical research has been performed, of which an overview is provided by Misaghi & Hassan [33]. These studies will not be discussed in this chapter, as they do not propose an answer to the more fundamental question *why* the human driver exhibits certain driving behavior.

### 2.2.3. Time to Line Crossing

Van Winsum & Godthelp [54] argued that only if the steering wheel angle perfectly matches the required steering wheel angle, the speed with which a curve can be driven is restricted by the vehicle's friction characteristics. They hypothesized that steering errors play a role in the *safety* as perceived by the driver and ultimately in the velocity choice. It is found that the increase in required steering wheel angle needed to negotiate curves of higher radii results in larger steering error, and it is assumed that this is accounted for by choosing a lower speed, so as to keep the *time to line crossing* (TLC), a concept earlier developed by Godthelp et al. [55], above a threshold acceptable for the driver. The TLC represents the time necessary for the vehicle to reach either edge of the driving lane and depends on the steering error, velocity, road width and offset from the lane center. Various ways to calculate the TLC exist, ranging from exact geometric methods to simple approximations [56, 57]. Godthelp et. al did not elaborate which method is applied in their study.

The results in Table 2.1 show the velocity, required steering wheel angle, steering error, steering error ratio and minimum TLC ($V$, $\delta_{s_{required}}$, $\delta_{s_{error}}$, $\delta_{s_{error}}/\delta_{s_{required}}$ and $TLC_{min}$, respectively) for four curves with different radii, averaged over all 16 participants. Note that the steering error ratio and TLC are approximately constant and that the absolute steering error increases as the curve radius decreases, which supports the hypotheses. In another experiment presented in this study, it is found that the TLC margin principle also holds for straight roads, where steering errors caused by reduced steering competence are compensated for by choosing a lower speed [54].

Table 2.1: Dependent variables averaged per curve in the experiment of Van Winsum & Godthelp [54].

| | $R_{curve}$ (m) | | | |
|---|---|---|---|---|
| | 40 | 80 | 120 | 180 |
| $V$ (m/s) | 11.23 | 14.92 | 17.58 | 17.99 |
| $\delta_{s_{required}}$ (deg) | 121.44 | 74.64 | 56.56 | 43.47 |
| $\delta_{s_{error}}$ (deg) | 14.20 | 7.47 | 5.54 | 4.75 |
| $\delta_{s_{error}}/\delta_{s_{required}}$ (-) | 0.12 | 0.10 | 0.10 | 0.11 |
| $TLC_{min}$ (s) | 2.52 | 2.70 | 2.89 | 2.79 |

### 2.2.4. Lateral acceleration margin

Reymond et al. [57] investigated the relation between velocity and road curvature by means of plotting the *lateral acceleration envelope*, which is defined by the convex set formed by all lateral accelerations plotted against velocity. They noted that when using the minimum TLC as an estimator for the curve speed, a significant decrease in maximum lateral acceleration with speed only occurs at small curve radii. This is depicted in Figure 2.8. Their set of experiments contradicted these findings. A sharper decrease in maximum lateral acceleration was found at higher speeds, both for real and simulated driving. Moreover, the lateral acceleration envelopes found in this data resembled a parabola, in contrast to the hyperbola as yielded with the TLC model.

A new model was proposed to describe their experimental data, in which it is assumed that drivers adjust speed in curves so as to keep the maximum lateral acceleration $\Gamma_{max}$ below a constant threshold based on their own experience, vehicle characteristics, road and weather conditions and a personal level of acceptable risk. It is argued that a driver wants to be able to deviate from the driven trajectory with a correcting maneuver with a curvature of magnitude $\Delta C$ at all times, which would result in an increased lateral acceleration $\Delta\Gamma$ of $\Delta C \times V^2$. Similar to $\Gamma_{max}$, the magnitude of $\Delta C$ is assumed to be constant, yet driver dependent. Considering that the total of the acceleration without such deviation ($\Gamma$) and this increased lateral acceleration can not exceed the driver's maximum lateral acceleration level, one yields Equation 2.2.

$$\Gamma \leq \Gamma_{max} - \Delta C_{max} V^2 \tag{2.2}$$

Moreover it is noted that at lower speeds, the maximum lateral acceleration is limited by the physical constraint of the steering angle. The lateral acceleration is then limited to $k \times V^2$, where $k$ accounts for the vehicle's restrictions on the trajectory's curvature. Together with the constraint from the lateral acceleration margin as given in Equation 2.2, this yields a lateral acceleration envelope as given in Figure 2.9.

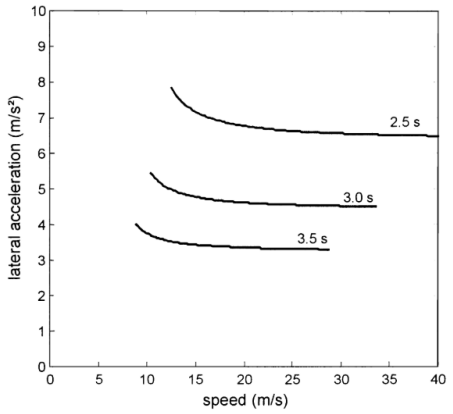


Figure 2.8: Lateral acceleration envelope for different TLCs. [57]

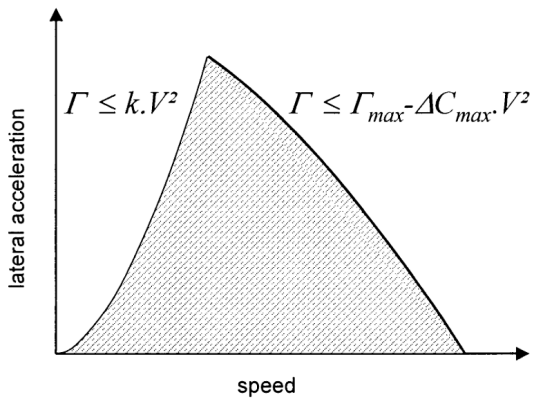


Figure 2.9: Model of the lateral acceleration envelope as a function of the velocity as proposed by Reymond et al. [57].

Linear regression is used to fit the acceleration envelope for each driver using data collected with a real vehicle, driving simulator with motion feedback and driving simulator without motion feedback. Results are shown in Table 2.2. No conclusions were drawn that relate the vehicle data to the simulator data, since the participant groups were dissimilar and small. Looking at the simulator data, the coefficient $\Delta C$ was found to decrease significantly when comparing the dynamic and static conditions. For illustrative purposes, Figure 2.10 shows the lateral acceleration envelope for one participant in both conditions. One can clearly see that the slope of the right part of the envelope is less steep for the static condition, which is the cause for the lower $\Delta C$. Differences between the models for the different motion condition contribute to the view that non-visual cues are taken into account in driving.

Table 2.2: Regression coefficients for the lateral acceleration margin model fitted for data collected with a real vehicle, dynamic simulator and static simulator. Standard deviations are added in parentheses. [57]

| | **Vehicle** | **Dynamic simulator** | **Static simulator** |
|---|---|---|---|
| $\Gamma$ (m/s$^2$) | 7.64 ($\pm$0.58) | 7.99 ($\pm$0.76) | 8.34 ($\pm$ 0.66) |
| $\Delta C$ (km$^{-1}$) | 6.32 ($\pm$1.88) | 8.34 ($\pm$0.66) | 3.82 ($\pm$ 0.77) |

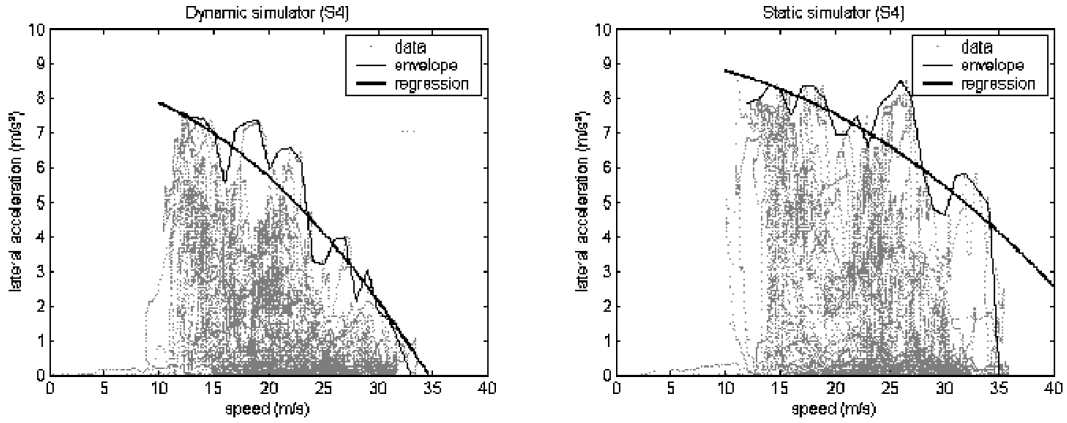


Figure 2.10: Lateral acceleration for one participant in a dynamic simulator (left) and static simulator (right). [57]

## 2.2.5. Two-thirds law

Bosetti et al. [49] noted that an inverse correlation between (angular) speed and curvature is known to be a general feature of human movement. Various studies have shown that when hand-tracing an arc, angular velocity is limited by two-thirds power of the local arc curvature [58–60]. A similar relationship is observed when humans walk curved paths [61]. This relationship is referred to as the *two-thirds law* and can be found in Equation 2.3, where $\kappa$ denotes curvature and $\alpha$ is a task-specific constant. Flash et al. [60] showed that when describing a hand tracing ellipses, the minimum jerk trajectory shows an exponent that closely resembles Equation 2.3. Minimizing jerk ensures smooth movements, a general computational principle of sensorimotor control [62]. This principle is generally referred to as *minimum variance* and is believed to be a byproduct of controlling movements in a way in which motor neuron noise is minimized by achieving an optimal trade-off between accuracy and speed.

$$\omega = \alpha \kappa^{\frac{2}{3}} \tag{2.3}$$

When relating velocity instead of angular velocity to curvature, Equation 2.4 is obtained. Bosetti et al. plotted velocity against radius of curvature on a log-log scale, using samples collected with an instrumented vehicle on urban roads, extra-urban roads and motorways. When fitting the *two-thirds law* as given in Equation 2.4, a value of $\alpha$ = 3.7 m$^{2/3}$s$^{-1}$ was found to represent 99.9% of the observed data, whereas $\alpha$ = 3.34 m$^{2/3}$s$^{-1}$ represents the median driver. It is noted that a speed limit of 90 km/h (25 m/s) restricts the speed at larger curve radii. Consequently, road radii larger than 1 km are considered irrelevant. A scatter of the collected data and lines representing the *two-thirds law*, the *lateral acceleration margin* theory as proposed by Reymond et al. [57] and a statistical relationship found by Levison [63] can be found in Figure 2.11. Bosetti et al. noted that using Reymond's model an overestimation of the speed envelope is obtained, due to using test track data opposed to real-world roads. After reparameterization of Reymond's model, it is slightly superior over the *two-thirds power law* at large curve radii. However, as previously stated, at large curve radii the speed is more likely to be determined by legal restrictions than by curve negotiation incentives.

$$V = \alpha \kappa^{-\frac{1}{3}} \tag{2.4}$$

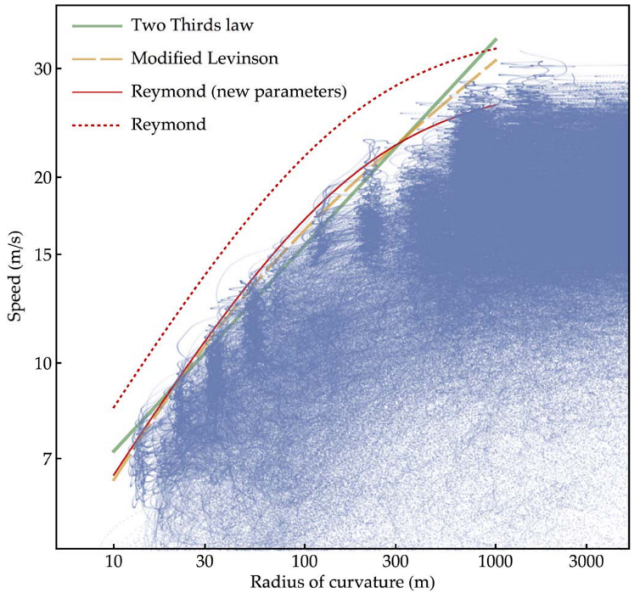


Figure 2.11: Velocity against radius of road curvature for Bosetti's data. [34]

Next to describing the maximum velocity while negotiating turns, Bosetti et al. [34] propose a kinematic human curve speed model, in which optimal control is used to keep velocity according to the *two-thirds law*. An optimization scheme is used to minimize a cost function that contains jerk and travel time. In the proposed model, this optimization is is solved for free flow as well as for curves ahead within a limited receding horizon. The maneuver with the lowest initial jerk is executed. This is illustrated in Figure 2.12, where $v_0$ and $a_0$ are the vehicle's initial velocity and acceleration, $v_d$ is a prediction of the desired velocity when neglecting road curvature and $v_1$ and $v_2$ are predictions of velocity used to anticipate curves 1 and 2, respectively. In this example, the maneuver from $A$ to $C$ would be executed, due to its lowest initial jerk. A trace of velocity calculated using the proposed model is shown in Figure 2.13. As can be seen, the model produces a velocity that approximately resembles the recorded drives.

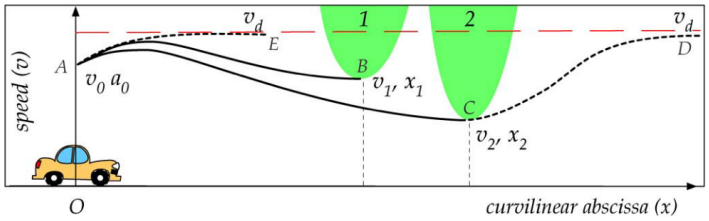


Figure 2.12: Maneuver planning for free speed and the anticipation of two curves. [34]

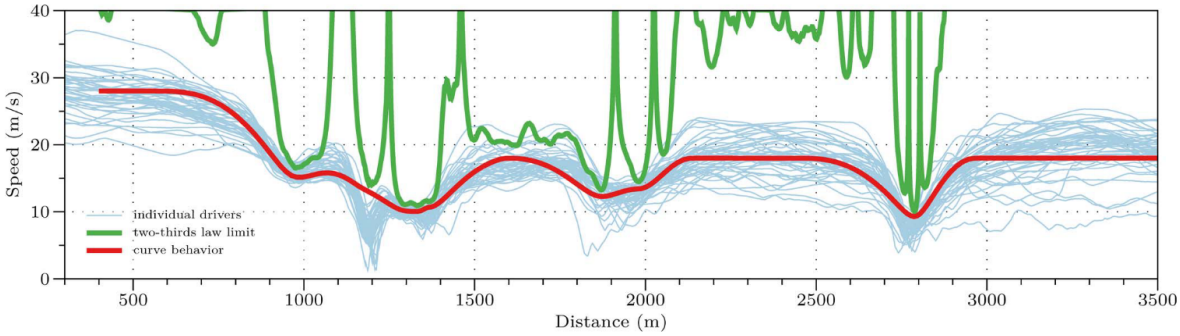


Figure 2.13: Velocity from data, as determined using the two-thirds law, and determined using an optimal driver model. [34]

### 2.2.6. Time to Extended Tangent Point

While investigating recordings of steering wheel angle and gaze direction along curved roads, Land & Lee [64] found that drivers pay a particular amount of attention to the *tangent point* (TP) on the inside of each curve. It is noted that the direction of this point provides a prediction of the curvature of the road ahead. However, it is also known that drivers do not solely fixate on this point, but scan areas further up the road and that in particular attention is paid to the *far road triangle*, which consists of the TP, the *occlusion point* (OP), which is the furthest point of the road that is not blocked by obstacles in the field of vision, and the opposite lane edge [65]. Gruppelaar proposed a velocity choice model using the *extended tangent point* (ETP), which is the point where the driver's line of vision through the TP intersects the opposite lane edge, as depicted in Figure 2.14. The *time to extended tangent point* (TETP) is defined as the time it would take for the vehicle to reach the ETP in a straight line, asuming a constant speed. The TETP depends on the vehicle's lateral offset from the lane center and can be interpreted as a measure of how much the road 'opens up' after a turn.

Next to modeling velocity, Gruppelaar proposed a model relating velocity choice of individual drivers to accelerator and brake pedal control. The proposed control model distinguishes between *acceleration, deceleration, braking, brake release* and *re-acceleration*, which each have a distinct set of equations for pedal control. Phase determination is based on the TETP and the time derivative of the TETP. When the TETP is above *deceleration threshold* $T_d$, the vehicle is accelerated. When the TETP is between $T_d$ and braking threshold $T_b$, the vehicle is either in the *deceleration* or *re-acceleration* phase, depending on the time derivative of the TETP w.r.t. TETP rate of change threshold $dT_a$. When the TETP is below $T_b$, the model assumes the driver to be either in the *braking* or *brake release* phase, again depending on the derivative of the TETP. This is depicted in a flowchart in Figure 2.15.

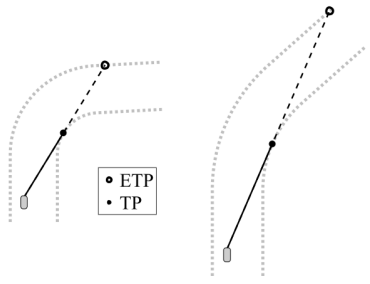


Figure 2.14: Location of the TP and ETP for two curves with different radii and deflection angles. [66]

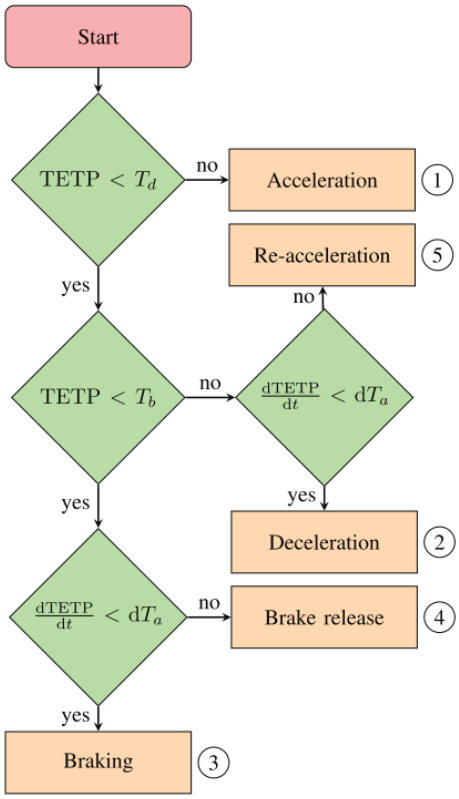


Figure 2.15: Flowchart of phase decision based on the TETP. [66]

Next to the TETP thresholds, the driver model contains gains that specify how quickly the driver lets go of the gas pedal, how strongly the driver presses the brake pedal and how strongly the driver presses the accelerator pedal. Validation using a road section that is not included in parameter estimation yields an averaged Variance Accounted For (VAF) of above 60%, implying that driver speed can be accurately described using the proposed model. The VAF found for acceleration accelerator control are below 30%. The lowest VAF scores are found for braking, which is assumed to be a result of the low variance caused by the sparsity of braking maneuvers.

## 2.3. Driver Intention Detection

Driver intention detection (DID) is attracting an increasing amount of interest [67–69]. It is believed that maneuver recognition can help to avoid mismatches between the driver's intention and the system's reaction in Advanced Driver Assistance Systems (ADAS) [70]. For example, a collision warning can be considered undesirable, in case a driver intends to overtake another vehicle. Another example use case of DID in vehicle design is improved gear shifting that incorporates estimates of future accelerations, yielding increased fuel efficiency [71]. DID models have been developed based on driver control inputs, dynamic vehicle states, gaze data and traffic situations as means to detect acceleration, braking, turns, lane changes and passing maneuvers. In the current section, the DID models are subdivided based on the model types, which are fuzzy logic, hidden Markov, and artificial neural networks.

### 2.3.1. Fuzzy logic

Peng et al. [72] noted that being often an effective means to simulate human reasoning, fuzzy logic can be used to describe driver intent. A fuzzy model is set up that relates the accelerator pedal position and velocity to membership of the fuzzy subset $[N, S, M, B]$, indicating negative, small, medium and big, respectively. Membership functions are shown in Figures 2.16 and 2.17.

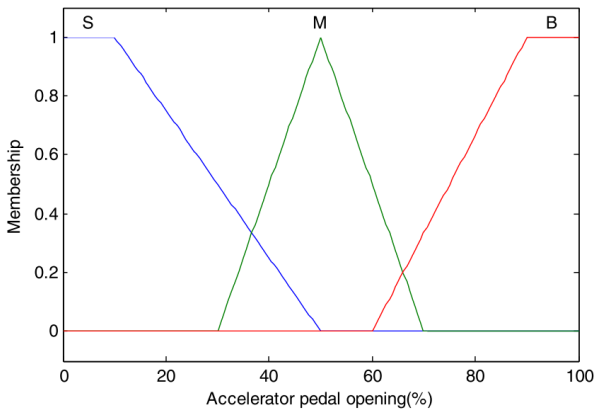


Figure 2.16: Membership functions of the accelerator pedal deflection. [72]

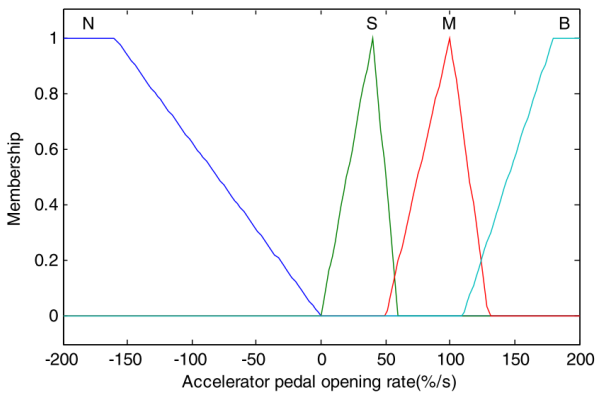


Figure 2.17: Membership functions of the accelerator pedal velocity. [72]

Fuzzy inference rules as shown in Table 2.3 are applied to relate the fuzzy subsets to driver intent, subdivided into adjustment acceleration (A) and emergency acceleration (E). In the latter case, large acceleration is required rapidly. Hereafter, both the membership functions and fuzzy inference rules are used together with a comparable fuzzy intention detection model for lateral maneuvering to improve torque distribution for an electric vehicle with in-wheel motors. The proposed method is found to be successful by means of improved vehicle control. Moreover, it is concluded that the lack of accuracy of the fuzzy rules limits the effectiveness of the solution.

Table 2.3: Fuzzy inference rules relating fuzzy subsets to driving intention, where A denotes adjustment acceleration and E denotes emergency acceleration. [72]

| **Pedal deflection** | **Pedal deflection rate** | | | |
|---|---|---|---|---|
| | $N$ | $S$ | $M$ | $B$ |
| $S$ | A | A | A | A |
| $M$ | A | A | A | E |
| $B$ | A | E | E | E |

## 2.3.2. Hidden Markov models

Liu & Pentland [73] were the first to use hidden Markov models (HMMs) for driver intention detection. In an HMM, it is assumed that an underlying process is happening, which consists of multiple discrete states. These states are unobservable, but the likelihood of transitions between states are constants obtained using model training. In later work, it was found that an increased similarity was found in maneuvers, when using predictions of the car's motion states made using the driver's control input, instead of raw control inputs [74]. It is reasoned that this is due to that the driver finds the sequence of control inputs less important than the actual vehicle movement. In a simulator study in which commands for maneuvers are provided to the driver making use of a display, over 95% of lane changes are discovered at 1.5 seconds after the beginning of lane changing. As can be seen in Figure 2.18, this is well before the part of the maneuver that contains that contains the most dynamics. As a remark, authors noted that this method of demanding maneuvers differs from naturalistic driving, where drivers choose a to-be-executed maneuver themselves.

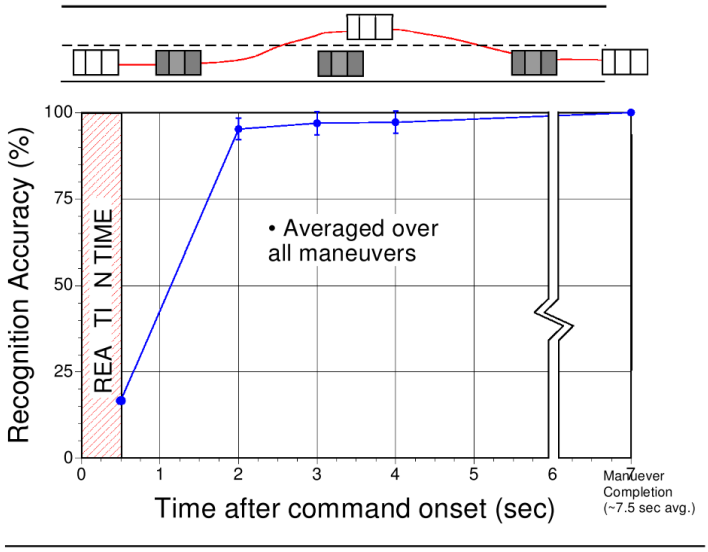


Figure 2.18: Recognition accuracy against time. [74]

In recent work of Zhao et al., [75] brake pedal and vehicle speed data are used to identify braking intention. The proposed model consists of three HMM models that determine the likelihood of slight, normal and emergency braking, based on the vehicle speed and brake pedal force, displacement and speed. It is found that the accuracy of the prediction can be improved by training NN models that relate the likelihoods of all three braking classes as calculated by the HMM models to the likelihood of each individual braking class. The resulting model identifies slight and normal braking with accuracies of over 95% within 0.7 seconds after actuation of the brake pedal. An illustration of the ANN model structure is provided in Figure 2.19.

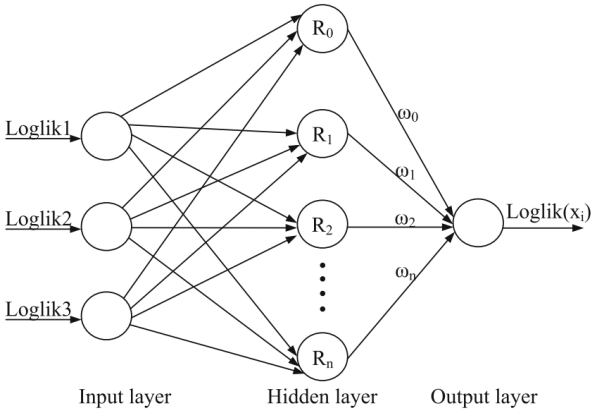


Figure 2.19: Illustration of NN model structure for enhancement of HMM outputs. [75]

Oliver & Pentland [76] first investigated the use of gaze data for DID purposes. In their proposed model, they used coupled hidden Markov models (CHMMs) to detect passing, lane changes, turning, starting and stopping of data collected with an instrumented test vehicle. CHMMs can be viewed as multiple HMMs coupled by conditional probabilities between hidden state variables [77]. Gaze was used as a discrete signal with six possible values: front road, rear view mirror, right mirror, right window, left window. On average, the models are able to recognize the maneuvers 1 second before the start of the dynamic part of a maneuver (i.e., 20% deviation of vehicle dynamics). It is concluded that gaze behavior is a relevant feature for driving maneuver prediction and recognition, especially when detecting lane changes, overtaking, and turns. More recently, Wu et al. [78] used gaze data as sole input for DID, to detect braking and turning maneuvers. Probabilistic Dynamic Time Warping (DTW) is used together with an HMM in order yield superior results when compared to a conventional HMM model. The proposed model can predict a driver maneuver 3 seconds before it occurs with an accuracy of 90%.

### 2.3.3. Artificial neural networks

Lethaus et al. [70] proposed artificial neural networks (NN) with one hidden layer to detect driving maneuvers. This NN converted gaze data as standalone predictor for lane change maneuvers. The data set used to train and validate the models is obtained with a dynamic driving simulator. Analogue to the work by Oliver & Pentland [76], gaze is subdivided into viewing zones. Two prediction window sizes are compared, consisting of the last 5 and 10 seconds. Both windows are split up in smaller sub-windows that form the inputs for the NNs. The labeled data set used to train the NNs, contains binary output data, since a maneuver of interest is either happening or not happening. Due to the structure of the NN, however, it outputs a value within the range of $[0, 1]$. A threshold is set to convert the non-binary NN output into a definitive maneuver estimate.

When choosing a higher threshold, false positives are reduced at the cost of a decrease in true positives. This is graphically shown in the Receiver Operating Characteristic (ROC) curves in Figures 2.20 and 2.20. In these plots, scores of identification are given for a look-ahead ranging from 0 to 2 seconds. A perfect score in an ROC curve would be true positive rate (TPR) of 1 and a false positive rate (FPR) of 0, which is found in the upper left corner of the plotting area. It can clearly be seen that higher performance is obtained for shorter look-ahead times. Moreover, it can be seen that the model with a 5 second detection window outperforms the model with a 10 seconds window. It is noted that this detection window should be chosen so as to include enough information to detect the pattern of interest, without including irrelevant previous behavior. The predictive value of the ANNs is validated by the fact that all points of the ROC curve are in the lower left half of the plot, indicating that the models outperform random classification.

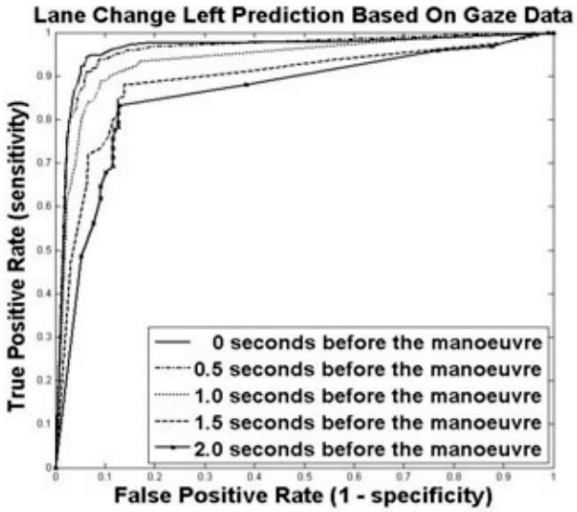


Figure 2.20: ROC curve for detection of left lane change maneuver using a 5 second detection window. [70]

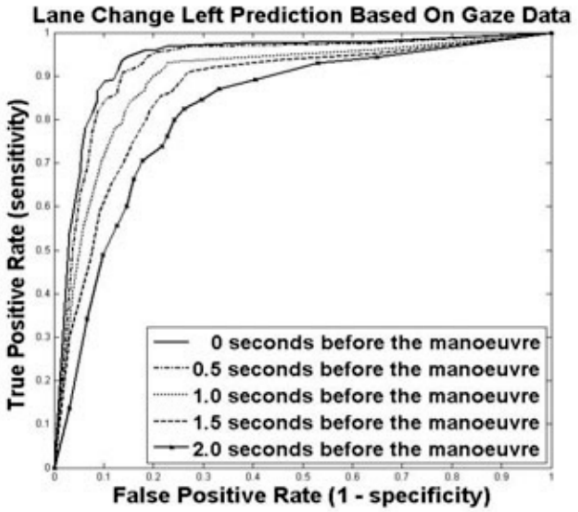


Figure 2.21: ROC curve for detection of left lane change maneuver using a 10 second detection window. [70]

Liu et al. [71] noted that traditional NNs may result in suboptimal identification results, as they do not consider inputs as time series. In contrast, Recurrent Neural Networks (RNNs), use internal memory states to be able to process sequences of inputs as time series. Various prediction models have been set up in the field of DID using RNNs [69, 79]. In the model proposed by Liu et al. a long short-term memory (LSTM) algorithm is trained to classify the driving behavior at the current time based on the (historical) degree of opening of the accelerator pedal, vehicle speed and brake pedal force. An LSTM is an enhanced RNN with a forgetting factor in each hidden layer that prevents gradient explosion, a major drawback from traditional RNNs. In a comparative study, both an LSTM and a traditional NN are trained to detect longitudinal driver intention using data collected with an instrumented vehicle. The models predicts 5 classes of longitudinal driving behavior, i.e.: acceleration, rapid acceleration, deceleration, rapid deceleration and cruise. Labeling of these subsets is done based on the actual vehicle acceleration, using K-means clustering. Recognition accuracies of 92.5% and 80.4% are found for the LSTM and traditional NN, respectively, implying that the LSTM model outperforms the traditional NN.

## 2.4. Discussion

From a control-theoretic viewpoint, the human driver is a non-linear element that adapts to situations and uses preview information so as to optimally control a vehicle. This would imply, that features that appear further ahead will have to be taken into account when modeling driving behavior. Research on *forced-paced* steering behavior using control theory is at an advanced stage, in contrast to velocity control. The latter is relatively complex, since the unknown desired velocity depends on the driver as well as many features of the driving scenario. Acceleration limits play a constraining role in vehicle maneuvering. Nevertheless, they do not define naturalistic driving, wherein levels of acceleration are generally much lower. Longitudinal acceleration maxima are only loosely related to the vehicle's velocity, which can be explained by that braking also occurs at lower velocities and that at higher velocities, accelerations also occur. This shows a limitation of solely basing PP on the vehicle's velocity. To what extent factors play a role depends on both the task and scenario and will thus have to be investigated for the data at hand.

As PP only has to offset the simulator to make a larger part of the workspace available for cueing, predicting exact specifications of future maneuvering is not required. For this reason, it could be useful to include simple relationships. The two-thirds law, as applied to curve velocity by Bosetti et al., could be such a relationship and will be investigated in this project. It contains only one parameter and is used do describe real world driving behavior, in contrast to the confined experimental tasks in control-theoretic studies. Control inputs can also be used in predictions and will also be included in this project.

Using control inputs in combination with gaze data and dynamic vehicle states is common in the field of DID. Here, high prediction scores are obtained with advanced models, but at best only a short instance before the maneuver is performed. This would most likely not suffice for the provision of PP, as offsetting the simulator's neutral point imperceptibly takes time. How much time is needed will have to be investigated for the current simulator. The geometry of the road ahead and legal speed limits have not been included in DID research described in literature. It is highly probable that these play a large role in velocity choice. A take-away from the advances in DID, is that a modeling technique suitable for time series is preferred over one that does not explicitly have a time dimension. However, this generally comes at the cost of higher model complexity. Noting the large gap between the state of the art of PP in literature and the advances in the field of DID, and assuming that in PP an accurate prediction is not always needed, a simpler approach such as regression could be a logical starting point for maneuver prediction in motion cueing. A probabilistic approach could be suitable, as deterministic models might be too rigid to describe driving behavior of all possible test drivers with realistic and thus complex driving task.

# 3

# Preliminary results

In this chapter, initial results are presented that relate the literature as described in Chapters 1 and 2 to the driving data and MCA made available by the BMW Group. Section 3.1 provides an overview of the driving scenario, and aims to find a preliminary answer to *RQ1: To what extent can longitudinal maneuvers be predicted in a driving simulation environment?* In Section 3.2, initial steps are taken to answer *RQ2: To what extent can motion cueing quality of a classical washout filter MCA be improved using PP based on predictions of longitudinal maneuvers?* Section 3.3 provides a discussion of the results provided in this Chapter and the implications for the subsequent work in this thesis.

## 3.1. Prediction

This section aims to provide a preliminary analysis on what data could be useful for the purpose of longitudinal maneuver prediction in the driving scenario at hand. It will start with a description of the scenario and data set in Section 3.1.1. Section 3.1.2 aims to describe the relation between the chosen velocity and environment features. Lastly, the possibility of using driver control inputs for motion cueing is discussed in Section 3.1.3.

### 3.1.1. Dataset

The provided set of driving simulator data consists of 154 csv-files, logged during an experiment in a static driving simulator [10]. Participants are asked to drive a predefined trajectory on a rural two-lane road as they would do during everyday-driving without time pressure and while respecting the road traffic regulations. No secondary tasks are performed. The data set contains logged time traces of vehicle states, control inputs and information on the driving environment, such as the road curvature and the offsets from the vehicle to the lane edges. The road is driven in both directions. Traffic is only present on the opposite driving lane. The vehicle model used is a 2018 BMW 530i with a 4 cylinder 2.0L engine. Figure 3.1 shows the trajectories and legal speed limit changes in both directions. Sections in which sustained longitudinal acceleration occurs are numbered and described in Table 3.1. This numbering will be used throughout the current report.

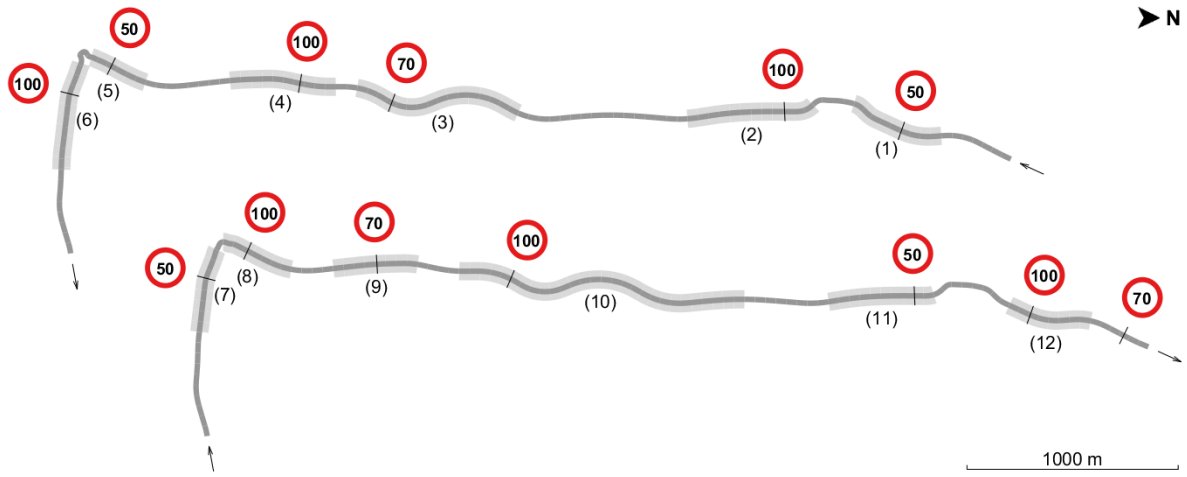


Figure 3.1: Course including legal speed limits and marked sections in which sustained acceleration/deceleration occurs.

Table 3.1: Sections in which sustained acceleration/deceleration occurs.

| Index | Description | Legal speed limit change |
|---|---|---|
| (1) | Entering village | 100 → 50 |
| (2) | Leaving village | 50 →100 |
| (3) | Sharp turn, reduced speed limit | 100 → 70 |
| (4) | Sharp hilltop, increased speed limit | 70 →100 |
| (5) | Approaching roundabout | 100 → 50 |
| (6) | Leaving roundabout | 50 →100 |
| (7) | Approaching roundabout | 100 → 50 |
| (8) | Leaving roundabout | 50 →100 |
| (9) | Sharp hilltop, reduced speed limit | 100 → 70 |
| (10) | Sharp turn, increased speed limit | 70 →100 |
| (11) | Entering village | 100 → 50 |
| (12) | Leaving village | 50 →100 |

The data set contains long drives spanning the whole scenario, as well as shorter drives. All drives that do not completely span one of the two trajectories shown in Figure 3.1 are removed from the dataset, so as to make sure that no start-up and stopping procedures are included, as these are considered exceptions and are therefore not included in the initial scope of this thesis. Hereafter, cleaning is done based on the RMS difference between individual drives and an average of all drives at the same location. One drive is ignored, since its velocity diverged on average more than 15% from the average velocity. As can be seen in Figure 3.2, the removed drive contains speeding throughout a large part of the scenario. After cleaning, 21 drives to the south and 16 drives to the north remain.

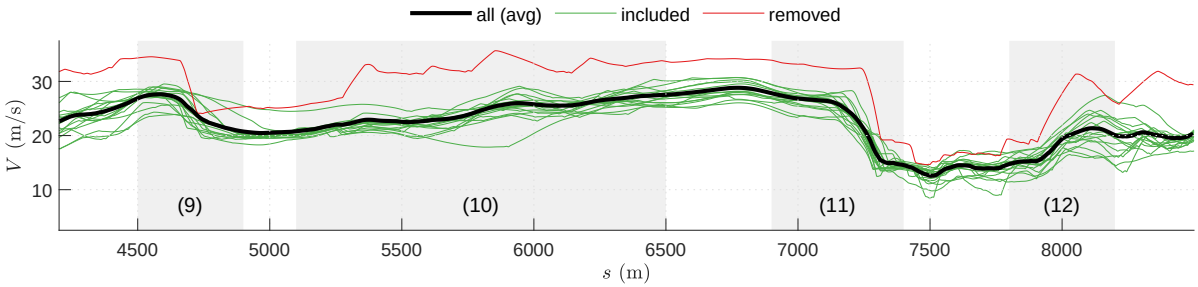


Figure 3.2: Cleaning of rides to the north, based on the RMS deviation from the average drive.

### 3.1.2. Velocity choice

In this section, aspects of the scenario will be related to the velocity choice. As described in Section 2.2.2, velocity choice with respect to road curvature has been studied extensively. The scenario as shown in Figure 3.1, contains several curves. The local road curvature at the middle of the lane, $\kappa$, is an attribute of the data and is available at each time step. It is defined as $1/R$, where $R$ is the local road radius in meters. Per definition, left curves have a negative curvature, and right curves have a positive curvature. The logged road curvature as available in the simulation environment is not smooth and contains many outliers. As this seems unrealistic, the curvature is recalculated using the $x-$ and $y-$coordinates of the road.[1] Figure 3.3 shows the logged curvature as well as the recalculated curvature, for a part of a drive. The recalculated curvature will be used in further analysis in this chapter.

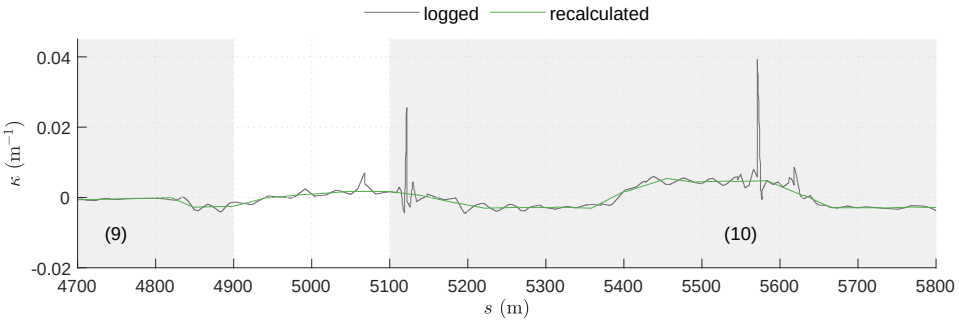


Figure 3.3: Logged and corrected road curvature of a part of a drive to the north.

As discussed in Section 2.2.2, the two-thirds law is used to relate the maximum velocity to the road radius for a real driving scenario. Figure 3.4 shows the velocity plotted against the road radius for all data points of the current data set, on a log-log scale. In contrast to Bosetti et al.'s data [34], one can observe a step-wise increase of velocity against curve radius for the current data set. This could be a result of the lack of variation of curves throughout the data set. The levels of 9, 16 and 31 m/s correspond to the maximum velocities driven on the roundabout, in the village and at the rural road when speed is unrestricted. When comparing the two-thirds law with $\alpha = 3.34$, corresponding to Bosetti et al.'s median driver, one sees that in the current data set, the chosen velocity is often higher. This can be the result of that the data set is obtained using a fixed-base simulator, whereas it is known that drivers drive faster in fixed-base simulators than when driving a real vehicle [6]. For this reason, the two-thirds law is re-fitted per driver, to account for 99.9% of the driver's data points. The resulting values for $\alpha$ range between 3.97 and 4.91, with a median of 4.36.

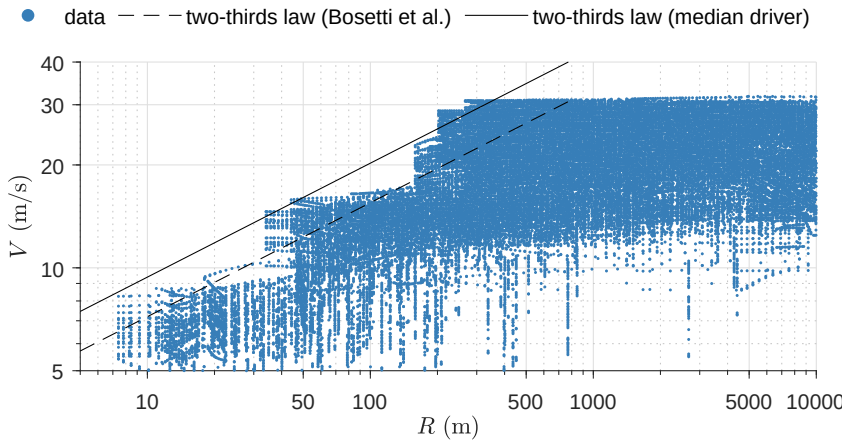


Figure 3.4: Velocity against road curvature, fitted with the two-thirds law.

[1] https://nl.mathworks.com/matlabcentral/fileexchange/32696-2d-line-curvature-and-normals

When plotting the maximum two-thirds law velocity for the median driver together with the actual velocity and legal speed limits as in Figure 3.5, one can see that for the current scenario, the maximum velocity seems to be determined more by the legal speed limit, than by road curvature. Clear exceptions are the roundabout (sections 5, 6, 7 and 8) and a curve in section 10.

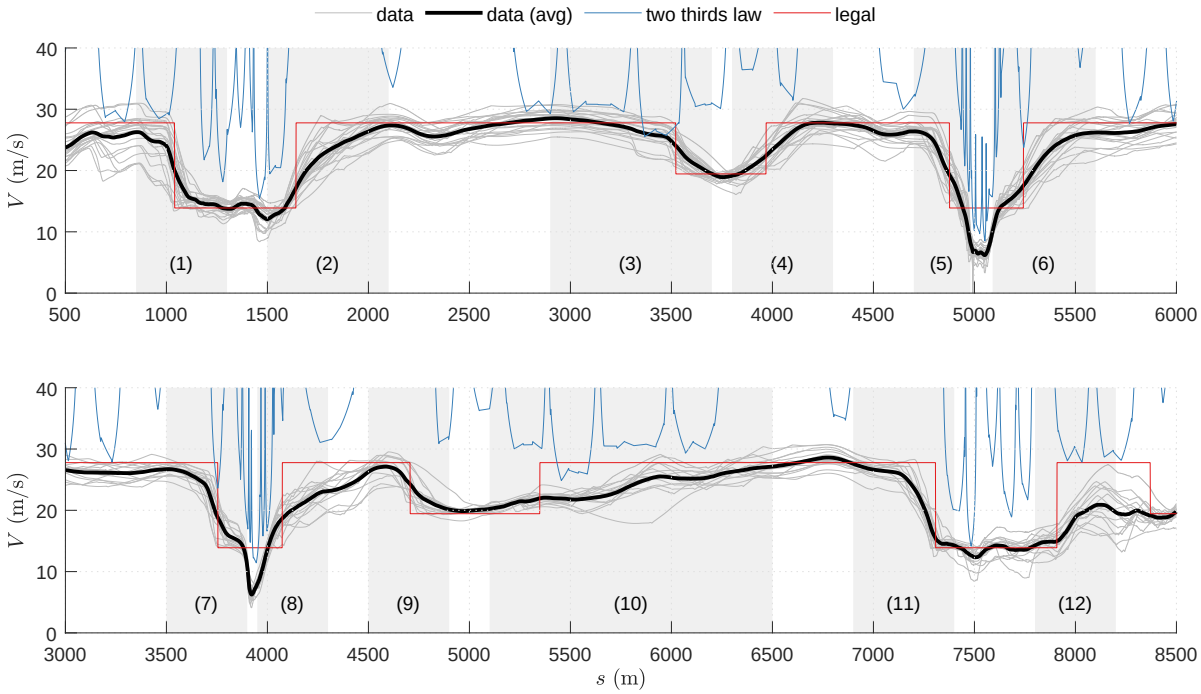


Figure 3.5: Chosen, two-thirds law and legal velocities for the drives to the south (top) and north (bottom).

Since in the current scenario, legal speed limits are the most defining factor for the velocity choice, it would be of interest to know where and when drivers anticipate to these. The current scenario only contains 4 speed limit signs that are not obstructed from sight in the preceding 200 m of road. These signs, located in sections 4, 5, 9 and 11, are examined to obtain insights into when the driver starts anticipating. Figure 3.6 shows the velocity and acceleration, for each driver and averaged over all drivers, plotted against the distance relative to the speed limit change. For the current analysis, acceleration/deceleration is detected when the magnitude of acceleration is larger than 0.5 m/s$^2$.

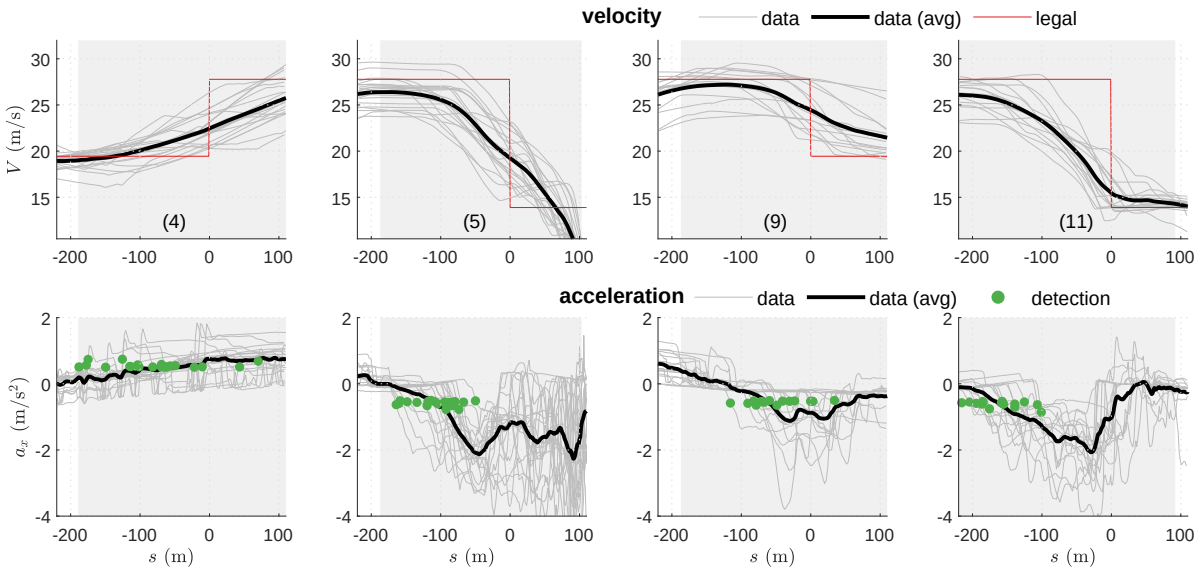


Figure 3.6: Detection of anticipation to changing legal speed limits.

The left plot in Figure 3.7 shows box plots of the detected anticipations to speed limits per location (4, 5, 9 and 11) and altogether. On average, anticipations occur at 99 m before a speed limit sign. Braking happens earlier in sections 5 and 11, which could be the result of the larger change in the legal speed limits. General conclusions like these can however not be drawn, since the amount road sections in this analysis is limited, and other factors could play a role. As described in Chapter 2, theories used to model drivers often assume that the driver makes use of time thresholds when controlling the vehicle. It would therefore be of interest to examine at what time anticipation to changes in speed limits takes place. Moreover, a constant look-ahead time would be preferred when using PP, since it could assure enough time to preposition the platform. The box plot on the right in Figure 3.7 shows the time at which the maneuver starts with respect to the time at which the speed limit sign is reached. On average, anticipation occurs 4.6 s before.

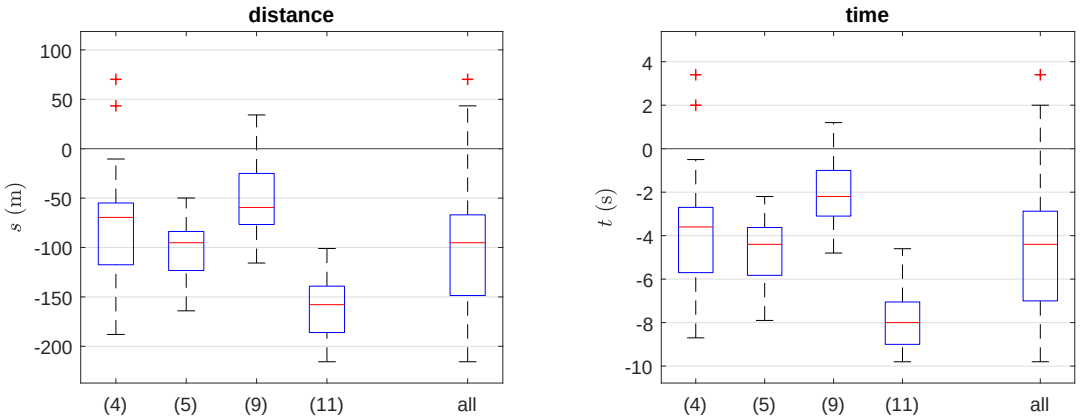


Figure 3.7: Distance and estimated time at which anticipation to changing legal speed limits is performed.

Whether look-ahead distance or look-ahead time is a more consistent predictor, can be assessed by normalizing the standard deviation using the absolute mean, yielding the coefficient of variation ($CV$). The means, standard deviations and $CV$s for both variables are shown in Table 3.2. The lower $CV$ of distance w.r.t. time, indicates that for the four maneuvers in the current analysis, time is not more consistent than distance. Figure 3.5 has shown that the velocity at which a maneuver is driven, differs per maneuver and per driver. However, faster drivers do not necessarily anticipate at a larger distance ahead of the road sign.

Table 3.2: Mean, standard deviation and coefficient of variation of the distance and time at which anticipation for speed limit changes occurs in sections 4, 5, 9 and 11 together.

| | $\mu$ | $\sigma$ | $CV$ |
|---|---|---|---|
| $s$ | -99 m | 60 m | 0.60 |
| $t$ | -4.6 s | 2.9 s | 0.63 |

### 3.1.3. Driver control inputs

This section provides a preliminary assessment of the suitability of control inputs for PP. Since the aim is to predict longitudinal acceleration, the accelerator- and brake pedals will be looked at. That an input on the accelerator yields an acceleration, and an input on the brake pedal results in a deceleration, is evident. However, to be useful for PP, it is of interest to know what time in advance a maneuver can be predicted. Moreover, it would be of interest to know whether the deflection rate could be of added value. Figure 3.8 shows the acceleration and pedal inputs during an acceleration and braking maneuver in sections 4 and 7 for one exemplary file. Generally, other drivers show comparable behavior. Again, acceleration and deceleration are detected at the first instance where the acceleration is larger than 0.5 $m/s^2$, or smaller than -0.5 $m/s^2$, respectively. The time on the $x$-axis is shown relative to the time of the detected maneuver, so as to show the offset at which pedal inputs are given.

The acceleration maneuver in the left of Figure 3.8 clearly results from the increased accelerator input. The vehicle accelerates before the desired accelerator position is reached. In conclusion, basing predictions solely on the accelerator position will not provide much time to preposition the platform. The accelerator's position is increased starting at 0.7 s before the vehicle accelerates, which means that an earlier detection could be possible when including the pedal velocity.

When looking at the braking maneuver in the right of Figure 3.8, one can see that the input on the brake pedal only occurs shortly before the vehicle accelerates (i.e., 0.2 s before the threshold of -0.5 m/s$^2$ is reached). However, the braking maneuver could for the current drive be detected earlier when looking at the accelerator pedal, which is released already 5 s before the vehicle is decelerating. When speaking in terms of the speed control phases as done by Gruppelaar et al. [66], the braking phase, in which a brake pedal is pushed, is usually preceded by a deceleration phase, in which the accelerator is released.

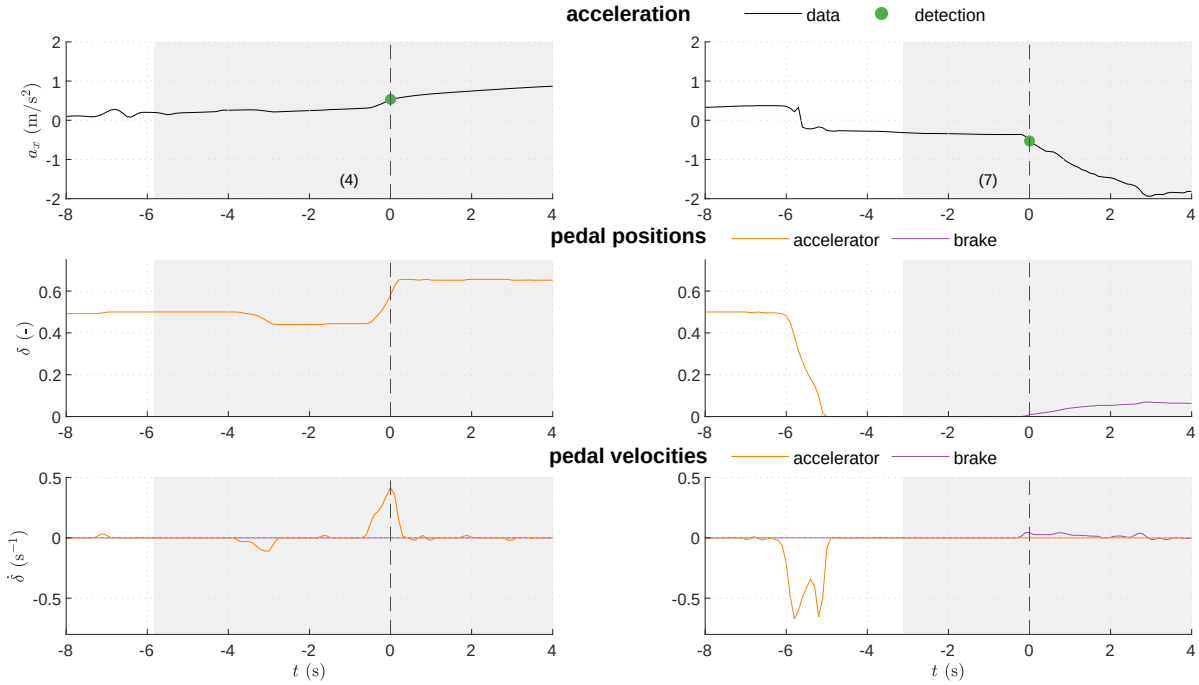


Figure 3.8: Pedal positions during accelerating in section 4 (left) and braking in section 7 (right) for one driver.

The third control input, the steering wheel angle, is not likely to be of added value for predictions of longitudinal maneuvers in the scenario at hand, in which the driver has to follow a predefined trajectory and steering will thus be done so as to follow the predefined trajectory. In conclusion, road curvature as discussed in Section 3.1.2 would be a more suitable predictor, as it is known further in advance.

## 3.2. Prepositioning

In the current section, preliminary findings on PP for the driving scenario, MCA and simulator at hand are discussed. The classical washout filter-based MCA is described in Section 3.2.1. Section 3.2.2 discusses the performance of the acceleration and jerk limiter used to preposition the simulator imperceptibly. Section 3.2.3 assesses optimal PP in the hypothetical case a future maneuver is completely known beforehand.

### 3.2.1. MCA

The MCA used throughout this report, is a simple classical washout filter MCA that is previously used and described in the work of Ellensohn [80]. A graphical overview is provided in Figure 3.9. Linear scaling is applied. Vehicle accelerations are split into high and low frequency content by high- and low-pass filters, respectively. High-frequency content leads to simulator translation. Low-frequency content leads to tilt coordination. No tilt rate limiter is present, which is overcome by using low cut-off

frequencies and gains on the tilt channel. The simulator position and orientation outputs of the MCA are sent through a workspace limiting block that ensures smooth behavior in case the they exceed the simulator's workspace.

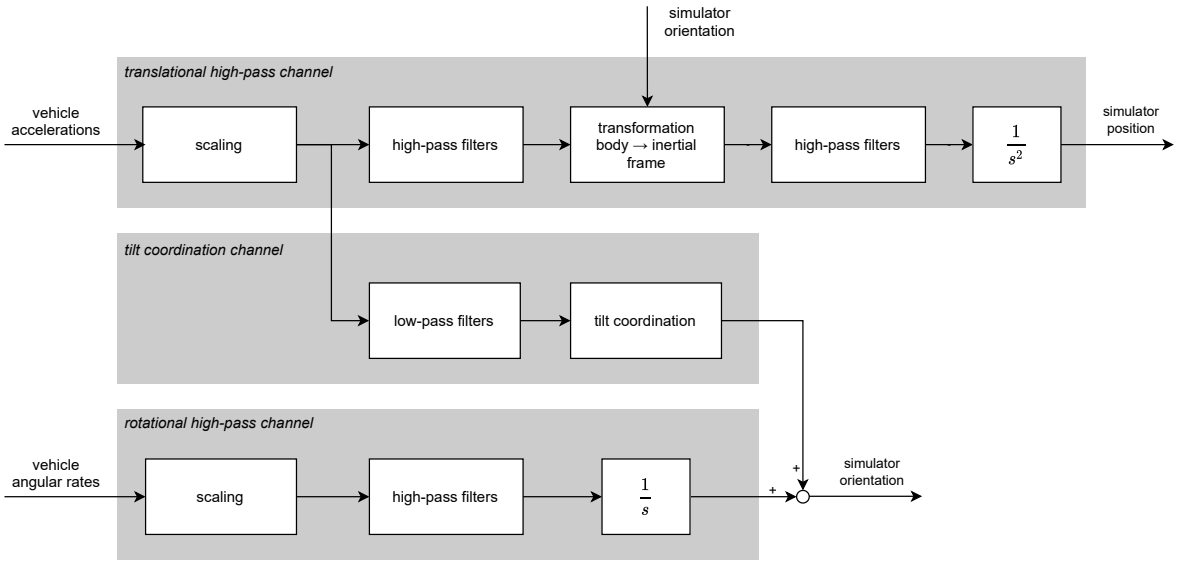


Figure 3.9: Schematic overview of the classical washout filter MCA used throughout this study.

### 3.2.2. Prepositioning controller

As discussed in Chapter 1, one can distinguish between the logic that determines a PP reference position from available information in the driving simulation environment, and the controller used to reached this desired position. Schematically, the prepositioning subsystem in coorporation with the MCA can be as in Figure 3.10. Note that the PP output is added to the MCA output, before being sent through the workspace limiting block, in order to ensure smooth behavior in case the combined output exceeds the workspace limits.

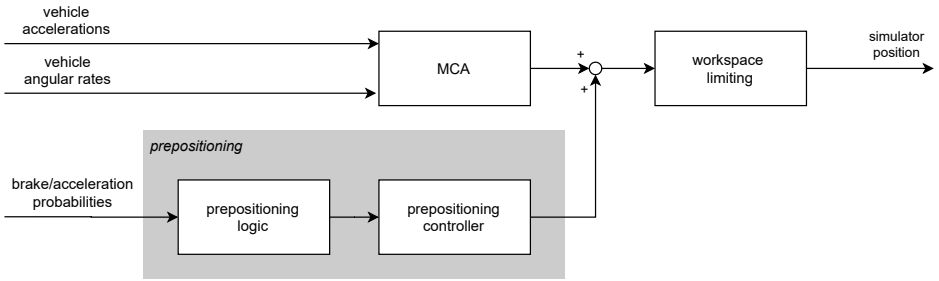


Figure 3.10: Schematic overview of the prepositioning subsystem.

The controller designed by Fischer [23] and applied for PP by Hansson & Stenbeck [12] is chosen, as it explicitly limits acceleration and jerk. A detailed description is given in Section 1.3. The acceleration and jerk limits for the controller are kept identical, but other parameters of the controller need to be tuned to the input signal. The magnitude of the uncontrolled PP signal depends on the workspace of the simulator. The small hexapod-based simulator used for the current analysis is described in detail in Section 4.3 and has an asymmetric workspace. When the platform is in its neutral position in all other DOFs, the extreme front and rear positions that it can reach are at 0.29 m and -0.36 m, respectively. A step input with a magnitude of 0.30 m will for now be used to tune the controller, as it covers a large part of the simulator's workspace. The parameters to be tuned are the inner loop gain $K$, and the $P$- and $D$-parameters of the $PD$-controller in the outer loop.

The controller has been tuned for the step input with the aim of reaching the desired position fast, without oscillations and with an overshoot that does not exceed the workspace boundaries. With the tuning parameters presented in Table 3.3, the response shown in Figure 3.11 is achieved. 95% of the final position is reached after 4.1 s. With an overshoot of 13%, the maximum excitation is 0.34 m. When the step input is applied, the jerk limit is directly reached, followed by the acceleration limit.

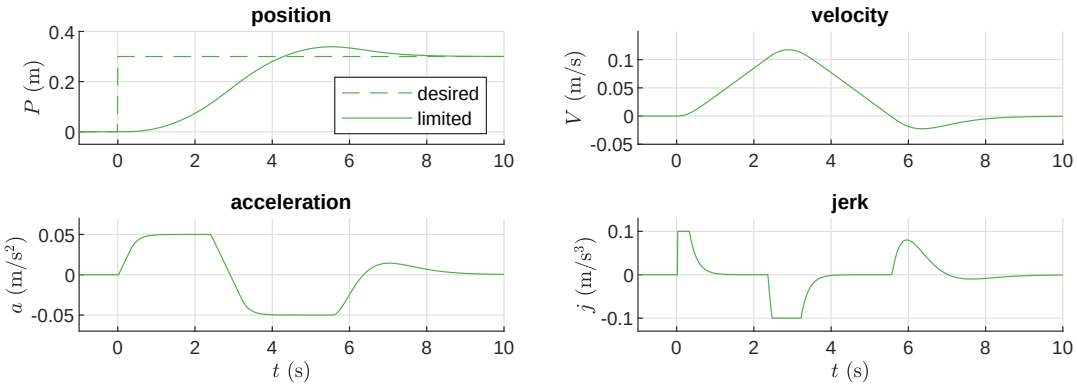


Figure 3.11: Step response of the prepositioning controller.

Table 3.3: Parameters of the prepositioning controller tuned for a step input of 0.3 m.

| Parameter | Value | Unit | Description |
|---|---|---|---|
| $a_{lim}$ | 0.05 | m/s$^2$ | acceleration limit |
| $j_{lim}$ | 0.1 | m/s$^3$ | jerk limit |
| $K$ | 5 | - | inner loop gain |
| $P_{PD}$ | 0.3 | - | $P$-value of the $PD$-controller |
| $D_{PD}$ | 1 | - | $D$-value of the $PD$-controller |

### 3.2.3. Oracle

In order to assess the potential effect of PP in combination with the MCA and simulator, PP is applied to a maneuver isolated from the data set. Perfect knowledge of the future maneuver (i.e., oracle) is assumed, so that it can optimally be anticipated. The maneuver is an acceleration from 47 to 104 km/h, of which the velocity and longitudinal acceleration of the vehicle are shown in Figure 3.12. For the sake of simplicity, vehicle motion other than surge acceleration is ignored and intensifying motion cueing will be done by means of increasing the translational surge gain, $K_x$. Alternatively, it could be opted to decrease the cut-off frequency of the high-pass filter for surge acceleration, $\omega_{w,trans,x}$, which would alter both the shape and the intensity of the cueing.

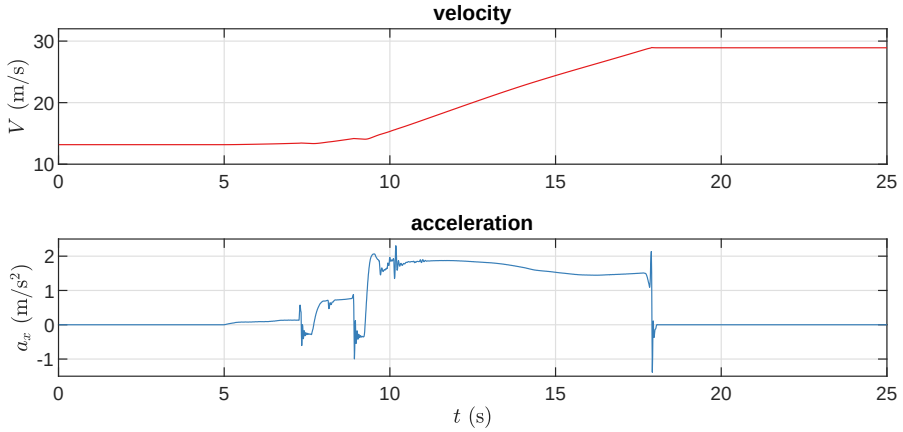


Figure 3.12: Velocity and acceleration of a pull-up maneuver after leaving a village.

The upper plot in Figure 3.13 shows the position output of the MCA without PP, together with the COW workspace limits as defined in Section 1.1.3. $K_x$ is increased to 0.34, which is the highest possible value that can be reached without exceeding the simulator's workspace. All other MCA parameters are taken from the parameter set that is tuned for the current scenario and can be found in Section III of the scientific paper in Part I of this report. Note that next to translational platform acceleration, tilt coordination is applied. In order to anticipate the maneuver, it could be opted to set the input of the PP controller to -0.30 between $t$ = 0 and 18 s, and 0 at any other time. As a result, the simulator's neutral position will be shifted, and a larger part of the simulator's workspace can be used. This is shown in the lower plot in Figure 3.13, where $K_x$ is increased to 0.74, to exploit the improved workspace usage.

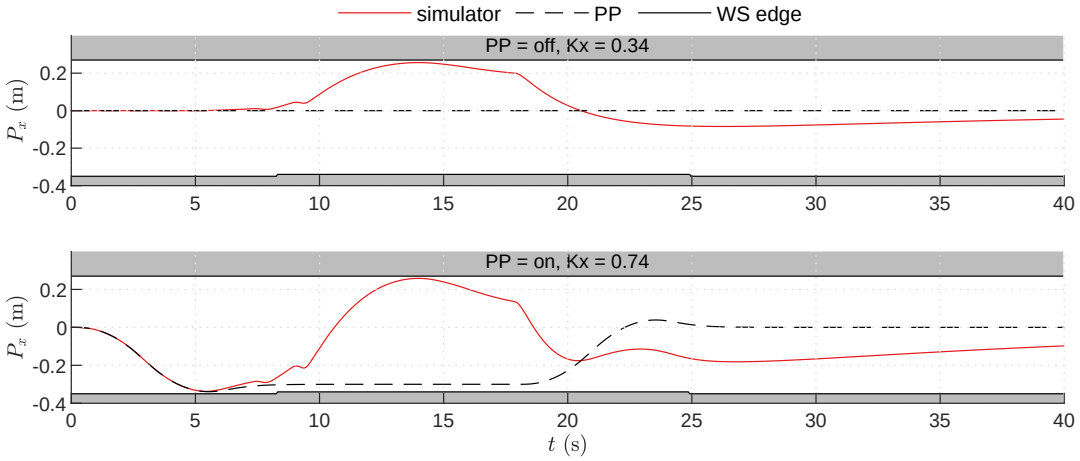


Figure 3.13: Simulator position with and without PP, with adapted gain settings.

Figure 3.14 shows the specific force in $x$-direction in the simulated vehicle and in the platform, for the previously described cases with and without PP. Although generally multiple phenomena occur simultaneously, one can clearly identify cues caused by the PP, translational cues of the MCA, tilt coordination cueing of the MCA, and false cues caused by the MCA. PP, denoted ①, consists of a small negative acceleration followed by a small positive acceleration, applied before the vehicle starts accelerating. When comparing the two MCA settings, no different perception is expected, due to the low magnitude of the acceleration and jerk of the prepositioning. The vehicle's acceleration consists of two stages, which are divided by a gear switch. The high-frequency content of both acceleration stages are cued by the platform by means of translation, denoted ②. Note that in the case where $K_x$ is increased, the magnitude of the translational acceleration of the platform increases. The lower frequency content is cued by means of tilt coordination, which is denoted ③. Since the MCA's parameters for tilt coordination are the same for both cases, the specific force due to tilting remains unchanged. At the end of the maneuver, the filters cause false cues, denoted ④. It can be seen that with a higher $K_x$, the magnitude of false cues is increased.

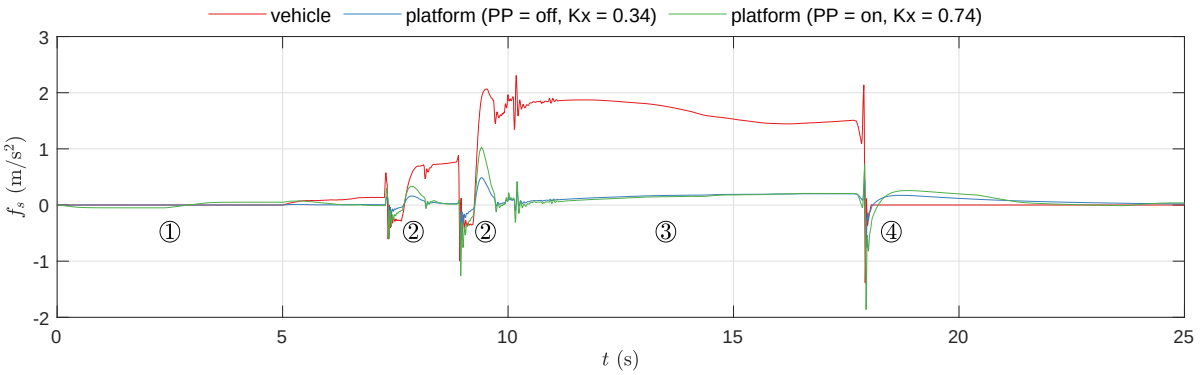


Figure 3.14: Specific force of the vehicle and simulator with and without PP, with adapted gain settings.

## 3.3. Discussion

In the current chapter, a preliminary analysis is made on what information can be of use to make predictions on longitudinal driving behavior and on how predictions could be exploited using PP. When using Bosetti et al.'s [49] two-thirds law to relate road curvature to velocity choice, it is found that it can be used to explain anticipation to some curves. However, for the available data, the velocity choice seems to be more related to the legal speed limits. The location and time at which anticipation to changes in the legal speed limits occurs are examined for four sections. When looking at the location, it is found that on average, anticipation occurs 99 m before the speed restriction sign. Looking at the timing, it is found that on average, anticipation takes place 4.6 s before reaching a speed limit sign. Clearly, road signs will have to be incorporated in a prediction model before they are reached. The coefficient of variation is calculated for both measures in order to examine consistency, where it is found the consistency is comparable. The speed limit at a time interval ahead will be evaluated as input for a prediction model in the remainder of this project, so as to ensure enough time for PP when driving at a higher velocity. It should be noted that during any realistic driving scenario, including the one at hand, more factors play a role than discussed here. The width and longitudinal slope of the road are known to play a role in velocity choice [53, 81]. However, these are assumed to be less relevant for the current scenario and therefore not taken into account in this project.

Next to information from the scenario, driver control inputs could provide hints on future maneuvers. By means of examples, it is shown that the time derivative of the pedal position can be used to predict a maneuver slightly earlier compared to only using the pedal positions. Moreover, it is shown that the position of the accelerator pedal can be useful to predict deceleration, since drivers release it before pushing the brake pedal. When one would want to accurately relate pedal positions to (future) vehicle accelerations, the (non-linear) vehicle model and the slope of the road should be taken into account. However, for the sake of simplicity, these will for now not be taken into consideration.

As elaborated in Chapters 1 and 2, the use of information from the driving environment and control inputs in motion cueing is fairly limited, in contrast to the more advanced models used in the field of driver intention detection. In the current thesis, the aim will be to obtain improved cueing using prediction. Longitudinal driving behavior is highly unpredictable due to differences between drivers. This does not necessarily have to be a problem, since instead of basing PP on exact predictions of future accelerations, a probabilistic approach might be suitable. Note that PP is only there to improve workspace management, while not providing any perceivable cues. As a next step, a model will be trained to identify the probability of a longitudinal driving maneuver continuously throughout a drive.

When choosing a model structure, the prediction accuracy is not the only criterion. As motion cueing is tuned for a driving scenario, simulator and use-case [82], the interpretability of any subsystem of the MCA can improve its usability. Interpretability of a model is the degree to which a human can understand the cause of a decision [83]. The high performance that can be reached with advanced ML methods as described in Section 2.4 can come at the cost of high complexity and reduced interpretability. For this reason, it would be preferred to use a simpler model, such as regression. Logistical regression will be applied in the remainder of this project, as it is a straight-forward method to predict probabilities of categorical dependent variables from multiple independent variables [84]. As model inputs, (future) speed limits and control inputs will be used.

In case of perfect knowledge on a future acceleration maneuver, an 118% increase in gain can be obtained for the onset of the movement with the small hexapod-based simulator that will be used throughout this thesis. Other ways to exploit the improved workspace usage exist, but are for now not taken into consideration. 4.1 s are needed to reach 95% of the 0.3 m PP without perceivable false cues. The prediction model that will be trained in the remainder of this project, will thus require a look-ahead of at least 4.1 s, so as to be able to finish PP before a predicted driving maneuver commences.

# 4

# Preliminary experiment design

This chapter describes the design of the human-in-the-loop experiment that will be performed at the BMW Group in Munich. The purpose of this experiment is to investigate the effectiveness of the proposed PP design. The research questions and hypotheses can be found in section 4.1. Section 4.2 provides a description of the participant group. The apparatus used for this experiment, a hexapod-based dynamic driving simulator, will be discussed in section 4.3. The conditions and measurements are elaborated in sections 4.4 and 4.5, respectively. Section 4.6 describes the procedures that will be followed during the experiment, including a detailed planning. The methods used to analyze the measurements are explained in section 4.7.

## 4.1. Research questions and hypotheses

The research questions (as posed in section ) that will be answered with the experiment, are:

- *RQ2b*: What is the effect of **PP** based on predictions of longitudinal maneuvering on the **workspace usage** of a hexapod-based driving simulator?
- *RQ2c*: What is the effect of **PP** based on predictions of longitudinal maneuvering on **motion cueing quality** as perceived by driving simulation participants?

**PP** itself is not likely to improve the motion cueing quality, as the goal of **PP** is to provide the simulator with a position imperceptibly. Only when improved **workspace usage** is exploited by changing the MCA tuning, improved **motion cueing quality** is expected. The independent variables are thus split into PP (on/off) and the MCA's surge motion cueing parameters (conservative/moderate tuning). Increasing surge motion will be done by re-tuning the classical washout filter MCA, in which the aim is to provide optimal motion cueing within the workspace of the hexapod, including a safety margin equal to 5% of the actuator deflection. Reviewing tuning sets will be done subjectively by experts. The methods that can be used to increase the surge motion are increasing the gain and decreasing the cut-off frequency (high-pass filter).

The dependent measures used to describe the **motion cueing quality**, are the absolute difference (AD) and the perceived motion incongruence (PMI). The AD is an objective motion cueing criterion which represents the error between the vehicle dynamics and the simulator dynamics. It is defined as the area of the error signal divided by the area of the reference signal [30]. The PMI is defined as the perceived deviation between expected vehicle motion and perceived simulator motion [85]. The dependent measure used to describe the **workspace usage** is the minimum workspace margin in $x$-direction. The workspace margin is the distance between the platform's center and the edge of the COW as described in Section 1.1.3. The simulator will make excursions outside of the center in order to provide motion cueing to the participants. Classical washout filter MCAs are generally tuned so as to keep a workspace margin at the anticipated worst-case vehicle acceleration [8]. Ranges of possible tuning parameters are thus constrained by the worst-case scenario. The minimum workspace margin for each drive provides an indication of how much more motion could be given to the platform.

The following hypotheses are formulated and will be tested with the experiment, based on the findings in literature described in Chapters 1 and 2 and results of simulations in Chapter 3:

- *H1:* Simultaneously adding **PP** and increasing **surge motion** decreases the **AD** and **PMI**.
- *H2:* Adding **PP** increases the **minimum workspace margin**.
- *H3:* Adding **PP** does not have an effect on the **AD** and the **PMI**.
- *H4:* Increasing **surge motion** decreases the **AD** and the **PMI**.

## 4.2. Sample description

The participant group will consist of around 50 BMW employees, in the possession of a valid driving license. Since motion perception is known to be correlated with gender and age [86], a diverse participant group will be aimed for. A within-subjects design will be used, in order to account for differences between individuals and in order to require less participants overall. Participants will not be compensated for their participation apart from their regular salary. They should give informed consent before taking part in the experiment. The Human Research Ethics Committee of Delft University of Technology has approved the procedures (application ID: 1103).

## 4.3. Apparatus

A Cruden AS1 hexapod-based driving simulator will be used in the experiment (see Figure 4.1). Motion is provided by a 6 DOF motion system with 400 mm stroke actuators. The simulator's workspace maxima and dynamic capabilities of the simulator are provided in Table 4.1. High frequency vibrations from the engine and road surface are provided using a separate vibration system. Visuals are shown on three 42" screens.[1] The steering wheel provides haptic feedback. Participants will be provided with sound from the engine, the vehicle's aerodynamics and other vehicles. The climate within the simulator room is controlled.

Figure 4.1: The Cruden AS1 driving simulator.[1]

Table 4.1: Dynamic capabilities of the Cruden AS1 driving simulator.

| | min. position | max. position | max. velocity | max. acceleration |
|---|---|---|---|---|
| $x$ | -0.37 m | 0.36 m | 0.6 m/s | 11 m/s$^2$ |
| $y$ | -0.38 m | 0.38 m | 0.6 m/s | 11 m/s$^2$ |
| $z$ | -0.26 m | 0.26 m | 0.5 m/s | 12 m/s$^2$ |
| $\phi$ | -23° | 23° | 40 °/s | 500 °/s$^2$ |
| $\theta$ | -23° | 26° | 40 °/s | 500 °/s$^2$ |
| $\psi$ | -22° | 22° | 40 °/s | 700 °/s$^2$ |

## 4.4. Experimental conditions

Participants will drive the trajectory shown in Figure 4.2 six times, with varying motion conditions. A detailed description of the numbered sections is given in Section 3.1.1. An overview of the conditions can be found in Table 4.2. Condition C1 is included as a baseline, against which the effects of adding PP and increasing surge motion will be tested. In condition C1, the surge motion will be tuned such that the simulator workspace is almost fully exploited, except for a safety margin to account for inter-driver variability. In conditions C2 and C3, the developed PP is active. In condition C2, the MCA motion cueing parameters will be kept unchanged w.r.t. the baseline condition, so as to be able to examine the effects of the PP by itself. In condition C3, surge motion will be intensified so as to exploit the increased simulator workspace made available by adding PP. Again, surge motion will be tuned such that the simulator workspace is almost fully exploited. Each of the three motion conditions will be driven two times per participant. A randomized latin square design will be used to sequence the experiment conditions differently per participant, in order to ensure a fair comparison. Participants will be briefed to drive as they would do in real life. Traffic will be present only on the opposite lane.

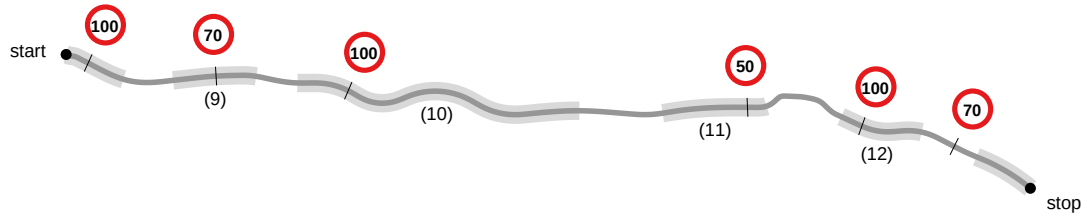


Figure 4.2: Experiment course including legal speed limits and marked sections in which sustained acceleration/deceleration occurs.

Table 4.2: Experimental conditions.

| Condition | Prepositioning | Surge motion |
|---|---|---|
| C1 | off | conservative |
| C2 | on | conservative |
| C3 | on | moderate |

## 4.5. Measurements

The PMI will be collected by means of post-hoc rating (PR) and section-wise post-hoc rating (SPR). In PR, participants are asked to orally rate the PMI on a scale from 0-10, where 10 indicates high PMI, thus indicating unrealistic motion. SPR is a novel measurement method, in which oral ratings similar to those in PR are given at the end of each section of the driving scenario as announced by the experiment leader [80]. The sections used for SPR are sections 9-11 as described in Table 3.1 in Section 3.1.1. Participants will be asked to only rate the longitudinal motion, since this is the only aspect that will change per condition. In order to obtain qualitative insights into the motion cueing provided in the three conditions, the following motion cueing questionnaire will be asked using 5-point Likert scales for agreement (*strongly disagree, disagree, undecided, agree, strongly agree*) and frequency (*never, rarely, sometimes, often, always*) [87]:

- *Q1:* Accelerating felt realistic. (agreement)
- *Q2:* Braking felt realistic. (agreement)
- *Q3:* Motion was too weak. (agreement)
- *Q4:* Motion was too strong. (agreement)
- *Q5:* No motion was provided at times motion was expected. (frequency)
- *Q6:* Motion was provided at times no motion was expected. (frequency)

[1] https://www.cruden.com/automotive-driving-simulators/

The minimum workspace margin will be calculated post-hoc from the recorded time traces of the simulator position using inverse kinematics as described in Section 1.1.2. A graphical representation of the forward and backward workspace margins for an exemplary position and orientation are shown in Figure 4.3. The minimum of both margins is defined as the minimum workspace margin.

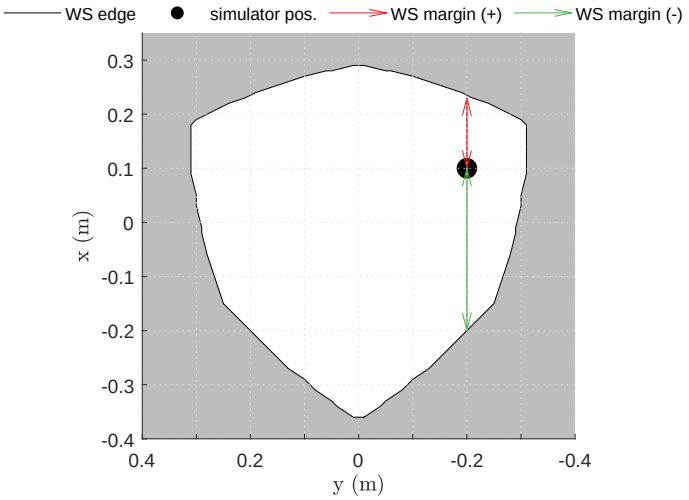


Figure 4.3: Forward (+) and backward (-) workspace margins for $[x\ y\ z] = [0.1\ -0.2\ \ 0]$ m and $[\phi\ \theta\ \psi] = [0\ 0\ 0]$ rad.

## 4.6. Procedure

An overview of the procedure can be found in Table 4.3. Participants will start filling out the informed consent form. Hereafter, instructions will be given at the desk and at the simulator, including safety instructions. The first drive will be a training drive, in which the participant will be able to get used to driving the simulator and reviewing motion queing using SPR, PR and the motion cueing questionnaire. Hereafter, the participant will drive the same trajectory six times. Note that the order differs per participant, using the randomized latin square. While driving, the participant will do SPR. At the end of each drive, participant will provide PR and fill out the motion cueing questionnaire. After the last drive, there is time for a Q&A. A buffer of 35 minutes is planned between experiments in order to ventilate the room, clean the setup and solve technical failures.

Table 4.3: Planning of the experiment procedures.

| **Procedure** | **Duration (minutes)** | **Notes** |
|---|---|---|
| Pick-up and welcome | 5 | |
| Instructions at desk | 5 | incl. informed consent |
| Instructions in simulator | 5 | incl. safety instructions |
| Familiarization drive | 8 | |
| Measurement drive (1) | 7 | incl. questionnaires |
| Measurement drive (2) | 7 | incl. questionnaires |
| Measurement drive (3) | 7 | incl. questionnaires |
| Break | 5 | |
| Measurement drive (4) | 7 | incl. questionnaires |
| Measurement drive (5) | 7 | incl. questionnaires |
| Measurement drive (6) | 7 | incl. questionnaires |
| Q&A | 5 | |
| Departure | 5 | |
| **Sum** | **80** | |

## 4.7. Data analysis

Statistical significance will be tested for the four hypotheses stated in Section 4.1. In every hypothesis, two motion conditions are compared. Since the experiment is within-subjects, a dependent t-test will be performed for data that meet the assumptions for parametric tests, whereas a Wilcoxon signed-rank test will be performed for data that do not meet these assumptions.

The minimum workspace margin, AD and PMI are considered interval data. The Lilliefors-test will be used to assess normality of the samples. In case normality holds, the paired t-test will be performed to test statistical significance of results. In case the samples are not normally distributed, the Wilcoxon signed-rank test will be performed. The Likert data from the questionnaire (Q1-Q6) are considered ordinal data, implying that a non-parametric test will be used, regardless of the normality of the samples. Thus, the Wilcoxon signed-rank test will be performed for the questionnaire data.

# 5

# Preliminary conclusions

The objective of this research is to assess the suitability of driver inputs and information from the simulation environment as triggers for PP of a dynamic driving simulator. In order to achieve this, a prediction model will be established from driving data, and prepositioning rules will be evaluated as extension to a classical washout filter MCA for a small hexapod-based simulator. As a first step, this preliminary thesis report discusses literature relevant to answer *RQ1: To what extent can longitudinal maneuvers be predicted in a driving simulation environment?* and *RQ2: To what extent can motion cueing quality of a classical washout filter MCA be improved using prepositioning based on predictions of longitudinal maneuvers?* Moreover, a preliminary analysis of data from previously recorded simulator drives is presented in this report. Together with the literature review, this analysis forms the basis for the PP algorithm that will be designed and evaluated later.

In contrast to simpler tasks usually described in control-theoretic modeling, the desired longitudinal response in real driving can have many forms. Real world driving scenarios generally consist of a multitude of features that form the basis for the velocity choice. The complexity of the driving scenario, combined with a high inter-driver variability, makes longitudinal driving behavior highly unpredictable. This is probably the reason that predictions in the field of driving simulation described in literature are fairly limited. In classical washout filter-based MCAs, predictions can be used by means of PP. A simulation has shown that for a small hexapod-based driving simulator, the gain of the translational $x$-acceleration can be increased with 118% in the hypothetical case a pull-up maneuver is completely foreseen. However, the only PP model that is fully described in literature assumes that it is not possible to predict whether acceleration or braking will occur and takes both possibilities into account at any time. Meanwhile, novel MPC-based MCAs depend on predictions of future vehicle movement, but as of now, prediction windows are short and highly relevant features of the environment such as road curvature and speed limits are not taken into account.

A preliminary data analysis is done to deduce how drivers choose their velocity in a driving scenario provided by BMW, which contains a rural area including a small village and roundabout. It is found that for this scenario, the legal velocity restrictions are leading. Road curvature only plays a role at a few locations. When a sign indicating a legal velocity restriction change is not obstructed from sight, anticipation occurs on average 4.6 s before the sign is reached, indicating that preview information should be taken into account when predicting longitudinal maneuvering. In a case study of one drive, it is shown that control pedal positions can also be valuable predictors. Especially the accelerator pedal is promising, as it is in many cases released a long time before a braking maneuver is performed.

In the remainder of this project, features of the environment and control inputs will be used to train a probabilistic model. A suitable candidate could be multinomial logistical regression, as it can handle multiple inputs to predict multiple outputs categories, with a low model complexity. Multiple combinations of predictors will be compared. Out of the predicted maneuvers, ideal PP will be calculated. The logic that transforms predictions to an ideal PP position will still have to be decided, based on the characteristics of the prediction model. The ideal PP position will be reached by the simulator using an

acceleration- and jerk limiter, to prevent false cues. Simulations presented in this preliminary thesis report have shown that a PP position that uses the majority of the workspace of the small hexapod-based simulator can be reached in 4.1 s. One thus needs a larger look-ahead in order to be able to finish PP before a maneuver takes place. The final implementation will be tested in a human-in-the-loop experiment of which the set-up is described in this report, to investigate the effectiveness of the workspace usage by the PP algorithm and the potential benefit in terms of motion cueing quality.

With an increasing amount of use cases for driving simulation, comes an increased relevance to obtain the most realistic motion feedback possible for a motion platform. Since the limited workspace of a simulator makes it impossible to exactly replicate the motion of a simulated vehicle, improving workspace usage can yield possibilities for motion cueing improvement. In the current thesis, this will be demonstrated using PP in combination with a classical washout filter-based algorithm, which is often used in driving simulation for its simplicity. Moreover, novel MPC-based MCAs use predictions of future maneuvers and could thus benefit from findings in the current thesis.

# Bibliography


[1] Van Driel, C. J., Hoedemaeker, M., and van Arem, B. (2007). Impacts of a Congestion Assistant on driving behaviour and acceptance using a driving simulator. *Transportation Research Part F: Traffic Psychology and Behaviour*, 10(2):139–152. ISSN 13698478. doi:10.1016/j.trf.2006.08.003.

[2] Brandenburg, S. and Skottke, E. M. (2014). Switching from manual to automated driving and reverse: Are drivers behaving more risky after highly automated driving? *2014 17th IEEE International Conference on Intelligent Transportation Systems, ITSC 2014*, pages 2978–2983. doi: 10.1109/ITSC.2014.6958168.

[3] Seeliger, F., Weidl, G., Petrich, D., Naujoks, F., Breuel, G., Neukum, A., and Dietmayer, K. (2014). Advisory warnings based on cooperative perception. *IEEE Intelligent Vehicles Symposium, Proceedings*, (Iv):246–252. doi:10.1109/IVS.2014.6856479.

[4] Hock, P., Kraus, J., Babel, F., Walch, M., Rukzio, E., and Baumann, M. (2018). How to design valid simulator studies for investigating user experience in automated driving - Review and hands-on considerations. *Proceedings - 10th International ACM Conference on Automotive User Interfaces and Interactive Vehicular Applications, AutomotiveUI 2018*, (September):105–117. doi:10.1145/3239060.3239066.

[5] Siegler, I., Reymond, G., Kemeny, A., and Berthoz, A. (2001). Sensorimotor integration in a driving simulator: contributions of motion cueing in elementary driving tasks. *Proceedings of the Driving Simulation Conference*, (September):21–32.

[6] Correia Grácio, B. J. (2013). *The effects of specific force on self-motion perception in a simulation environment*. ISBN 978-94-6203-467-9.

[7] Aykent, B., Merienne, F., Guillet, C., Paillot, D., and Kemeny, A. (2014). Motion sickness evaluation and comparison for a static driving simulator and a dynamic driving simulator. *Proceedings of the Institution of Mechanical Engineers, Part D: Journal of Automobile Engineering*, 228(7):818–829. ISSN 09544070. doi:10.1177/0954407013516101.

[8] Garrett, N. J. I. and Best, M. C. (2010). Driving simulator motion cueing algorithms–a survey of the state of the art. *Proceedings of the 10th International Symposium on Advanced Vehicle Control (AVEC)*, pages 183–188.

[9] Pitz, J.-O. (2017). *Vorausschauender Motion-Cueing-Algorithmus für den Stuttgarter Fahrsimulator*. Springer Vieweg. ISBN 9783658170325. doi:10.1007/978-3-658-17033-2.

[10] Parduzi, A., Venrooij, J., and Marker, S. (2020). The Effect of Head-Mounted Displays on the Behavioural Validity of Driving Simulators. In *DSC 2020 Europe*, pages 125–132. Antibes.

[11] Chapron, T., Colinot, J.-p., and Peugeot-citroën, P. S. a. (2007). The new PSA Peugeot-Citroën Advanced Driving Simulator Overall design and motion cue algorithm. *DSC 2007 North America*.

[12] Hansson, P. and Stenbeck, A. (2014). *Prepositioning of driving simulator motion systems*. Ph.D. thesis, Chalmers University of Technology.

[13] Weiß, C. (2006). *Control of a Dynamic Driving Simulator : Time-Variant Motion Cueing Algorithms and Prepositioning*. Ph.D. thesis, Deutsches Zentrum für Luft- und Raumfahrt.

[14] Gough, V. and Whitehall;, S. (1962). Universal tyre test machine. In *International Automobile Technical Congress. Ninth. Proceedings, Institution of Mechanical Engineers*, pages 117–137.

[15] Stewart, D. (1965). A Platform with Six Degrees of Freedom. *Proceedings of the Institution of Mechanical Engineers*, 180(1):371–386. ISSN 0020-3483. doi:10.1243/pime_proc_1965_180_029_02.

[16] Conti, J. P., Clinton, C. M., and Zhang, G. Workspace variation of a hexapod machine tool.

[17] Kurutas, S. (2006). *Modellierung der Dynamik eines Hexapods*. Ph.D. thesis, Universität Duisburg-Essen.

[18] Merlet, J.-p. and Sophia-antipolis, C. (2008). Springer Handbook of Robotics. *Springer Handbook of Robotics*, (May 2014). doi:10.1007/978-3-540-30301-5.

[19] Merlet, J. P. (1995). Determination of the orientation workspace of parallel manipulators. *Journal of Intelligent & Robotic Systems*, 13(2):143–160. ISSN 15730409. doi:10.1007/BF01254849.

[20] Pitz, J., Rothermel, T., Kehrer, M., and Reuss, H. (2016). Predictive motion cueing algorithm for development of interactive assistance systems. In *Internationales Stuttgarter Symposium*, pages 213–226. doi:10.1007/978-3-658-13255-2_86.

[21] Benson, A. J., Spencer, M. B., and Stott, J. R. R. (1986). Thresholds for the detection of the direction of whole-body, linear movement in the horizontal plane. *Aviation Space and Environmental Medicine*, 57(11):1088–1096. ISSN 00956562.

[22] Grant, P. R. and Haycock, B. (2008). Effect of jerk and acceleration on the perception of motion strength. *Journal of Aircraft*, 45(4):1190–1197. ISSN 00218669. doi:10.2514/1.33757.

[23] Fischer, M. (2009). Motion-Cueing-Algorithmen für eine realitätsnahe Bewegungssimulation (Dissertation). *Berichte aus dem DLR-Institut für Verkehrssystemtechnik*. ISSN 1866-721X.

[24] Dagdelen, M., Reymond, G., Kemeny, A., Bordier, M., and Maïzi, N. (2009). Model-based predictive motion cueing strategy for vehicle driving simulators. *Control Engineering Practice*, 17(9):995–1003. ISSN 09670661. doi:10.1016/j.conengprac.2009.03.002.

[25] Ellensohn, F., Schwienbacher, M., Venrooij, J., and Rixen, D. (2018). Motion Cueing Algorithm for a 9 DoF Driving Simulator: MPC with Linearized Actuator Constraints. *SAE Technical Paper Series*, 1:1–10. doi:10.4271/2018-01-0570.

[26] Augusto, B. and Loureiro, R. (2009). *Motion cueing in the Chalmers driving simulator: A model predictive control approach*. Ph.D. thesis, Chalmers University of Technology.

[27] Ellensohn, F., Venrooij, J., Schwienbacher, M., and Rixen, D. (2019). Experimental evaluation of an optimization-based motion cueing algorithm. *Transportation Research Part F: Traffic Psychology and Behaviour*, 62:115–125. ISSN 13698478. doi:10.1016/j.trf.2018.12.004.

[28] Bruschetta, M., Cenedese, C., Beghi, A., and Maran, F. (2018). A motion cueing algorithm with look-Ahead and driver characterization: Application to vertical car dynamics. *IEEE Transactions on Human-Machine Systems*, 48(1):6–16. ISSN 21682291. doi:10.1109/THMS.2017.2776207.

[29] Mohammadi, A., Asadi, H., Mohamed, S., Nelson, K., and Nahavandi, S. (2016). Future reference prediction in model predictive control based driving simulators. *Australasian Conference on Robotics and Automation, ACRA*, 2016-Decem(March 2017):177–184. ISSN 14482053.

[30] Grottoli, M., Cleij, D., Pretto, P., Lemmens, Y., Happee, R., and Bülthoff, H. H. (2018). Objective evaluation of prediction strategies for optimization-based motion cueing. *Simulation*, 95(8):707–724. ISSN 17413133. doi:10.1177/0037549718815972.

[31] Boyd, S. and Vandenberghe, L. (1999). Convex Optimization Copyright c. page 716.

[32] Ellensohn, F., Spannagl, M., Agabekov, S., Venrooij, J., Schwienbacher, M., and Rixen, D. (2020). A hybrid motion cueing algorithm. *Control Engineering Practice*, 97(January):104342. ISSN 09670661. doi:10.1016/j.conengprac.2020.104342.

[33] Misaghi, P. and Hassan, Y. (2005). Modeling operating speed and speed differential on two-lane rural roads. *Journal of Transportation Engineering*, 131(6):408–418. ISSN 0733947X. doi:10.1061/(ASCE)0733-947X(2005)131:6(408).

[34] Bosetti, P., Da Lio, M., and Saroldi, A. (2015). On Curve Negotiation: From Driver Support to Automation. *IEEE Transactions on Intelligent Transportation Systems*, 16(4):2082–2093. ISSN 15249050. doi:10.1109/TITS.2015.2395819.

[35] Sagberg, F., Selpi, Bianchi Piccinini, G. F., and Engström, J. (2015). A review of research on driving styles and road safety. *Human Factors*, 57(7):1248–1275. ISSN 15478181. doi:10.1177/0018720815591313.

[36] Macadam, C. C. (2003). Understanding and Modeling the Human Driver. *Vehicle System Dynamics*, 40(734):101–134. doi:10.1076/vesd.40.1.101.15875.

[37] Yoshimoto, K. (1982). Self-Paced Preview Tracking Control Model of an Automobile Driver. *IFAC Proceedings Volumes*, 14(2):3495–3500. ISSN 1474-6670. doi:10.1016/S1474-6670(17)63989-2.

[38] Gipps, P. G. (1981). A behavioural car-following model for computer simulation. *Transportation Research Part B*, 15(2):105–111. ISSN 01912615. doi:10.1016/0191-2615(81)90037-0.

[39] Nise, N. S. (2011). *Control Systems Engineering*. Wiley, sixth edit edition. ISBN 978-0470-54756-4.

[40] Miller, R., Jagacinski, R., Nalavade, R., and Johnson, W. (1981). Plans and the structure of target acquisition behavior. In *Proceedings of the Human Factors Society*, 1, pages 571–575.

[41] Van der Steen, H. (1998). *Self-motion perception*. Ph.D. thesis, Delft University of Technology.

[42] Berger, D. R. (2006). *Sensor Fusion in the Perception of Dissertation*. Ph.D. thesis, Universität Ulm.

[43] McLane, R. C. (1974). *The influence of motion and audio cues on driver performance in an automobile simulator*. Ph.D. thesis, Virginia Polytechnic Institute and State University.

[44] Mcruer, D. T. and Jex, H. R. (1967). A Review of Quasi-Linear Pilot Models. *IEEE Transactions on Human Factors in Electronics*, HFE-8(3):231–249. ISSN 21682852. doi:10.1109/THFE.1967.234304.

[45] Van Der El, K. (2018). *How humans use preview information in manual control*. Ph.D. thesis. doi:10.4233/UUID.

[46] Sheridan, T. (1966). Three Models of Preview Control. *IEEE Transactions on Human Factorc in Electronics*, HFE-7(2):91–102.

[47] Lechner, D. and Perrin, C. (1993). Actual use of the dynamic performances of vehicles. *Proceedings of the Institution of Mechanical Engineers, Part D: Journal of Automobile Engineering*, 207(4):249–256. ISSN 09544070. doi:10.1243/PIME_PROC_1993_207_190_02.

[48] Bielaczek, C. (1999). Die auswirkung der aktiven fahrerbeeinflussung auf die fahrsicherheit. *ATZ Automobiltechnische Zeitschrift*, 101(9):714–715. ISSN 00012785. doi:10.1007/bf03224277.

[49] Bosetti, P., Da Lio, M., and Saroldi, A. (2014). On the human control of vehicles: An experimental study of acceleration. *European Transport Research Review*, 6(2):157–170. ISSN 18668887. doi:10.1007/s12544-013-0120-2.

[50] Ritchie, M. L., Mccoy, W. K., and Welde, W. L. (1968). A Study of the Relation between Forward Velocity and Lateral Acceleration in Curves During Normal Driving. *Human Factors: The Journal of Human Factors and Ergonomics Society*, 10(3):255–258. ISSN 15478181. doi:10.1177/001872086801000307.

[51] Liu, R. and Zhu, X. (2017). Driving Data Distribution of Human Drivers in Urban Driving Condition. *IEEE Conference on Intelligent Transportation Systems, Proceedings, ITSC*.

[52] Levison, W. H. (1998). Issues Related to Driver Modeling. *Transportation Research Record: Journal of the Transportation Research Board*, 1631(98):20–27.

[53] Cruzado, I. and Donnell, E. T. (2010). Factors affecting driver speed choice along two-lane rural highway transition zones. *Journal of Transportation Engineering*, 136(8):755–764. ISSN 0733947X. doi:10.1061/(ASCE)TE.1943-5436.0000137.

[54] Van Winsum, W. and Godthelp, H. (1996). Speed choice and steering behavior in curve driving. *Human Factors*, 38(3):434–441. ISSN 00187208. doi:10.1518/001872096778701926.

[55] Godthelp, H., Milgram, P., and Blaauw, G. J. (1984). The development of a time-related measure to describe driving strategy. *Human Factors*, 26(3):257–268. ISSN 00187208. doi:10.1177/001872088402600302.

[56] Van Winsum, W., Brookhuis, K. A., and De Waard, D. (2000). A comparison of different ways to approximate time-to-line crossing (TLC) during car driving. *Accident Analysis and Prevention*, 32(1):47–56. ISSN 00014575. doi:10.1016/S0001-4575(99)00048-2.

[57] Reymond, G., Kemeny, A., Droulez, J., and Berthoz, A. (2001). Role of lateral acceleration in curve driving: Driver model and experiments on a real vehicle and a driving simulator. *Human Factors*, 43(3):483–495. ISSN 00187208. doi:10.1518/001872001775898188.

[58] Lacquaniti, F., Terzuolo, C., and Viviani, P. (1983). The law relating the kinematic and figural aspects of drawing movements. *Acta Psychologica*, 54(1-3):115–130. ISSN 00016918. doi:10.1016/0001-6918(83)90027-6.

[59] Viviani, P. and Flash, T. (1995). Minimum-Jerk, Two-Thirds Power Law, and Isochrony: Converging Approaches to Movement Planning. *Journal of Experimental Psychology: Human Perception and Performance*, 21(1):32–53. ISSN 00961523. doi:10.1037/0096-1523.21.1.32.

[60] Flash, T., Meirovitch, Y., and Barliya, A. (2013). Models of human movement: Trajectory planning and inverse kinematics studies. *Robotics and Autonomous Systems*, 61(4):330–339. ISSN 09218890. doi:10.1016/j.robot.2012.09.020.

[61] Hicheur, H., Vieilledent, S., Richardson, M. J., Flash, T., and Berthoz, A. (2005). Velocity and curvature in human locomotion along complex curved paths: A comparison with hand movements. *Experimental Brain Research*, 162(2):145–154. ISSN 00144819. doi:10.1007/s00221-004-2122-8.

[62] Bays, P. M. and Wolpert, D. M. (2007). Computational principles of sensorimotor control that minimize uncertainty and variability. *Journal of Physiology*, 578(2):387–396. ISSN 00223751. doi:10.1113/jphysiol.2006.120121.

[63] Levison, W. H. (2007). Development of a Driver Vehicle Module for the Interactive Highway Safety Design Model. *Fhwa-Hrt-08-019*, (November).

[64] Land, M. F. and Lee, D. N. (1994). Where we look when we steer. *Nature*, 369(6483):742–744. ISSN 00280836. doi:10.1038/369742a0.

[65] Lappi, O., Rinkkala, P., and Pekkanen, J. (2017). Systematic observation of an expert driver's gaze strategy-An on-road case study. *Frontiers in Psychology*, 8(APR):1–15. ISSN 16641078. doi:10.3389/fpsyg.2017.00620.

[66] Gruppelaar, V., Van Paassen, R., Mulder, M., and Abbink, D. (2019). A Perceptually Inspired Driver Model for Speed Control in Curves. *Proceedings - 2018 IEEE International Conference on Systems, Man, and Cybernetics, SMC 2018*, pages 1257–1262. doi:10.1109/SMC.2018.00220.

[67] Elamrani Abou Elassad, Z., Mousannif, H., Al Moatassime, H., and Karkouch, A. (2020). The application of machine learning techniques for driving behavior analysis: A conceptual framework and a systematic literature review. *Engineering Applications of Artificial Intelligence*, 87(March 2019):103312. ISSN 09521976. doi:10.1016/j.engappai.2019.103312.

[68] Tran, D., Sheng, W., Liu, L., and Liu, M. (2015). A Hidden Markov Model based driver intention prediction system. *2015 IEEE International Conference on Cyber Technology in Automation, Control and Intelligent Systems, IEEE-CYBER 2015*, pages 115–120. doi:10.1109/CYBER.2015.7287920.

[69] Zyner, A., Worrall, S., and Nebot, E. (2018). A Recurrent Neural Network Solution for Predicting Driver Intention at Unsignalized Intersections. *IEEE Robotics and Automation Letters*, 3(3):1759–1764. ISSN 23773766. doi:10.1109/LRA.2018.2805314.

[70] Lethaus, F., Baumann, M. R., Köster, F., and Lemmer, K. (2011). Using pattern recognition to predict driver intent. *Lecture Notes in Computer Science (including subseries Lecture Notes in Artificial Intelligence and Lecture Notes in Bioinformatics)*, 6593 LNCS(PART 1):140–149. ISSN 03029743. doi:10.1007/978-3-642-20282-7_15.

[71] Liu, Y., Zhao, P., Qin, D., Li, G., Chen, Z., and Zhang, Y. (2019). Driving Intention Identification Based on Long Short-Term Memory and A Case Study in Shifting Strategy Optimization. *IEEE Access*, 7:128593–128605. ISSN 21693536. doi:10.1109/ACCESS.2019.2940114.

[72] Peng, B., Zhang, H., Xuan, F., and Xiao, W. (2018). Torque Distribution Strategy of Electric Vehicle with In-wheel Motors Based on the Identification of Driving Intention. *Automotive Innovation*, 1(2):140–146. ISSN 2096-4250. doi:10.1007/s42154-018-0024-x.

[73] Liu, A. and Pentland, A. (1997). Towards real-time recognition of driver intentions. *IEEE Conference on Intelligent Transportation Systems, Proceedings, ITSC*, pages 236–241.

[74] Pentland, A. and Andrew, L. (1999). Modeling and prediction of human behavior. *Neural Computation*, 11(1):229–242. ISSN 08997667. doi:10.1162/089976699300016890.

[75] Zhao, X., Wang, S., Ma, J., Yu, Q., Gao, Q., and Yu, M. (2019). Identification of driver's braking intention based on a hybrid model of GHMM and GGAP-RBFNN. *Neural Computing and Applications*, 31(s1):161–174. ISSN 09410643. doi:10.1007/s00521-018-3672-1.

[76] Oliver, N. and Pentland, A. (2000). Graphical models for driver behavior recognition in a SmartCar. (Mi):7–12. doi:10.1109/ivs.2000.898310.

[77] Brand, M., Oliver, N., and Pentland, A. (1997). Coupled hidden Markov models for complex action recognition. *Proceedings of the IEEE Computer Society Conference on Computer Vision and Pattern Recognition*, pages 994–999. ISSN 10636919. doi:10.1109/cvpr.1997.609450.

[78] Wu, M., Louw, T., Lahijanian, M., Ruan, W., Huang, X., Merat, N., and Kwiatkowska, M. (2019). Gaze-based Intention Anticipation over Driving Manoeuvres in Semi-Autonomous Vehicles. *IEEE International Conference on Intelligent Robots and Systems*, pages 6210–6216. ISSN 21530866. doi:10.1109/IROS40897.2019.8967779.

[79] Patel, S., Griffin, B., Kusano, K., and Corso, J. J. (2018). Predicting Future Lane Changes of Other Highway Vehicles using RNN-based Deep Models.

[80] Ellensohn, F. (2019). *Urban Motion Cueing Algorithms – Trajectory Optimization for Driving Simulators*. Ph.D. thesis, TU München.

[81] Feng, Z., Yang, M., Kumfer, W., Zhang, W., Du, Y., and Bai, H. (2018). Effect of longitudinal slope of urban underpass tunnels on drivers' heart rate and speed: A study based on a real vehicle experiment. *Tunnelling and Underground Space Technology*, 81(August):525–533. ISSN 08867798. doi:10.1016/j.tust.2018.08.032.

[82] Kolff, M., Venrooij, J., Pool, D. M., and Mulder, M. (2020). Comparison of Quality Metrics between Motion Cueing Algorithms in a Virtual Test Environment. pages 9–11.

[83] Biran, O. and Cotton, C. (2017). Explanation and Justification in Machine Learning: A Survey. *IJCAI Workshop on Explainable Artificial Intelligence (XAI)*, pages 8–13. ISSN 13563289. doi: 10.1108/13563281111156853.

[84] Dobson, A. and Barnett, A. (2008). *An Introduction to Generalized Linear Models*. Chapman & Hall/CRC, third edit edition. ISBN 9781584889502. doi:10.2307/1269239.

[85] Advisory Group for Aerospace Research and Development (1980). Fidelity of simulation for pilot training.

[86] Gilmore, G. C., Wenk, H. E., Naylor, L. A., and Stuve, T. A. (1992). Motion perception and aging. *Psychology and aging*, 7(4):654–660. ISSN 08827974. doi:10.1037/0882-7974.7.4.654.

[87] Likert, R. (1932). A technique for the measurement of attitudes. *Archives of Psychology*, 22 140(55).

[88] Chinchor, N. (1992). MUC-4 Evaluation Metrics. In *Proceedings of the Fourth Message Understanding Conference*, pages 22–29.

# III

# Appendices

# A

# Effect of workspace limiting on motion cueing quality

In the scientific paper presented in Part I of this report, drives wherein workspace limits were reached, were excluded in the analysis of the motion cueing quality results. The current appendix presents a comparison between the motion cueing quality of limited drives and that of clean drives (i.e., drives in which the simulator's workspace limits were not reached). As in the current analysis individual drives are looked at, no averaging of double data points was performed.

Figure A.1 shows the objective motion cueing criterion results for the whole drive except the starting and stopping maneuvers. Note that the AD denotes the normalized difference between the specific forces in the platform and the simulated vehicle, and that an AD score of 0 indicates perfect cueing [30]. It is clearly visible that in all conditions, the drives in which limiting occurs yielded a larger AD w.r.t. the clean drives.

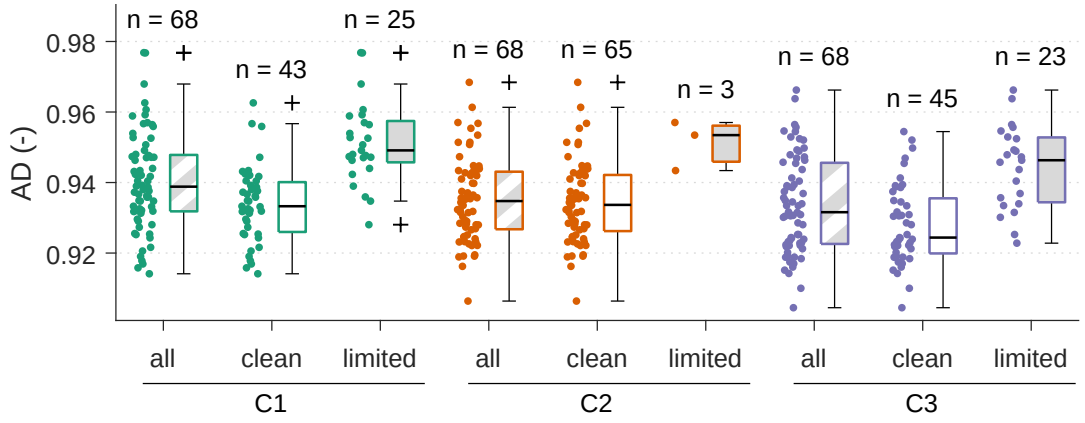


Figure A.1: Subdivision of objective motion cueing quality over the whole drive except the starting and stopping maneuvers into clean and limited drives.

Figure A.2 shows the subjective PMI ratings for sections N1 to N4. Most limiting cases occurred in sections N1 and N3. In section N1, no clear differences are found between the clean and limited drives. In section N3, however, higher PMI scores were obtained for the limited rides under all conditions. The latter is in line with the findings on the AD. In conclusion, it would have been better to opt for a more conservative tuning in the human-in-the-loop experiment, so as to not obscure results with the effect of limiting.

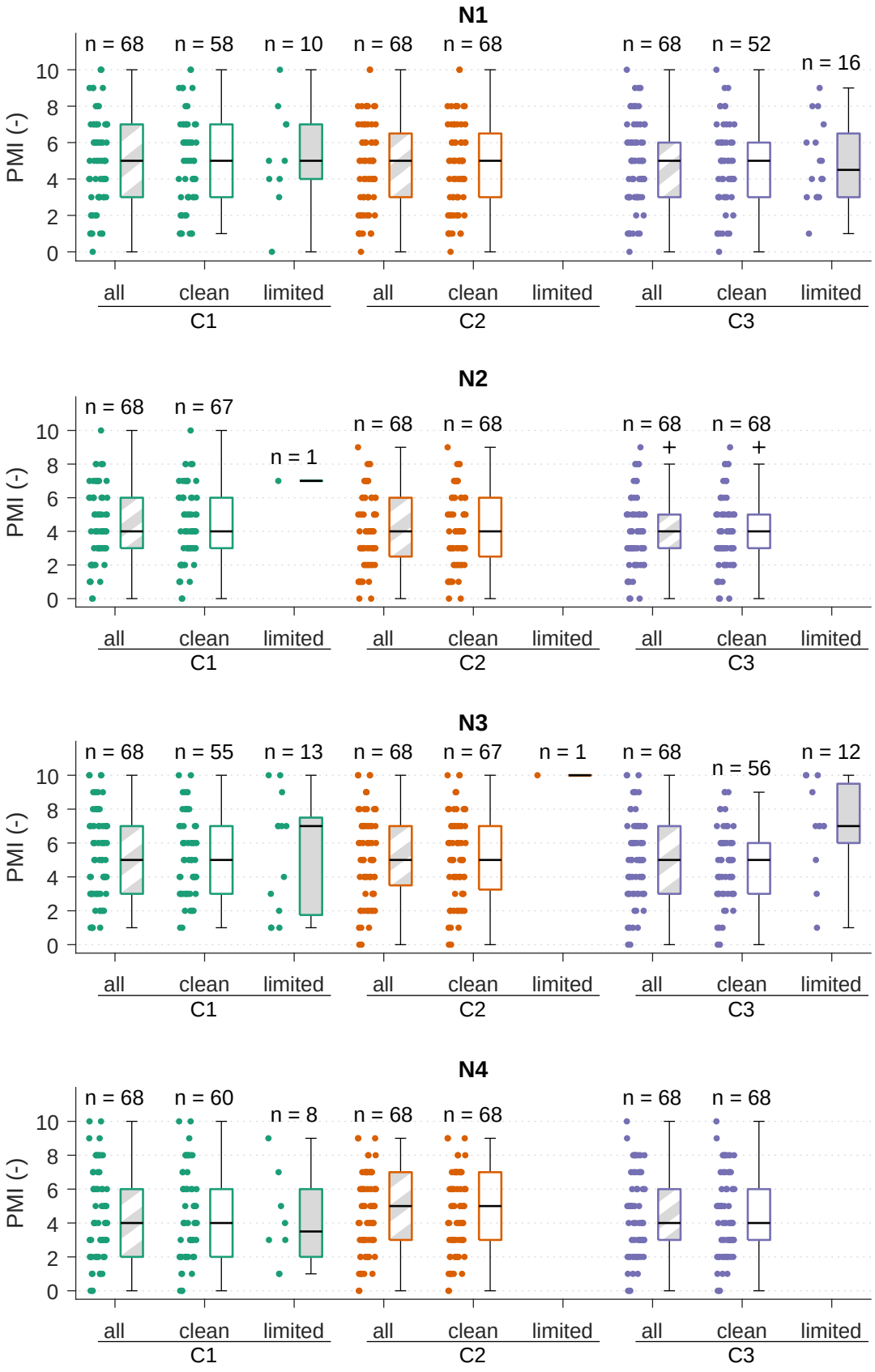


Figure A.2: Subdivision of subjective motion cueing quality per section into clean and limited drives.

# B

# Post-hoc questionnaire results

The current appendix provides the results obtained using the post-hoc motion cueing questionnaire described in Appendix D. Workspace limits were reached in the starting and stopping procedures of almost all drives. Workspace limiting could induce false cues due to braking of the simulator and missing cues due to the inability to accelerate further in the direction of the workspace edge. Consequently, it was not possible to observe the effect of adding PP and increasing the translational surge gain of the MCA. For completeness, measurements are presented here.

The resulting PMI per experimental condition as presented in Figure B.1 shows that in the post-hoc ratings of the complete drives, no clear differences were found when comparing the three motion conditions. This is in line with the inconsistency found in the SPR ratings as presented in the scientific paper in Part I of this report. Figure B.2 shows the response to the motion cueing questionnaire. The aim was to provide qualitative insights that could explain the resulting PMI ratings. Nevertheless, again no clear differences were found between the three conditions.

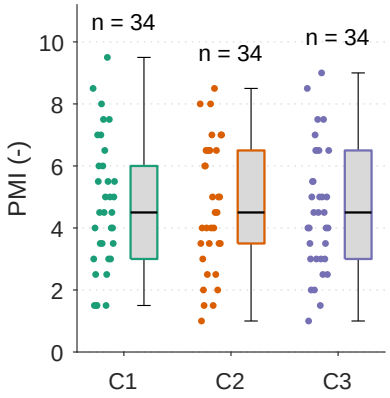


Figure B.1: Subjective ratings of motion cueing quality.

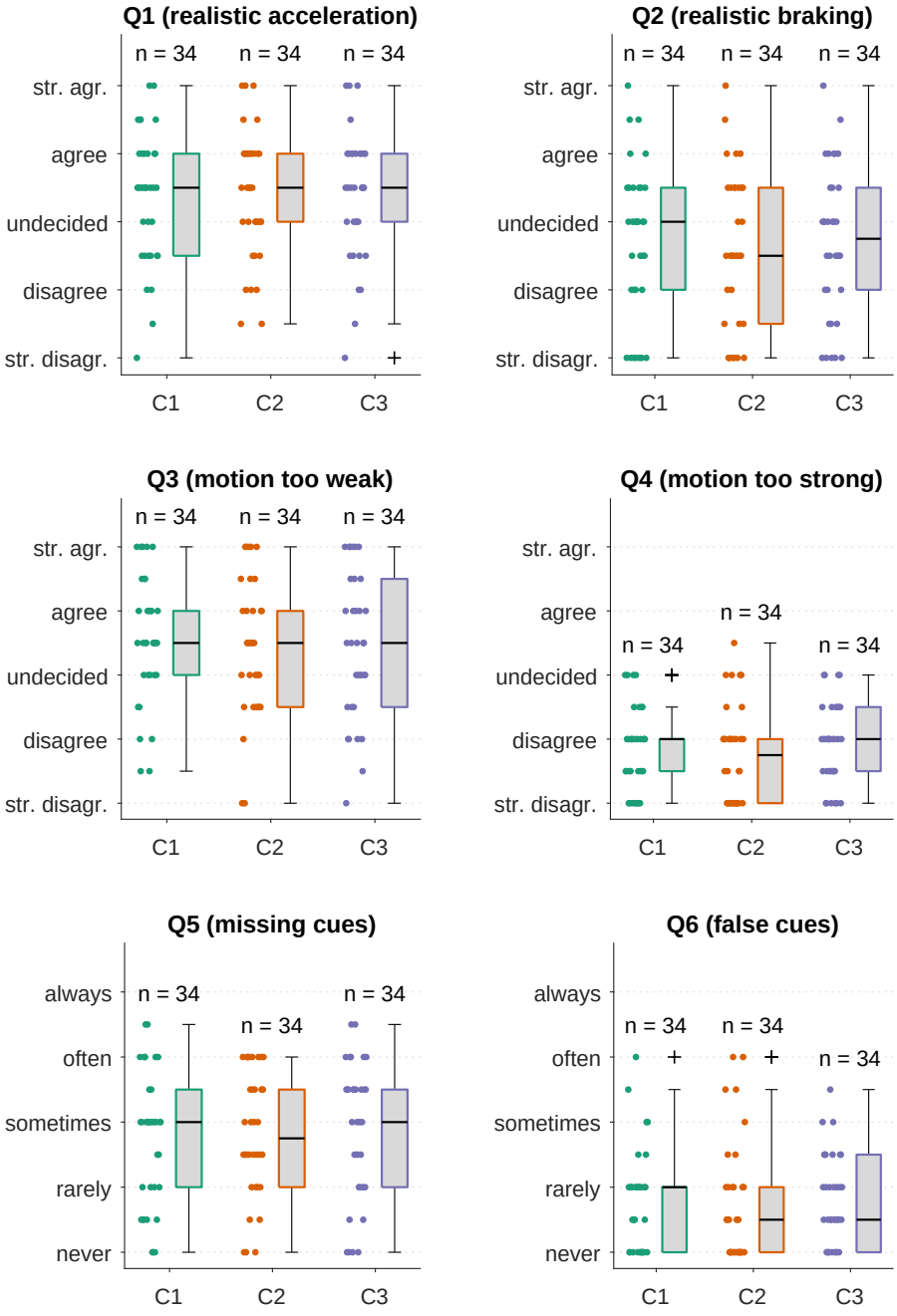


Figure B.2: Motion cueing questionnaire responses.

# C

# Experiment briefing

## C.1. Allgemeine Information für Teilnehmende

In der heutigen Studie wird es um die Qualität der Simulatorbewegung gehen. Ihre aufgabe als Fahrer wird sein, die strecke zu fahren in Ihrem normalem Fahrstil und Abweichungen zwisschen der erwarteten und der gegebenen Bewegung zu bewerten.

## C.2. Aufgabe und Messungen während der Fahrt

Die Bewegung des Simulators unterscheidet sich von der Bewegung eines realen Fahrzeugs. Diese Abweichungen können in verschiedenen Formen auftreten. Einerseits können Bewegungen zu schwach anfühlen oder ganz fehlen, das heißt es ist zu wenig Bewegung bei einem spezifischen Fahrmanöver spürbar. Andererseits kann Simulatorbewegung zu stark sein im Vergleich zum realen Fahrzeug und kann der Simulator sich bewegen, während das reale Fahrzeug das nicht tut. Die Abweichungen zwischen der Bewegung des Simulators und des realen Fahrzeugs sollten nach eigenem Empfinden beurteilt werden. Die Skala reicht von 0 bis 10, wobei 0 keine Abweichung zu einer realen Fahrt und 10 eine sehr Große Abweichung zur Realfahrt repräsentiert:

**Reales Fahrempfinden** **Sehr große Abweichung**

| 0 | 1 | 2 | 3 | 4 | 5 | 6 | 7 | 8 | 9 | 10 |
|---|---|---|---|---|---|---|---|---|---|---|
| | | | | | | | | | | |

Ziel ist, für verschiedene Abschnitte die Abweichung pro Abschnitt zu bewerten. Der Versuchsleiter wird während der Fahrt anzeigen wann ein Abschnitt beginnt und endet. Wen ein Abschnitt endet, Sie bewerten die Bewegung im gesamten Abschnitt mündlich. Bitte bewerten Sie ausschließlich die Längsbewegung des Simulators (gefühl beim beschleunigung und bremsen). In die Bewertung nicht mit einfließen sollen:

- Querdynamik des Simulators (gefühl beim drehen)
- Visualisierungsfehler, bspw. Verpixelungen, Rand vom Bildschirm
- Fehlende Straßenbeschaffenheiten, bspw. Schlaglöcher, Abwasserdeckel
- Soundeffekte, bspw. Motorsound, Fahrtwind
- Störgeräusche vom Simulator, bspw. von Elektromotoren
- Unmittelbarer Beginn und Ende der Fahrt. Der Simulator fährt in die neutrale Position, dies ist nicht Bestandteil der Messfahrt ist
- Unrealistische Gegebenheiten im Fahrerraum, bspw. Lenkrad und Fußpedale bewegen sich nicht
- Gerüche

## C.3. Ablauf der Studie

Das Experiment besteht aus 6 vierminütige Fahrten. Insgesamt dauert das Experiment etwa 1 Stunde und 10 Minuten. Die Studie wird dabei nach folgendem Ablaufplan durchlaufen:

- Nachdem Sie diese Studieninformation gelesen haben, werden Sie einen Fragenbögen ausfüllen.
- Danach dürfen Sie in den Simulator einsteigen. Nachdem Sie Platz genommen haben, werden Sie eine kurze Einweisung bekommen. Auch die mündliche Bewertung von Abschnitte in eine Testfahrtwird hier geübt.
- Nachdem die Testfahrt abgeschlossen ist und Sie keine weiteren Fragen haben, beginnt die erste Messfahrt.
- Während der Messfahrt führen Sie die beschriebenen Aufgaben aus. Bitte teilen Sie dem Versuchsleiter unbedingt mit falls Ihnen unwohl ist. Sie können zu jeder Zeit den Versuch abbrechen.
- Nach jeder Messfahrt, wird die Simulation kurz unterbrochen, und werden Sie ein paar Fragenbogen ausfüllen.
- Zum Abschluss des Experiments, wenn Sie wieder aus dem Simulator ausgestiegen sind, werden Sie noch einen Fragenboge ausfüllen. Anschließend ist die Studie beendet.
- Wer vor der Fahrt auf die Toilette möchte, hat jetzt die Gelegenheit dazu.
- Ich bitte Sie außerdem, für die Zeit der Studie Ihr Handy auf lautlos zu stellen und während der Fahrt nicht Ihr Handy zu benutzen.
- Sollten Sie noch Fragen haben wenden Sie sich bitte an den Versuchsleiter.

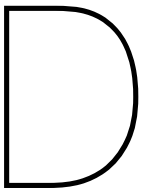

# Post-hoc motion cueing questionnaire

**Reales Fahrempfinden** **Sehr große Abweichung**

| 0 | 1 | 2 | 3 | 4 | 5 | 6 | 7 | 8 | 9 | 10 |
|---|---|---|---|---|---|---|---|---|---|---|
| | | | | | | | | | | |

| | **Trifft nicht zu** | **Trifft eher nicht zu** | **Teils-teils** | **Trifft eher zu** | **Trifft zu** |
|---|---|---|---|---|---|
| Beschleunigung fühlte sich realistisch an | | | | | |
| Bremsen fühlte sich realistisch an | | | | | |
| Bewegung war zu schwach | | | | | |
| Bewegung war zu stark | | | | | |

| | **Nie** | **Selten** | **Manchmal** | **Oft** | **Immer** |
|---|---|---|---|---|---|
| Es gab kein Bewegung wenn Bewegung erwartet war | | | | | |
| Es gab Bewegung wenn kein Bewegung erwartet war | | | | | |

# E

# Latin square design

Ordering of experimental conditions was done as in Table E.1. Here, $A_i$ is the $i$-th realization of a row- and column-randomized version of matrix $A_0$, which is shown in Equation E.1.

Table E.1: Latin square matrix design used in the experiment.

| | **Drive 1** | **Drive 2** | **Drive 3** | **Drive 4** | **Drive 5** | **Drive 6** |
|---|---|---|---|---|---|---|
| Participant 1 | $A_1$ | | | $A_2$ | | |
| Participant 2 | | | | | | |
| Participant 3 | | | | | | |
| Participant 4 | $A_3$ | | | $A_4$ | | |
| Participant 5 | | | | | | |
| Participant 6 | | | | | | |
| ⋮ | ⋮ | | | ⋮ | | |

$$A_0 = \begin{bmatrix} \text{C1} & \text{C2} & \text{C3} \\ \text{C2} & \text{C3} & \text{C1} \\ \text{C3} & \text{C1} & \text{C2} \end{bmatrix} \tag{E.1}$$

# F

# Effect of drive number on subjective ratings

The Latin Square design as described in Appendix E was applied in order to balance out order effects. In order to provide a look into these effects, Figure F.1 shows the PMI ratings of all of the drives per drive number. After the third drive, a 5-minute break was held. Hereafter, the PMI is rated slightly lower than before the break. It is hypothesized that the increased acceptance of motion cueing over time is a result of that participants tend to forget the experience of realistic motion.

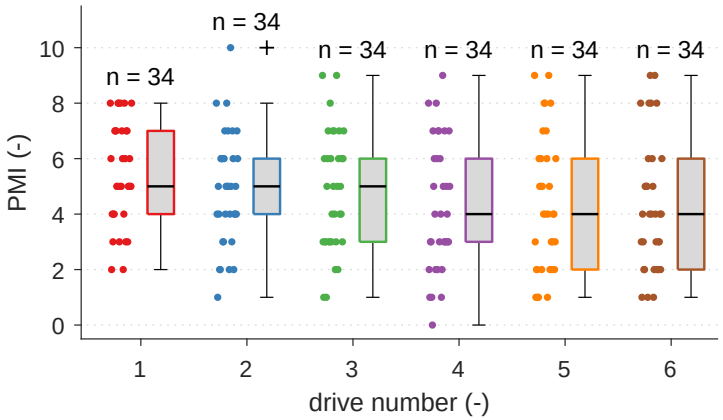


Figure F.1: Subjective ratings over the whole ride per drive number, not distinguishing between conditions.

# G

# Sensitivity of F1-scores to detection thresholds

In section III of the scientific paper in Part I, the use of detection thresholds was proposed for prepositioning. The $F_1$-score [88] was calculated for each threshold and the thresholds that yielded the highest scores were used in the proposed prepositioning logic. The current appendix is added to show the sensitivity of the $F_1$-scores to the detection thresholds, for the logistic regression model with predictor variables $V_{veh} - \hat{V}_{r,t+8}$ and $\delta_a$ (i.e., the selected model).

In Figure G.1, the thresholds are indicated on the ROC curves for acceleration and deceleration detection. It can be seen that for equivalent thresholds, the TPR of deceleration detection is lower than that of acceleration detection. Consequently, a lower threshold has to be chosen in order to detect maneuvers.

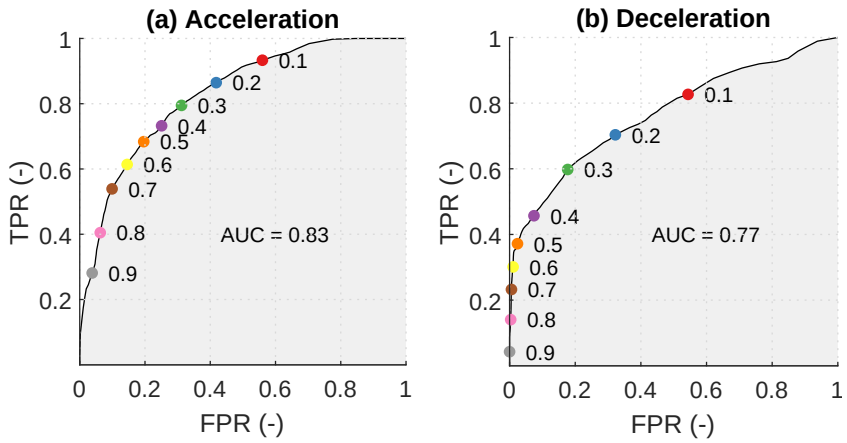


Figure G.1: ROC curves with indication of detection thresholds.

Figure G.2 shows the $F_1$-scores against threshold values for the acceleration and deceleration prediction models. It can be seen that the $F_1$-score of the deceleration prediction is more sensitive to the detection threshold than the $F_1$-score of the acceleration prediction. Note that even though the $F_1$-score of the acceleration detection is relatively insensitive to the detection threshold, changing the detection threshold still changes the characteristics of the classifier. As can be seen in Figure G.1, a higher acceleration detection threshold yields an increased TPR at the cost of an increased FPR.

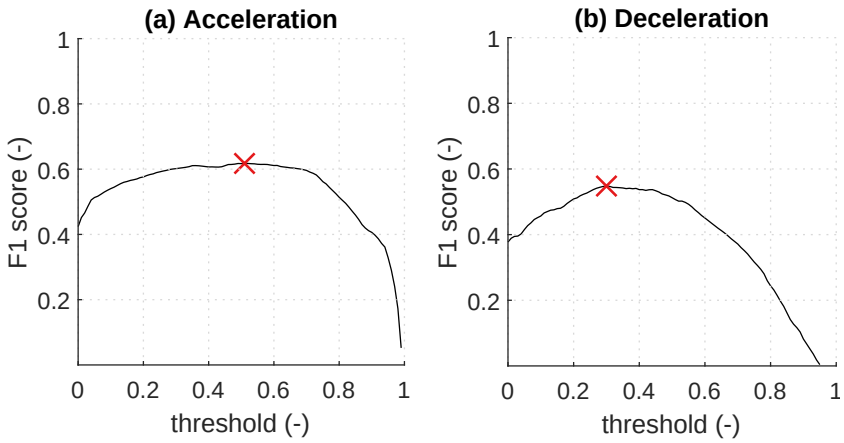


Figure G.2: $F_1$-scores plotted against the detection thresholds. The optima are denoted by $\times$.

# H

# Comparison with velocity-based prepositioning

The only prepositioning algorithm that is explicitly described in literature, is that of Hansson & Stenbeck [12]. In their implementation for a curvy race track, the possibilities of braking and acceleration were taken into account at all times. The mean of the range of possible vehicle accelerations was calculated at each time step, and from this mean, a reference PP offset was calculated. As the range of possible vehicle accelerations was assumed to be a function of the vehicle's velocity only, this will be referred to as velocity-based PP.

In the scientific paper presented in Part I, low AUCs and $F_1$-scores were obtained for the prediction of acceleration and deceleration when the vehicle's velocity was used as only predictor variable. For this reason, a comparison between the PP algorithm proposed in the scientific paper and the PP algorithm proposed by Hansson & Stenbeck was omitted. For completeness, it is included in the current appendix.

## H.1. Equations

$$a_{acc,max} = \begin{cases} 6 & V \leq 8.64 \text{ (m/s)} \\ 51.84 \cdot V^{-1} & V > 8.64 \text{ (m/s)} \end{cases} \tag{H.1}$$

The mean possible acceleration is calculated using to Equation H.2, where the maximum deceleration is equal to -5 m/s and thus independent of the vehicle's velocity.

$$\bar{a}(V) = \frac{a_{acc,max}(V) + a_{brake,max}}{2} \tag{H.2}$$

Equation H.3 was used to calculate a PP offset ($x_{PP}$) out of the mean of possible accelerations, which cannot exceed the maximum allowed PP offset ($x_{PP,max}$).

$$x_{PP}(V) = -x_{PP,max} \frac{\bar{a}(V)}{\max\left(\bar{a}(V_{max}), |\bar{a}(V_{min})|\right)} \tag{H.3}$$

## H.2. Evaluation

Equivalent to the comparison between the threshold-based and linear PP types in Section III-B of the scientific paper presented in Part I, a grid search was performed to find the optimal settings for the velocity-based PP described in the current appendix. The maximum translational surge gain that could be set without activating the workspace limiting in any of the 16 drives ($K_{x,max}$), was calculated for various settings of $P_{pp,max}$. Results are shown in Table H.1. Note that for the velocity-based PP, $P_{pp,min}$ is not an optimization parameter, as it is defined as -$P_{pp,max}$. The velocity range parameters $V_{min}$ and $V_{max}$ were set to 0 and 120 km/h, respectively.

Table H.1: Maximum surge gains and corresponding $P_{pp,min}$ and $P_{pp,max}$ values per PP type.

| **PP logic** | $K_{x,max}$ | $P_{pp,min}$ | $P_{pp,max}$ **(m)** |
|---|---|---|---|
| None | 0.24 | - | - |
| Velocity-based (Hansson & Stenbeck) | 0.26 | -0.06 m | 0.06 m |
| Linear (proposed in this thesis) | 0.33 | -0.14 m | 0.20 m |

As can be seen in Table H.1, higher gains could be set using velocity-based PP than when not using PP. Nevertheless, the potential increase in surge gain was 8.3 %, which is little compared to the 38 % increase that was could be obtained using the linear PP logic proposed in this thesis. In order to be able to elaborate on the shortcomings of velocity-based PP, H.1 shows the vehicle velocity, PP (reference and final) and the simulator position (with and without PP) for one of the drives, with a $K_x$ value of 0.27 (i.e., slightly higher than possible within the simulator's workspace). One can see that the critical maneuver in this drive occurs in section N3. In this maneuver, the vehicle decelerates from 28 m/s (±100 km/h) to 14 m/s (±50 km/h). At the end of this deceleraton maneuver, the velocity is low and consequently, PP is approximately zero. Nevertheless, the simulator is still located in the rear. Consequently, the simulator reaches the workspace limits, despite the slight compensation by PP. Increasing the value for $P_{pp,max}$ would improve workspace management in this deceleration maneuver, but would yield the same problem at the end of acceleration maneuvers.

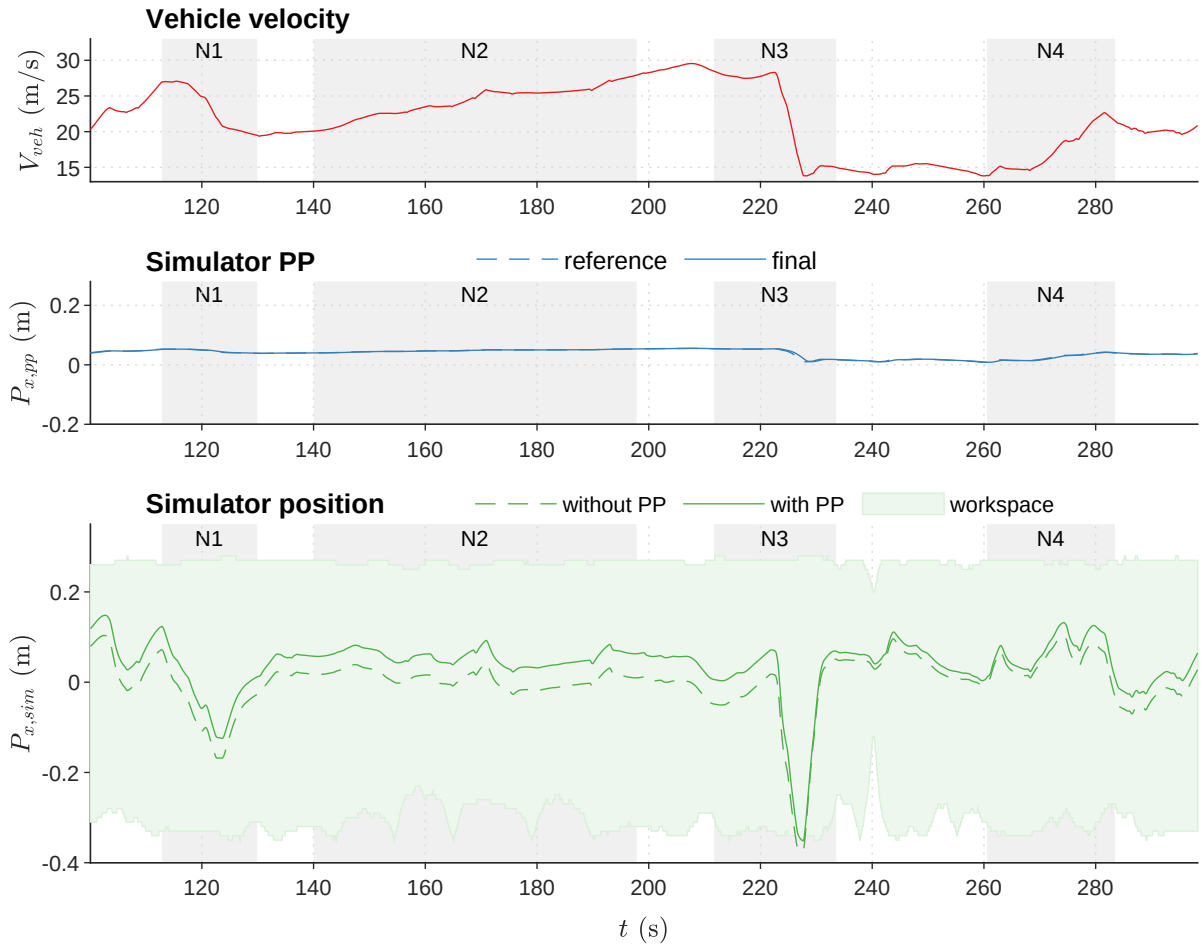


Figure H.1: Vehicle velocity, velocity-based PP and the resulting simulator surge position.

Figure H.2 shows the PP (reference and final) and the simulator position (with and without PP) for the same drive, but now using the linear PP as proposed in this thesis. Larger PP excursions (i.e., ranging between -0.14 and 0.20 m) could be made, as the velocity, speed limit and accelerator pedal deflection accurately predicted future maneuvering. Consequently, the prepositioned simulator did not reach the workspace limits in section N3.

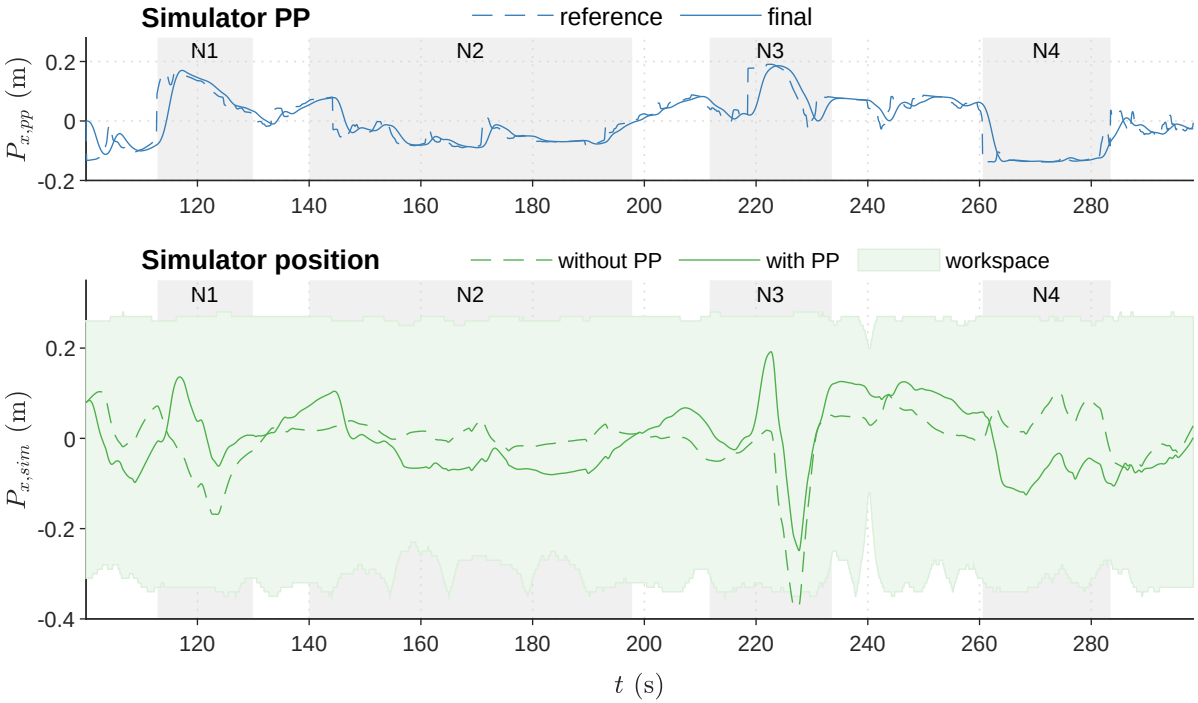


Figure H.2: Linear PP and the resulting simulator surge position.